Watching Sugar Transport in Real Time in Single Cells and Cell Populations

TITLE PAGE

Watching Sugar Transport in Real Time in Single Cells and Cell Populations

A Dissertation Presented

By

Andrew H. Simon

Submitted to the Faculty of

University of Massachusetts

Graduate School of Biomedical Sciences, Worcester

in partial fulfillment of the requirements for the degree of

Doctor of Philosophy

February 23rd, 2018

Biochemistry and Molecular Pharmacology

SIGNATURE PAGE

Watching Sugar Transport in Real Time in Single Cells and Cell Populations

A Dissertation Presented

By

Andrew H. Simon

Approved as to style and content by:

Dr. Daniel Bolon, Chair of Committee

Dr. José Argüello, Member of Committee

Dr. Osman Bilsel, Member of Committee

Dr. William Royer, Member of Committee

Dr. Sean Ryder, Member of Committee

Dr. Anthony Carruthers, Thesis Advisor

Dr. Anthony Carruthers
Dean of the Graduate School of Biomedical Sciences

Department of Biochemistry & Molecular Pharmacology

February 23rd, 2018

COPYRIGHT NOTICE

ABSTRACT

The facilitative glucose transporter GLUT1 catalyzes the passive translocation of glucose across plasma membranes. Previous studies have demonstrated that regulation of GLUT1 activity is complex and subject to modulation by a variety of environmental and allosteric effectors. Mathematical models of GLUT1 kinetics have been derived which successfully account for subsets of these factors, though efforts to develop a single kinetic theory has not yet been achieved. Limitations in conventional experimental methodologies cannot provide kinetic data with the precision and continuity needed for further refinement of said models. We utilized a glucose-sensitive fluorescent protein (GlcSnFR) to develop novel experimental methodologies to facilitate elucidation of the GLUT1 kinetic mechanism. Characterization of the kinetic and optic properties of GlcSnFR and glucose binding (k_{on}: 389.5 ± 12.1 $M^{-1}s^{-1}$, k_{off}: 0.593 ± 0.103 s^{-1}, k_D: 1.52 ± 0.31 mM) allowed us to construct analyses which continuously estimate glucose flux through GLUT1 with subsecond temporal resolution and spacial resolution of a single human erythrocyte. We additionally revised the analytic methodology for interpreting the collected kinetic data sets to reduce the *a priori* assumptions regarding equilibrium states of the GLUT1 enzyme ensemble, which provided more flexible, model-independent characterizations of transporter activity. Using resealed human erythrocyte ghosts containing GlcSnFR, we applied techniques in confocal microscopy and fluorometry to achieve new insights into the kinetics of GLUT1. By microscopy, we observed transport in single cells to achieve conclussive evidence that populations of resealed ghosts are homogeneous in their composition, a previously unachieved result which retroactively validates to a great many previous studies. Further, we confirmed, unambiguously, that ATP induces directional asymmetry in GLUT1 through a reduction in rates of sugar efflux. By fluorometry, we demonstrated that previous measurements of the endofacial KM of GLUT1 for glucose are underestimated (~4 mM) and closer to ~20 mM. Finally, these new methods provide access to a new paradigm for measuring glucose transport in general and will serve to advance the field significantly in years to come.

ACKNOWLEDGMENTS

I would like to thank my mentor, Tony Carruthers, for his continued support and insight throughout the long course of my graduate career. We started a very different project than we finished, but ultimately achieved something significant both now and in time to come. I would also like to thank my advisory committee for their steadfast guidance and encouragement. It was only through their advice that I was able to follow a course which led somewhere rather than anywhere. I would also like to thank the entirety of my family. I could not have achieved this without their unending love and support and infinite willingness to help in every way possible.

Most of all, I want to thank my wonderful, brilliant wife, Kailene Simon. Without you I would have neither embarked upon nor completed this personal odyssey. You are the ship that protects me, the star that guides me, and the sea that creates my place in the world. Thank you for everything.

ATTRIBUTIONS

We would like to thank the Looger lab at Janelia Research Facility for their contributions to this work. Their collaboration provided us with the GlcSnFR probe which gave us the means to complete this body of work.

TABLE OF CONTENTS

Table of Contents

LIST OF FIGURES

Chapter 1

LITERATURE REVIEW

Solute flux across phospholipid membranes

The homeostatic regulation of a cell depends on its ability to prevent and effect changes in its chemical state quickly and with a high degree of accuracy. Of fundamental importance to this capacity is the phospholipid bilayer, whose structure results from the organization of amphipathic phospholipids into two sheets with a hydrophobic center. This layer of hydrophobicity prohibits the free movement of chemicals between the enclosed volume and its environment (Widdas, 1952). In order to enable the movement of solutes between membrane-enclosed spaces, cells utilize specific proteins which can facilitate the transmembrane flux of specific molecules (Stein, 1986). Through the coordination of the individual activities of these proteins, a cell can dynamically regulate its contents with up to single solute molecule precision. Different classes of proteins achieve this result with varied structural compositions and mechanisms, but perhaps the most fundamental delineation is whether they do work on the system or permit work to be done by the system. Thermodynamically, these proteins can be separated into two major classes: active and passive (Alberts B et al., 2002).

Passive transporters enable the diffusion of a specific substrate, but do not prefer one direction of flux over the other. This results in a net movement of the transported substrate down its chemical gradient and equilibration of concentrations in the separated volumes. Transporters of this variety are often responsible for the transport of chemical species used or produced by constitutively active cell processes like metabolism and the biogenesis of macromolecules. Specific examples of this type of transporter are ion channels and aquaporins (Hille, 2001). These proteins allow the cell to maintain strict control over transmembrane traffic while providing permeability to chemicals whose flux can be automatically regulated by their rates of utilization or production (Alberts B et al., 2002).

Active transporters can catalyze substrate translocation using a variety of potential energy stores generated previously by other biochemical processes. A common example is the potential stored in chemicals such as adenosine triphosphate (ATP) which contain high energy bonds. The coupling of bond lysis with transporter activity allows the transporter to preferentially select the direction of flux, often shifting the solute concentration gradient away from equilibrium. Examples of this type of transporter include the Cu^{+}-ATPase, whose catalytic mechanism uses ATP hydrolysis to move copper (I) ions out of the cytoplasm, against its concentration gradient (Argüello et al., 2016), and the protein complexes of the electron transport chain which use the high reduction capacity of chemicals like NADH and $FADH_2$ to enact a sequence of reductions which catalyze the unidirectional transfer of protons into the intermembrane space (Friis et al., 1997). The activity of such transporters can enable another class of active transporters which catalyze reactions using potential stored entropically in unequilibrated concentration gradients. Facilitating the equilibration of this gradient allows the transporter to simultaneously enact a second, thermodynamically unfavorable action. Such is the case with the ATP synthase complex which allows the transport of protons back into the mitochondrial matrix while simultaneously synthesizing ATP from adenosine diphosphate (ADP) and inorganic phosphate (P_i) (Taurino and Gnoni, 2018).

As stated above, the cell achieves precise control over its physical and chemical state first by maintaining compartmentalized spaces whose conditions can be changed through selective and dynamically regulated transporters (Alberts B et al., 2002). As biochemical processes involve a great many different chemical species, cells must have a proportionally large arsenal of transporters to control their passage across its constituent plasma membranes. To date, over 1,400 individual human proteins have been characterized as transporters (Elbourne et al., 2017). As each plays its own role in the human physiology, it is not surprising that conditions leading to the loss, malfunction, or dysregulation of these proteins are the causes of many diseases or play important roles in their pathologies. Examples of

diseases and their dysregulated substrates include chloride ions in cystic fibrosis (Cheng et al., 1990), glucose in diabetes (Bell et al., 1989), amino acids in cystinuria (Calonge et al., 1994), and calcium in polycystic kidney disease (Brook-Carter et al., 1994).

Glucose transporters catalyze the facilitated diffusion of glucose

The glycolytic pathway forms the axis of cellular glucose utilization and thus exists at the core of metabolic function in human physiology. The energy resulting from the catabolic breakdown of glucose is stored in the molecular bonds of molecules like ATP and NADH which the cell can later use to catalyze a variety of biochemical processes. The existence of similar glycolytic machinery in the majority of known organisms speaks to an ancient origin (Romano and Conway, 1996) and helps explain the high connectivity of glycolytic intermediates to other catabolic and anabolic pathways (Court et al., 2015). Glucose is the preferred metabolic substrate in many cells types and is kept in abundant supply by the body, circulating in the serum at concentrations between 4-12 mM(Wright, 2009). An adult body can utilize upward of 300 g of glucose per day, the majority of which (50-75%) is consumed in the brain (Richter, 2010). Consistent availability of glucose is accomplished primarily though diet with the consumption of carbohydrate-containing foods, but can be internally regulated through the generation and mobilization of sugars stored as glycogen in specific tissues, mainly the liver and skeletal muscles(Wasserman, 2009), but also in a variety of other cells like astrocytes(Hertz et al., 2007). Maintaining glucose-rich environments around cells which readily consume it through highly active routines is a physiological strategy whose utility is realized only if glucose can move between the two spaces.

The highly polar nature of carbohydrates effectively prohibits their spontaneous translocation across plasma membranes. Measurements of the unfacilitated translocation of glucose revealed a membrane permeability coefficient of approximately 10^{-10} cm/s (Wood et al., 1968), a value 5 to 6

orders of magnitude lower than that seen for glucose movement across the glucose carrier-rich membrane of the human erythrocyte. For context, this has been estimated to result from a decrease in the activation energy of crossing from ~80 kJ/mol to 16 kJ/mol as a result of carrier activity (Naftalin and Holman, 1977). The diffusion of sugars across membranes is catalyzed by a variety of transmembrane proteins which belong to a broad class of transporters called the major facilitator superfamily (MFS) (Pao et al., 1998), with the nomenclature for the human orthologues referring to them as solute linked carriers (SLCs) (Perland and Fredriksson, 2017). Transporters of the MFS effect membrane permeability for varied substrates, but only through thermodynamically passive means. This includes simple uniporters as well as secondary-active symporters and antiporters (Marger et al., 1993). This contrasts with the mechanisms of the other major superfamily of transporters, the ATP-binding cassette (ABC) transporters, which catalyze their transport cycle through the association and hydrolysis of ATP (Jones and George, 2004).

The SLC2A family of transporters, commonly known as the glucose transporters (GLUTs), comprises 14 known members: GLUTs 1-12, HMIT (GLUT13), and GLUT14 (Jones et al., 2000). Most members appear to function as uniporters, enabling facilitated diffusion through the passive catalysis of sugar translocation between the membrane-partitioned volumes of cells and organelles (Stein, 1986). HMIT is an exception, enacting the exchange or symport of protons and inositol (Uldry et al., 2001).

Structure of the glucose transporters

GLUT-1 comprises of 492 amino acid residues, sharing the greatest amount of sequence homology with GLUT2, GLUT3, GLUT4 and GLUT14. Collectively, these 5 isoforms represent Class 1 within the GLUT protein family. This distinction, which is based on sequence similarity, also identifies fructose transporter GLUT5, GLUT7, GLUT9 and GLUT11 as Class 2, and the remaining isoforms, GLUT6, GLUT8, GLUT10, GLUT12 and the H+/myo-inositol symporter (HMIT or GLUT13) as Class 3. Taken

together, the relative sequence homology between GLUT1 and other GLUT protein family members ranges from 25% with Class 3 members to roughly 80% within its own class (Long and Cheeseman, 2015; Taylor and Holman, 1981).

GLUT1 carries a predicted molecular weight of approximately 55 kDa, and has been shown to exist in humans with two distinct degrees of glycosylation (Yu and Ding, 1998). In its heavily glycosylated form, which is found in high abundance on erythrocytes and in endothelial cells of the vasculature, GLUT1 will migrate to this predicted location of 55kDa on a gel when analyzed using SDS-PAGE. In contrast, cells present in the non-vascularized portion of the brain, specifically the astrocytes and oligodendrocytes, express a more modestly glycosylated form of GLUT1, which migrates to 45kDa on SDS-PAGE (Maher et al., 1994; Yu and Ding, 1998). The lower-than-expected size migration seen is likely due to a combination of a more compact shape from the lack of heat denaturation in membrane protein sample preparation for SDS-PAGE and the tendency for hydrophobic sequences to bind a greater number of detergent molecules and maintain a higher charge:mass ratio, both of which can cause membrane proteins to run slightly faster than their predicted molecular weight markers.

With the 2014 publication of the 3.2Å crystal structure by the Yan lab at the University of Beijing, the structure of human GLUT-1 has been definitively determined and reported (PDB ID: 4PYP) (Deng et al., 2014b). This structure, which contained two stabilizing mutations to facilitate crystallization (N45T, which removed glycosylation heterogeneity, and E329Q, which has been shown to lock GLUT1 in an inward-facing conformation) represents a detergent-purified, monomeric form of GLUT1 (Deng et al., 2014b; Schurmann et al., 1997). In addition to this apo structure, the Stroud lab at UCSF has published three additional WT-hGLUT1 co-structures with inhibitors bound: one with Cytochalasin B (PDB ID: 5EQI), one with glucose transporter-inhibitor 1 (GLUT-i1)(PDB ID: 5EQG), and one with glucose transporter-inhibitor 2 (GLUT-i2)(PDB ID: 5EQH) (Kapoor et al., 2016). The basic

topology of GLUT1, along with other members of the major facilitator superfamily (MFS), is that of a multi-pass integral membrane protein (IMP) consisting of two transmembrane domains (TMDs), both with six α-helical transmembrane segments (TM). Each TM is connected by intra- and extra-cellular hydrophilic loops of various lengths, the longest of which connects the two TMDs at TM6 and TM7, and holds four short intracellular α-helices (Deng et al., 2014b; Joost et al., 2002; Travis et al., 2004). This region, known as the intracellular helical bundle (ICH), appears to be a feature unique to the sugar porter subfamily, as it has been seen in fellow subfamily members XylE and GlcP, however not in other MFS transporters (Deng et al., 2014a; Yan, 2013).

Of the 12 membrane-spanning α-helices that make up the majority of GLUT1, eight are amphipathic and likely form an aqueous translocation pathway that makes glucose transport possible in both directions across a plasma membrane (Mueckler et al., 1985). The four remaining helices, 3, 6, 9 and 12, are strongly hydrophobic, as evidenced by their resistance to α-chymotrypsin digestion (Blodgett et al., 2008). This experimentally-determined topology is supported by the positioning of the transmembrane domains of the published crystal structures (Deng et al., 2014a; Kapoor et al., 2016).

Similar to other members of the GLUT protein family, the N- and C-termini of GLUT1 are intracellular (Augustin and Mayoux, 2014), with a single N-linked glycosylation site at Asn45 on the α-helical extracellular loop between TMs 1 and 2 (Deng et al., 2014a; Gorga and Lienhard, 1981; Jones et al., 2000; Mueckler and Thorens, 2013; Taylor and Holman, 1981; Travis et al., 2004). See figures 1.1 and 1.2 for crystal structure of GLUT1 and secondary structure topology respectively.

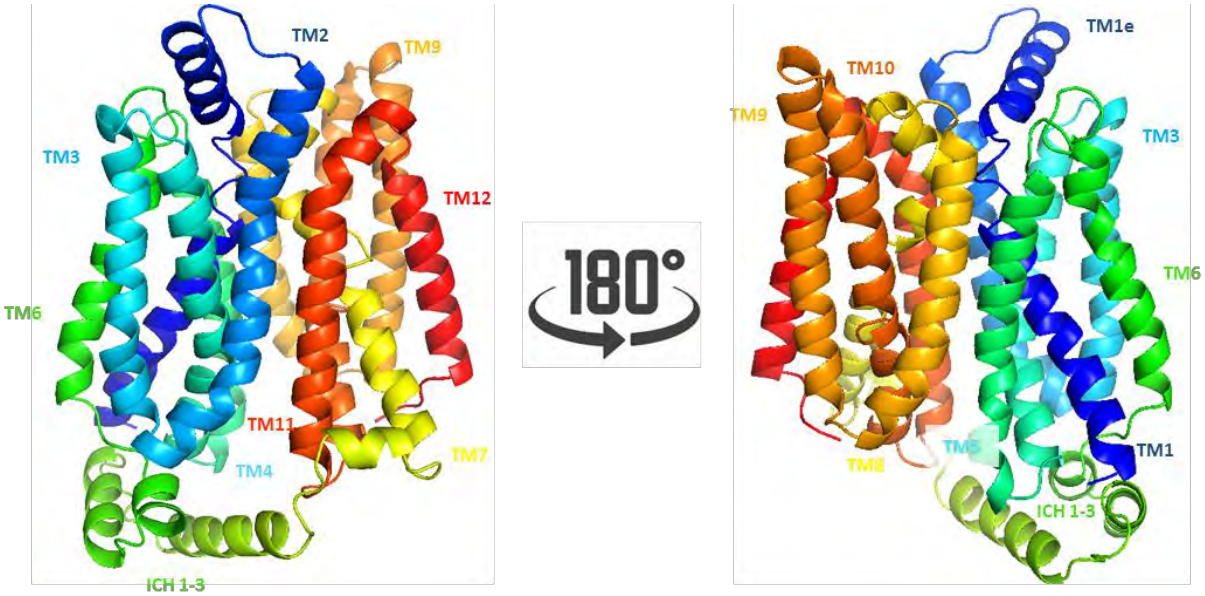

Figure 1.1. Crystal structure of hGLUT1. Published crystal structure of hGLUT1 in two orientations with the n-terminus colored blue and c-terminus colored red. For this figure, PDB ID 4PYP was obtained from RCSB (http://www.rcsb.org) and formatted using PyMOL. (Deng et al., 2014a)

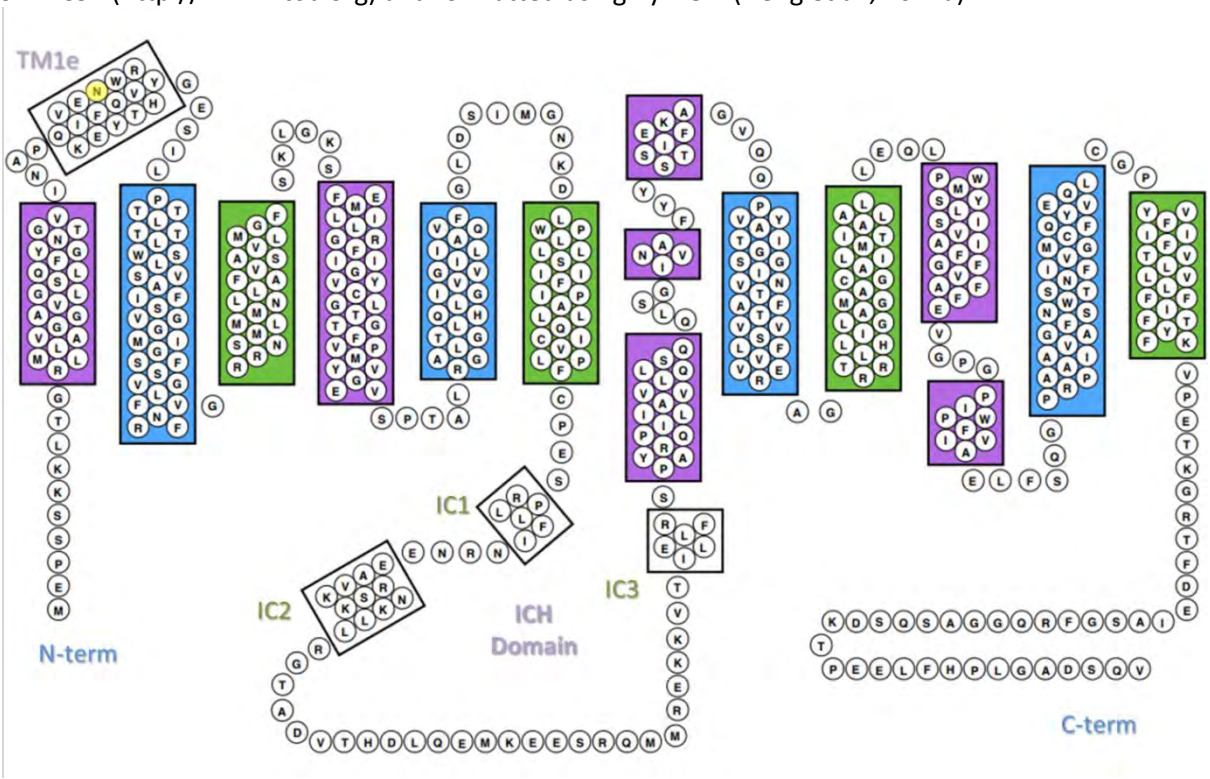

Figure 1.2. Topology map of GLUT1 secondary structure GLUT1 topology map showing transmembrane domains.

Oligomerization

Published crystal structures of detergent-purified GLUT1 show a monomeric protein comprising 12-transmembrane helices in the inward-open conformation. Biochemical studies, on the other hand, demonstrate that endogenous GLUT1 exists not as a monomer, but as non-covalent homodimers and tetramers in both erythrocytes and transfected cell lines (Hebert and Carruthers, 1991). Additionally, unpublished work from this lab has shown that when GLUT1 is purified from either erythrocyte or HEK293 cell membranes using the amphipathic polymer styrene-maleic acid, the resulting nanodiscs are a mixture of GLUT1 dimers and tetramers, as evidenced by NativePAGE immunoblotting and mass spectroscopy (Simon and Simon, unpublished). This oligomerization may be the key to explaining cooperative interactions between exofacial and endofacial glucose binding sites in cells, may provide insight into certain ligand binding behaviors, and may be the driving force behind GLUT1 trans glucose interactions and ATP-modulated transport kinetics.

To that end, the ability to purify, and biochemically and structurally characterize GLUT1 and its ligands is of great value to the field of sugar transport. However, due to the nature of IMPs, which are predominantly embedded in the lipid bilayer, purification of these proteins requires disruption of its stabilizing hydrophobic surroundings, usually with a bilayer-disrupting detergent, effectively disturbing its natural state. If this solubilization from the native lipid bilayer is successful, it is often necessary for lipids to be reintroduced to the suspension and detergent removed through the use of Bio-Beads or some similar method, in order to return the protein back to a more stable environment for functional analysis (Rigaud and Levy, 2003). All of this is accomplished through a lengthy protocol of spins, incubations and reconstitution with many synthetic detergents, often in the presence of reducing agents such as DTT or TCEP (Heard et al., 2000). It is fair to assume, then, that this high level of manipulation of the protein and its intrinsic surroundings during purification may be stripping GLUT1 of key molecular interactions and potentially affecting tertiary folding in the process, particularly in cases where some

commonly-used detergents such as dodecyl maltoside (DDM) or CHAPS are used (Graybill et al., 2006). In fact, much work has been done to understand the impact on GLUT1 oligomerization when the protein is solubilized using various detergents, and in the presence or absence of certain reductants (Graybill et al., 2006; Hebert and Carruthers, 1992; Hermansen et al., 1967). When GLUT1 is purified using octyl glucoside in the presence of reducing agent, for example, and analyzed using freeze-fracture electron microscopy, the resulting particles measure to the approximate size of a GLUT1 dimer (Graybill et al., 2006). When the transporter is purified in a non-reduced setting, though, particle sizes suggest GLUT1 tetramers (Graybill et al., 2006).

Several cross-linking and mutation studies have been carried out (by our lab and by others) that help explain GLUT1's sensitivity to certain detergents and reducing agents. This work has shown that the structural integrity of tetrameric GLUT1 relies on a specific transporter fold that results from a disulfide bond involving Cys347 and Cys421 (Hebert and Carruthers, 1992). More recent work involving homology-scanning mutagenesis and GLUT1-GLUT3 chimeras has shown that TM9 of GLUT1 is critical for GLUT1 dimerization (De Zutter et al., 2013). When TM9 is spliced into GLUT3, it is determined to be 4-fold more active than its inverse counterpart, GLUT1 containing GLUT3 TM9, and can also lead to dimerization of GLUT1 and GLUT3 when spliced in to the otherwise unassociated GLUT3, yet the same is not true for GLUT3 TM9 (De Zutter et al., 2013). Linking this peripheral α-helix with intermolecular interactions, rather than with glucose transport pathway, is quite logical, given what we now know about GLUT1 structure.

ATP regulation of GLUT1

It is well-established that human GLUT1 is an adenine nucleotide binding protein, but not an ATPase, and that the presence or absence of ATP will impact the sugar transport properties of the molecule (Carruthers and Helgerson, 1989). When cytosolic ATP cooperatively binds to GLUT1, the

export site ligand cytochalasin B demonstrates a higher affinity, which leads to sustained substrate occlusion and a reduction in overall net sugar uptake of glucose into the cells (Cloherty et al., 2002; Levine et al., 2002). When human erythrocyte ghosts are resealed with ATP, they take on a traditional concave "diskocyte" shape of red blood cells, however when filled with AMP or no nucleotide is present, the ghost takes on a spiculated morphology, and is known as an "echinocyte" (Anderson and Lovrien, 1981). In kinetic studies discussed in chapter 4, as well as reported by others, differences in glucose transport profiles are measured between these two populations of ghosts. In ATP-containing ghosts, equilibration of sugar by equilibrium exchange occurs in two phases (one slower, one faster relative to each other). However, in ghosts lacking ATP or with AMP, GLUT1 transport complexity is lost, and movement of sugar appears monophasic. This difference in transport rate has been attributed to structural changes in GLUT1 that occur upon nucleotide binding, which likely impact intramolecular interactions within a GLUT1 homodimeric complex, and impedes movement of sugar through the carrier (Cloherty et al., 2002; Levine et al., 2002). In trypsin cleavage experiments involving nucleotide-bound GLUT1, the presence of ATP protects several cytosolic lysine residues in the c-terminus (K477) and along loop 6 (K256 and K257), suggesting there is movement at the c-terminus upon binding, and that this change may be required for glucose transport (Blodgett et al., 2008; Heard et al., 2000).

Mechanistic models for the GLUT1 catalytic cycle

While the topological relationships of the GLUT1 structure are being refined with increasing precision through the recent, excellent crystallography work mentioned above, the sequence of dynamic GLUT1 conformation changes and substrate:GLUT1 interactions, which ultimately results in the transmembrane transition of the substrate, is still quite opaque. In the absence of more complete data related to the structure-specific mechanism of sugar transport by GLUT1, abstracted models of the carrier's behavior are used instead. Kinetic models make broad characterizations of the major

thermodynamic states of the system components and the parameterized transitions that occur between them, allowing the construction of a mathematical framework that can approximate outcomes from various theoretical conditions. By attempting to match the construction of a model and its parameters to experimental observations, investigators can learn a great deal about the practical functionality of a biological mechanism. And, as the distance decreases between the theoretical and structural understandings of the system, such models can provide researchers with increasingly predictive capacity and allow for the rational and targeted modification of molecules of interest. It follows that the difficulty associated with direct measurements of GLUT1 structure as it relates to its function has resulted in a great deal of work done by researchers to develop rational kinetic models whose behaviors can account for those seen in GLUT1 transport experiments. Many models have been used to describe the specific and general behaviors of GLUT1, but most of these fall into one of two categories based on their fundamental assumptions of enzyme mechanism: i) simple carrier, also known as the alternating access carrier, or ii) the fixed site carrier.

Prior to describing these models in detail, it is useful to first establish some common conventions in the nomenclature of their description as well as the fundamental techniques used in the laboratory to establish certain boundary conditions for carrier behavior. Except in complicated kinetic schema, the abstracted reaction space is partitioned into two volumes separated by an impermeable membrane: the inside, usually the cytosol of a cell, is side 1, and the outside is side 2. Substrate populations in one volume or the other are indicated with an appropriate subscript. However, when describing the schema of transport experiments or kinetic simulations, the terms *cis* and *trans* are used to describe compartments relative to the starting location of tracked substrate. The compartment in which the substrate begins is the *cis* side of the membrane and the *trans* side is the other. Additional terminology may be used to orient the direction of flux relative to the interior of a cell. “Exit” experiments track sugar transport rates from cytosol to interstitium while “entry” experiments track

rates of translocation from interstitium to cytosol. There are four important types of transport experiments used to measure the kinetic properties of carrier proteins (Figure 1.4).

1. Zero-*trans* transport experiments measure the rate of substrate translocation from *cis* to *trans* with an initial sugar concentration of 0 in the *trans* compartment. Net transport is measured by the appearance of sugar in the *trans* compartment. Sequential experiments vary initial *trans* sugar concentration from low to high and observe increasing initial rates to allow measurement of V_{max} and K_M parameters exclusively in the direction of initial flux.
2. Equilibrium exchange experiments begin with equal substrate concentration on both sides of the membrane with only one side initially containing traceable sugar. Sequential experiments vary initial sugar concentrations on both sides from low to high, observing increasing initial transport rates to allow measurement of V_{max} and K_M for exchange.
3. Infinite *cis* experiments begin with saturating sugar conditions on the *cis* side (multiple times higher than the K_M for the *cis* side as measured by zero-*trans*) and measures sugar transport rates into the *trans* compartment when it initially contains a specific subsaturating substrate concentration (saturating conditions being relative to the K_M on the *trans* side). Sequential experiments vary the initial *trans* sugar concentration from 0 to saturating and observe the sequential decrease in initial transport rates. This provides a measurement of V_{max} in the *cis* to *trans* direction and the K_M for transport into saturating opposing substrate in the *trans* to *cis* direction.
4. Infinite *trans* experiments begin with subsaturating sugar on the *cis* side and measure transport rates with saturating sugar on the *trans* side. Sequential experiments vary the initial *cis* sugar concentration from low to saturating and observe the increase in initial transport rates up to conditions of equal starting concentrations. This provides a

measurement of V_{max} for exchange specifically in the *cis* to *trans* direction and the K_M for transport into saturating opposing substrate in the *cis* to *trans* direction.

Because of the high degree of interaction between cellular components and glucose in the cytosol, certain technical considerations are needed to ensure the successful execution of the techniques above. The canonical foundation for glucose transport measurements is the use of radiolabeled substrate to trace the movement of molecules from one side of the membrane to the other. The progress of the experimental system is sampled periodically by isolating subsets of the transporting cell population and measuring their radioactive contents. This introduces a complication in interpreting what is actually being measured. The radioactivity of the tracer does not influence its chemical profile in any way that alters its interactions with cellular elements. Symmetrically, the radioactivity of the reporter atom is independent of the fate of its parent molecule. As such, there is no guarantee that a given signal was generated from within a glucose molecule. And, given the rate of cellular glucose utilization, it is not likely. This must be overcome during experimental design with careful *a priori* planning for data collection and interpretation, otherwise the convolution of transporter and metabolic activity can introduce insurmountable ambiguity into the results. There are three design principles which can be altered to address this problem:

1. Experimental temperature can have a dramatic effect on the kinetic rates of both transport and metabolism. The rate at which both of these phenomena proceed at physiological temperature can place early time points beyond the capacity of the sampling device, especially when initial velocities are highly transient, which is the case at non-saturating sugar concentrations (Lowe and Walmsley, 1986).
2. Metabolic consumption rates can vary dramatically between cell types. As such, selecting an appropriate cell type can lessen the effects of substrate sequestration away from the transport mechanism by host metabolism. It is for this reason that a large portion of the foundational

work done to characterize GLUT1 kinetics was undertaken using human erythrocytes. Not only do they have an uncommonly high density of GLUT1 in their membrane, but their metabolic rates are extremely low compared to their transport capacities, which are 50- to 500-fold higher (Jacquez, 1984). This benefit can be extended even farther by creating erythrocyte ghosts whose cytosolic contents are removed, all but eliminating metabolism in these cells (Jung et al., 1971).

3. A great deal of experimental flexibility is granted through the use of glucose homologues. GLUT1 demonstrates the capacity to transport a variety of hexose substrates, two of which have been used extensively because of their level of interaction with the glycolytic enzymes. 2-Deoxy-D-glucose (2DG) is a substrate for hexokinase (Bachelard, 1972) which converts it to 2-deoxy-D-glucose-6-phosphate (2DGP). This product is trapped within the cytosol as 2DGP, is not transported by GLUT1, nor is it a substrate for any downstream enzymes of the cellular metabolism. This can provide measures of total transporter activity over the course of an experiment. The other substrate of note is 3-O-methylglucose (3MG) which is transported by GLUT1, but is not phosphorylated by hexokinase (Jay et al., 1990). This allows researchers to completely dissociate transport and metabolism.

The simple carrier model was first put forward by Widdas as a potential mechanism for thermodynamically passive membrane permeability (Widdas, 1952). Its mathematical framework was later refined (Lieb and Stein, 1971) and it is still commonly used today to describe the mechanistic action of GLUT1 and MFS members in general. In fact, many of the experiments above were designed and refined as kineticists worked to harmonize its construction with the phenomena observed in GLUT1 transport experiments. The defining characteristic of the simple carrier is that the transport protein contains two separate substrate binding domains, one on each of its intra- and extracellular surfaces, but provides solvent access to them on an exclusive basis, occluding one when the other is solvent-

exposed. Transitions in enzyme conformation which reverse this cardinality occur spontaneously in both directions for both *apo* and substrate-bound carrier species, the latter case giving the bound substrate access to alternating solvent volumes and forming the basis of the model's execution of the translocation process. A complete transport cycle, following sugar transport from solvent to cytoplasm, begins with binding of exofacial sugar (S_2) to the outward facing apo carrier (e_2), conformational inversion of the bound carrier ($e.S_2$ becomes $e.S_1$), release of substrate into the cytosol (S_1), and the conformational reinversion, or "relaxation", of the inward (e_1) to outward apo carrier. The simple carrier model also presents an intuitive basis for chemical inhibition of the transporter. The binding of a non-translocatable substrate on either face will prohibit conformational inversion, effectively sequestering the carrier in an inactive state. A King-Altman diagram for the basic concepts of this model is shown in Figure 1.3.

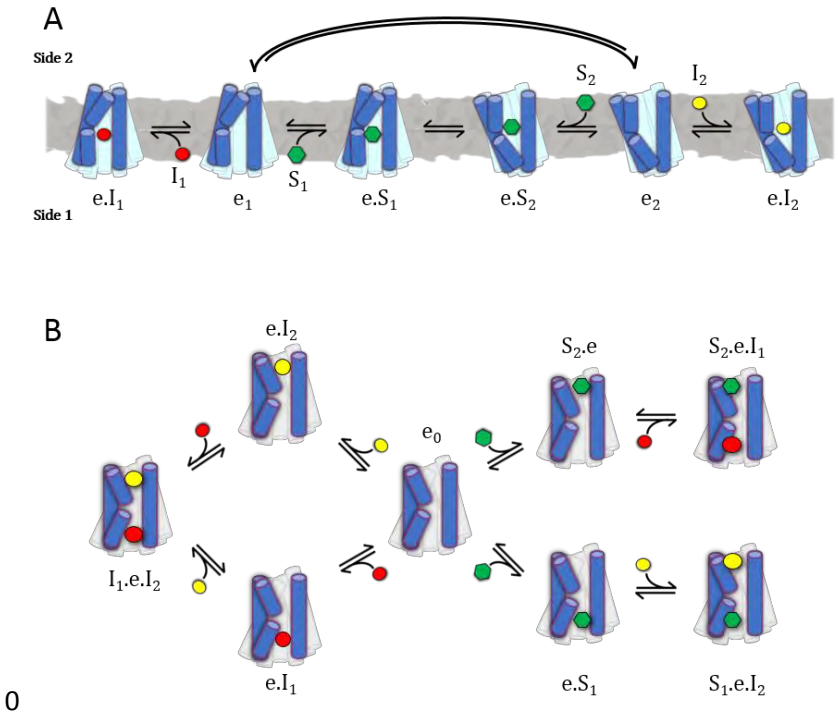

Figure 1.3 King-Altman diagram for simple carrier and fixed-site carrier models. Blue cylinders: GLUT1; Red circles: intracellular inhibitor; Yellow circles: extracellular inhibitor; Green hexagon: glucose. A: King-Altman diagram for the simple carrier kinetic model. In this model, GLUT1 protein has two apo

forms, e_1 and e_2, which face the cytosol and interstitium, respectively, and can transition from one to the other through conformational changes. The exposed surface of GLUT1 can bind substrates and inhibitors in the solvent volume it faces. The protein can also transition between substrate-bound forms ($e.S_1$ and $e.S_2$) to effect transport, but is unable to transition in the inhibitor-bound form ($e.I_1$ and $e.I_2$). B: King-Altman diagram for the fixed-site carrier kinetic model. In this model, GLUT1 has distinct cytosolic and interstitial substrate binding sites. Bound substrate can transition from one site to the other in the absence of any other bound substrate in the destination site. Inhibitors can bind the site exposed to their solvent, but do not transition between the two.

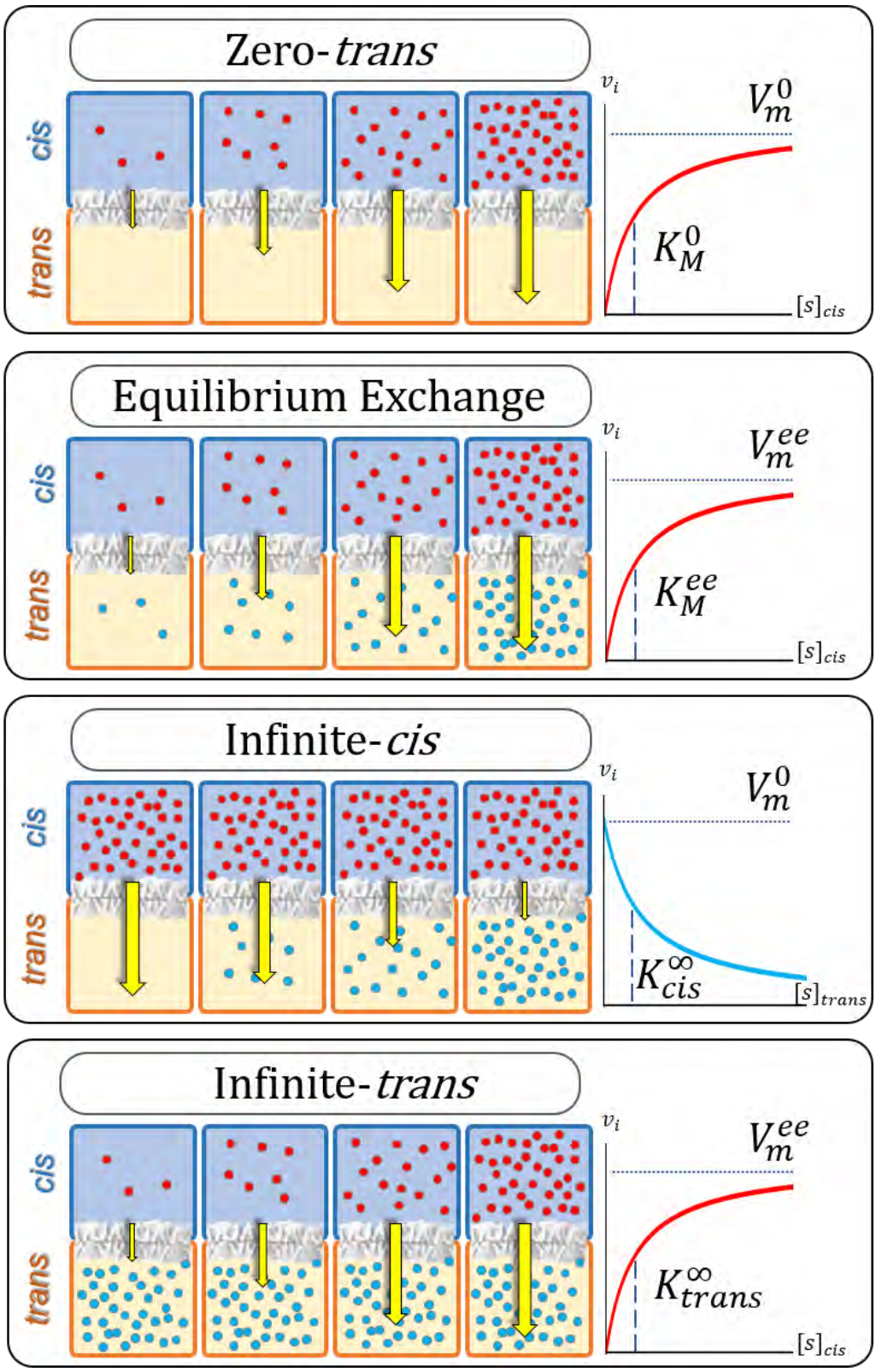

Figure 1.4 Standard transport experiments. Shown are the basic schemes for the four major classes of transport experiment used to evaluate glucose transporter kinetics. Red circles: labeled, traceable substrate; Blue circles: unlabeled substrate; Yellow arrows: relative magnitude of measured sugar flux.

Diagrams for each experimental class show the general pattern of substrate titration. Graphs indicate the general shape of Michaelis-Menten plots constructed from these titrations and the kinetic properties of the transporter they measure.

Chapter 2

CHARACTERIZATION OF GLUCOSE SENSOR AND MUTANTS

Abstract

Canonical measurement of glucose transport utilize radiolabeled hexose substrates whose time courses of accumulation or loss are constructed through series of singular, destructive measurements from individual samples. Previous studies have achieved excellent results through ingenious applications of this technique, though certain technical constraints cannot be overcome. Specifically, the loss of resolution during the early seconds of equilibration results in a significant reduction in the analytic capacity of the method. Additionally, the lack of sample continuity introduces a significant uncertainty to the data set which further confounds analyses. Through a collaboration with the Looger Lab at Janelia Farms, we obtained a glucose-sensitive protein sensor called GlcSnFR which demonstrates an increased fluorescence output proportional to local glucose concentrations. We expressed, purified, and characterized this probe in order to determine its utility as a foundation for new methods to investigate glucose transport kinetics. We found that that its binding and release of glucose has kinetic properties which make it useful for measuring glucose concentrations within the normal physiological range in human tissues (k_{on}: 389.5 ± 12.1 $M^{-1}s^{-1}$, k_{off}: 0.593 ± 0.103 s^{-1}, k_D: 1.52 ± 0.31 mM) with a signal-to-noise ratio between 3:1 and 4:1. We also demonstrate that its sensitivity to environmental variables such as pH and temperature are not prohibitive to its utility in a cellular context. We conclude that GlcSnFR is a suitable to achieve continuous measurement of glucose concentrations in a non-disruptive manner with greatly increased temporal resolution.

Introduction

As an axial substrate in the metabolisms of almost all cells and tissues, glucose and the mechanisms that regulate its availability play foundational roles in homeostasis on all scales of an

organism. Due to its critical importance, disorders in cellular functions related to the utilization of glucose often result in a complete loss of viability. As a result, there are few diseases in which the pathology prohibits the cellular use of glucose. Instead, most disorders related to glucose stem from impairment in the body's ability to regulate glucose distribution. This is seen in both type I and II diabetes, a well-known and active area of research, where there is disruption in the capacity for insulin-induced, increased GLUT4 membrane content and a proportional stimulation of glucose uptake in targeted tissues. As a result, serum glucose levels are poorly regulated which leads to a variety of symptoms, some severe or lethal. Another example is the dysregulation of GLUT1 surface expression and gross overabundance of the protein in the membranes of many varieties of cancer cells to facilitate their highly increased rates of metabolism and anabolism. And while the abnormal regulation of sugar uptake in cancer is not the direct cause of the disease, its widespread use by many forms of the disease are leading researchers to develop therapeutics which restrict or eliminate the tumor's ability to use GLUT1 as an enabler of their increased metabolic demand. In both of the above cases, and in any research related to cellular glucose permeability, the ability to accurately measure the transition of glucose from one side of a membrane to the other is of fundamental importance.

The chemical nature of glucose, its ubiquitous presence in relatively high concentrations throughout the bodies of higher organisms, and its role as a highly utilized metabolic substrate create challenges when measuring its flux between compartments. While molecules such as electrolytes are highly abundant and concentrated, their electrical potential permits highly sensitive monitoring of their transport through the change in membrane potential generated by such movement. This can allow investigators resolution up to a single channel of activity. However, the same methodologies cannot be employed when studying glucose transport due to its lack of a charge. Further, the glucose transporters facilitate passive diffusion of their substrates, so passage through the GLUTs cannot be tracked by the secondary report of cofactor hydrolysis. This is compounded by a continuous presence of millimolar

glucose concentrations, maintained in relative equilibrium, on both sides of the membrane. This equilibrium is achieved through the cell's careful regulation of its glucose consumption rate to match substrate availability and can rapidly respond to changes in this availability. As a result, perturbing the equilibrium will shift both transport and utilization rates and this simultaneous adjustment in two different glucose pathways can confound results if not taken into account.

Methods currently employed to measure glucose transport utilize radioactive substrate which serves as a reporter for trans-membrane flux. By controlling the starting location of the tracer and direction of the concentration gradient, researchers can observe the progress of glucose translocation by sampling the amount of tracer on specific sides of the membrane at different times. The greatest limitation inherent in this technique is the need to destroy the sample in order to measure the signal. Consequently, experiments utilizing this method contain many duplicate samples that will be harvested individually at the predetermined times to generate a more complete picture of the equilibration process. Further, it is necessary to rapidly halt transporter activity when collecting samples to ensure an accurate relationship between time of collection and signal. This becomes hyperbolically difficult as the time of collection gets closer to the start time of the experiment and introduces increasing issues with precision as the sampling is usually done by hand. Despite this, researchers have found various ways to ameliorate these difficulties through manipulation of experimental conditions or the use of glucose substrates with helpful properties. The activity of the GLUTs is greatly reduced at lower temperatures, providing conditions in which the early activity can be observed more readily. The use of the glucose homologue 2-deoxy-D-glucose (2DG) is a comparable substrate for the transporters and hexokinase. However, once phosphorylated, it is not acted upon by any other cellular enzymes. This allows for its accumulation within the cell without being a substrate for GLUT-mediated exit. Another homologue, 3-O-methylglucose (3MG), can be transported by the GLUTs, but is not a substrate for hexokinase. This allows the design of experiments which can discount the cell's metabolic response to shifts in glucose

availability. However, all of these methods introduce some degree of distance between the measured results and the physiological paradigm being studied. A large step toward shortening this distance could be taken with the development of a technology that allowed continuous monitoring of transporter activity without significant loss of the sample being studied.

The use of fluorescent molecules as reporters of biochemical activity has been applied to many areas of study. Tryptophan fluorescence is sensitive to its chemical environment, a fact which has been used as the basis of countless biochemical assays designed to study the structural state of proteins and the processes which affect them. Many other small molecules, often aromatics, with inherent fluorescence such as NADH, are used to study the biological processes in which they are involved without disrupting the system. The development of genetically encodable sensors, like green fluorescent protein (GFP), has provided the basis for an ever-growing toolkit used to investigate the inner workings of cell mechanism, select rare events from large populations, and follow genetic processes. Modifications to these proteins which make their fluorescent efficiency proportional to the local concentration of a secondary molecule have given rise to sensors with dynamic reporting of changing cellular contexts. The use of calcium (GCaMP) and neurotransmitter (gluSnFR) sensors in the field of neurobiology allows non-invasive real-time imaging of cerebral activity and has made an incredible impact on our ability to study and understand the often opaque mechanisms of cognitive biology.

The Looger lab at the Janelia Research Campus has engineered a green fluorescent protein (GFP) whose signal is proportional to glucose concentration, herein referred to as GlcSnFR. This was achieved through the fusion of a circularly permuted GFP (cpGFP) into a glucose binding protein (GBP) from *T. thermophilus* (Figure 2.1, A). Binding of glucose in the GBP domain induces a positive shift in the cpGFP domain's fluorescent efficiency, increasing its rate of fluorescence conversion of blue into green light. As such, this protein enables the design of experiments in which dynamics in glucose concentrations can

be observed without need for membrane disruption allowing for continuous measurement from the same cell or cell population (Figure 2.1B). While this opens new avenues of research, it does introduce new complications as well. The use of a reporter molecule to measure the concentration of another adds another kinetic interaction whose behavior must be known in order to convert the observed signal into a concentration of the target substrate. Additionally, many factors can affect fluorescent output from a reporter molecule, including pervasive qualities of the solution such as temperature and pH. With these considerations, any investigation using this reporter will require a thorough *a priori* characterization of its properties.

Here we describe the *in vitro* expression, purification, and analysis of GlcSnFR. Additionally, we have generated several affinity mutants with altered specificities for glucose, 2DG, and 3MG.

A

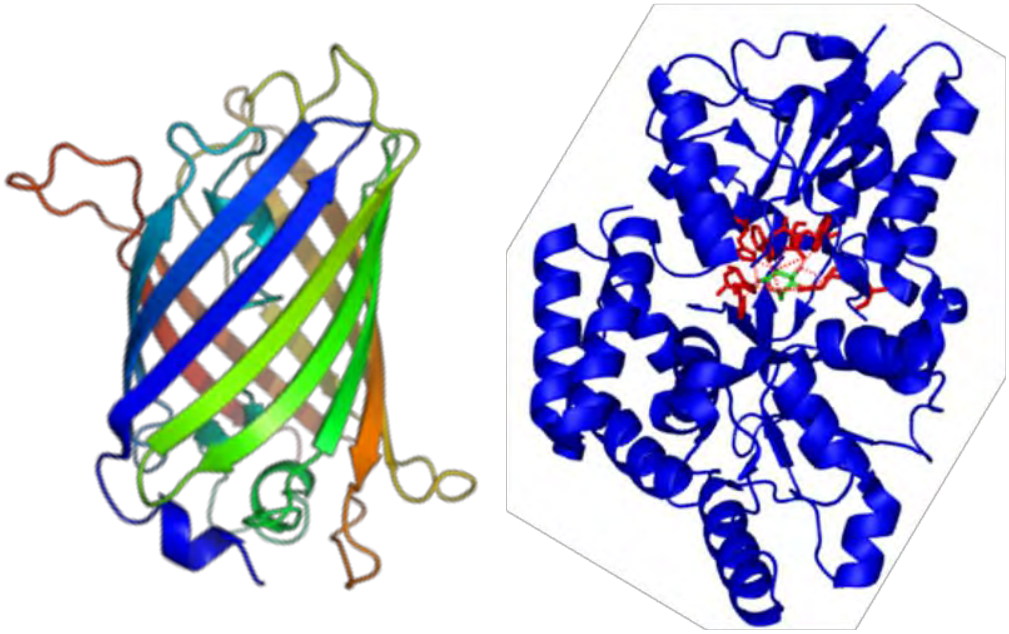

B

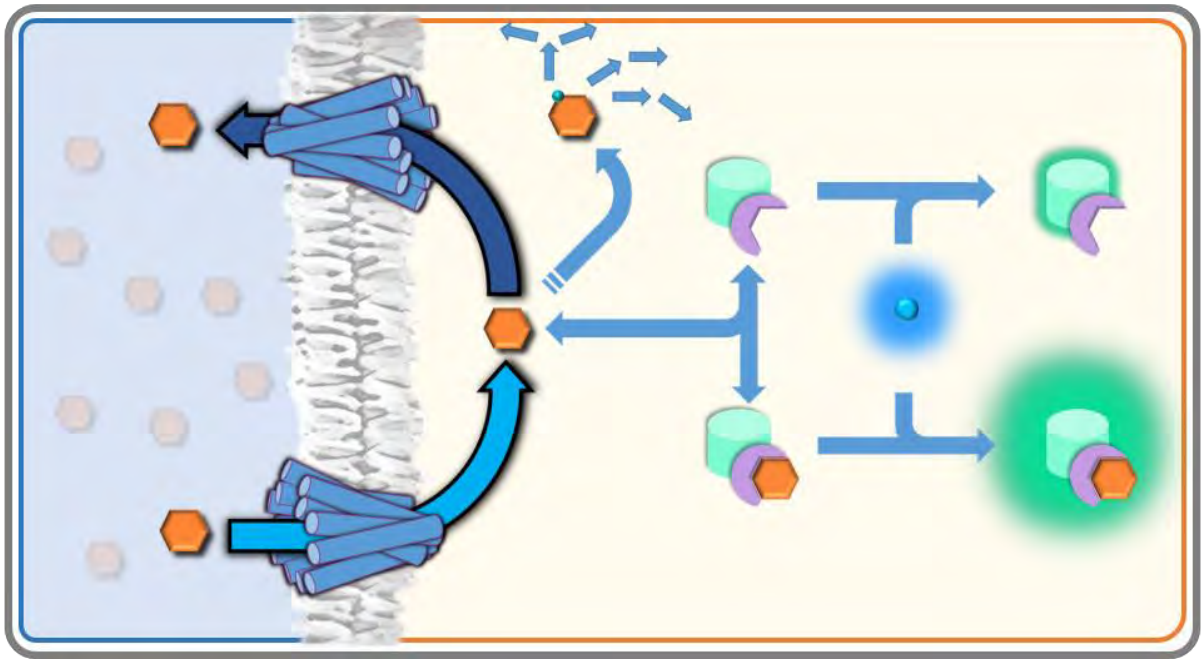

Figure 2.1 GlcSnFR is a genetically encoded glucose sensor. **A:** Crystal structures [PDB: 1GFL (green fluorescent protein), 2B3B (glucose binding protein)] from individual proteins used in the engineering of GlcSnFR and linear schematic of protein domains in GlcSnFR. The circularly-permuted form of GFP was inserted into the GBP sequence as indicated in the linear topology. **B:** Proposed use of GlcSnFR to measure carrier-mediated kinetics of glucose transport. Blue cylinders: glucose transporter protein; Orange hexagons: sugar substrate; Green cylinder with purple crescent: GlcSnFR protein; Green circle: phosphorylation; Blue circle/glow: 488 nm light; Green glow: fluorescent emission ~510 nm. The binding of glucose by the GlcSnFR probe increases its fluorescent efficiency. We intend to express or otherwise entrap the probe within cells and continuously monitor changes in output to evaluate changing sugar concentrations as a function of emitted light.

Materials and Methods

Materials

Human whole blood (#100-17) from purchased from Biological Specialty Corporation. Any other chemicals not mentioned above were purchased from Sigma Chemicals.

Solutions

Kaline buffer contains 150 mM KCl, 5 mM HEPES, 0.5 mM EDTA, and the pH is adjusted to 7.4 at experimental temperature. Erythrocyte lysis buffer contains 10 mM Tris·HCl, 4 mM EDTA, and the pH is adjusted to 7.4 at 4 °C.

Cloning of GlcSnFR into expression vectors

Glycerol stocks of GlcSnFR in two different expression vectors were obtained from the Looger Lab, pCYTO (derived from pcDNA3.1) and the pDisplay vector (Invitrogen).

Expression in *E.* coli was carried out by cloning the GlcSnFR open reading frame (ORF) into the pRSET vector (Invitrogen). This was facilitated by first removing a HindIII restriction site via the introduction of a silent mutation in the GlcSnFR sequence for serine 612, changing the codon AGC to AGT. Then the ORF was PCR amplified using a forward primer which introduced a BamHI site to the 5' end of the product and a reverse primer which included a HindIII site from the template sequence 3' end. The PCR product was run out on a 1% (m/v) agarose gel and purified using a Qiagen gel purification kit followed by a PCR purification kit then ligated into the compatibly linearized pRSET vector.

Affinity mutants were made by site-directed mutagenesis PCR using QuikChange Site-Directed mutagenesis kits (Agilent). All cloning, unless otherwise specified, was completed using reagents obtained from New England Biolabs.

Expression and purification of GlcSnFR and affinity mutants

For expression of the sensor, plasmids containing the GlcSnFR –pRSET variants were transformed into E. Coli BL21-Gold (DE3) cells. Starter cultures of 100mL were incubated overnight at

37°C, 225 RPM with supplemental ampicillin at 100µg/mL. The following morning, 10mLs of the starter culture was added to each of six 1L flasks of Luria broth (unsupplemented) and incubated at 37°C, 225 RPM for four hours, after which time, expression was induced by adding Isopropyl β-D-1-thiogalactopyranoside (IPTG) at 1.5 mM and the temperature was reduced to 30°C. Cultures were protected from light and incubated with rotation at 30°C overnight. After approximately 16 hours, cells were pelleted (6,000g for 15min) and pellets were resuspended in lysis buffer (50mM Tris pH 7.4, 100mM NaCl, 0.2mM EDTA, [X] DNase I). Cell lysis was accomplished using two rounds of passage through a pneumatic cell disruptor. The lysate was then centrifuged at 20,000g for 10 minutes to remove large debris, and the remaining supernatant was incubated in a rotating shaker with Ni^{2+}-charged agarose beads according to the recommended protocol (His·Bind Resin kit, Novagen). Agarose beads were loaded into a drip column, and protein was eluted from the resin using 1M imidazole. Eluted protein was then dialyzed against 12L kaline (3x4L) to remove elution buffer and residual imidazole, and then concentrated using Amicon Ultra-15 spin filters with a 50kD molecular weight cut-off (EMD-Millipore).

96-well plate fluorescence detection assay

A 96-well fluorescence detection assay was performed to evaluate fluorescence output of the sensor upon exposure to increasing amounts of glucose. Glucose was titrated in kaline buffer (pH 7.4 at experimental temperature, unless otherwise indicated) to final concentrations ranging from 1µM to 100mM in clear, flat-bottom 96-well plates. A fixed volume of GlcSnFR was added to each well, and the plate was read using a Victor X5 Fluorescent plate reader (PerkinElmer) at excitation/emission wavelengths of 488/515 using a long-pass filter. Data were analyzed using GraphPad Prism.

Stopped-flow measurement of k_{on} and k_{off}

The time course of ligand binding induced fluorescence increase of GlcSnFR protein was monitored using a Hi-Tech Scientific SF-61DX2 stopped-flow system. All buffers described herein were

made using standard kaline as the base. A pneumatic drive system mixed equal volumes of GlcSnFR (constant concentration across runs) and glucose (varied concentrations) and forced the solution through the light path of the flow cell. Flow was stopped with a dead time of 1 ms and fluorescence was monitored for up to 60 seconds. Excitation was at 488 nm and readings were collected at 508 nm with monochrometer slit widths of 3 nm.

Assuming GlcSnFR and glucose interact via simple binding kinetics and that glucose is in excess at each concentration, time courses of binding-induced fluorescence should follow pseudo-first order kinetics:

$$F_1[t] = b + (A - b)(1 - Exp[-k'\,t]) \qquad \textbf{EQ 2.1}$$

where

$$k' = k_{on}[Glc] + k_{off} \qquad \textbf{EQ 2.2}$$

Individual data sets were fit by nonlinear regression to a single exponential binding curve (EQ 2.1), two-phase exponential binding curve (EQ 2.3), or a convolution of a single exponential with a gaussian with domain shifted to $t \in [0, \infty]$ (see below, EQ 2.5). Linear regression was performed on plots of k' vs. $[Glc]$ to estimate the parameters k_{on} and k_{off}.

$$F_2[t] = b + (A - b)(p\left(1 - Exp\left[-k_{fast}t\right]\right) + (1 - p)(1 - Exp[k_{slow}t])) \qquad \textbf{EQ 2.3}$$

$$G[t] = \frac{2}{\sqrt{2\pi\sigma^2}} e^{-\frac{t^2}{2\sigma^2}} \qquad \textbf{EQ 2.4}$$

$$\int_0^\infty F_1[\tau]\, G[t - \tau]\, d\tau$$

$$= (A + b)Erf\left[\frac{t}{\sqrt{2}\sigma}\right] + Ae^{\frac{k}{2}(k\,\sigma^2 - 2t)}(Erf\left[\frac{k\,\sigma^2 - t}{\sqrt{2}\sigma}\right] - Erf[\frac{k\,\sigma}{\sqrt{2}}]) \qquad \textbf{EQ 2.5}$$

Nonlinear regression was carried out using GraphPad Prism (single and double exponentials), or with Mathematica software (exponential/gaussian convolution).

Results and Discussion

Sensitivity of GlcSnFR to glucose and glucose homologues

To better prepare to use GlcSnFR in various experimental settings, we first endeavored to measure the sensitivity of its fluorescence to specific chemical and environmental factors. We expressed a 6·His-tagged fusion of GlcSnFR in *E. coli* and purified the protein using his-tag ion chromatography followed by dialysis against kaline buffer. We began by comparing the excitation and emission profiles to those previously measured for GFP. Using a fluorimeter, the resulting protein was analyzed for fluorescent output of 510 nm light following excitation by a range of wavelengths. Two peaks were observed at excitation wavelengths of 488 and 492 nm (Figure 2.2A). We then conducted an emission scan using an excitation wavelength of 488 nm and found the peak to be at 509 nm (data not shown). These values are in good agreement with the published results for eGFP. We evaluated the equilibrium kinetics of glucose binding to GlcSnFR by titrating the glucose concentration with a fixed amount of sensor and then measuring fluorescent output in a plate reader. This was done with two independent protein preps to evaluate the consistency of the sensor's behavior. We found that at 4 °C in kaline, the sensor demonstrated, in the two separate preparations, k_D values of 800 and 771 μM for glucose binding with maximum ratios of output to background of 2.750 and 2.864-fold, respectively (Figure 2.2B). We repeated this experiment at 20 °C and used glucose, 2DG, and 3MG as substrates (Figure 2.2C). The increase in temperature caused the k_D for glucose binding to increase to 1.3 mM and the maximum signal ratio to increase to 3.3-fold over background. The k_D and maximum output for 2DG were measured to be 5.6 mM and 3.82-fold, respectively. GlcSnFR binding of 3MG was too weak to accurately measure either parameter. We also found a complete lack of response by GlcSnFR when using either trehalose or glucose-6-phosphate as substrates (data not shown).

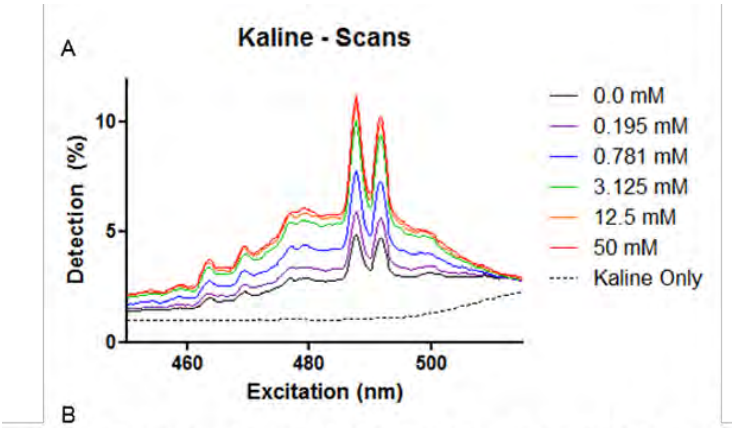
A
Kaline - Scans
Detection (%)
10
5
0
460
480
500
Excitation (nm)
0.0 mM
0.195 mM
0.781 mM
3.125 mM
12.5 mM
50 mM
Kaline Only

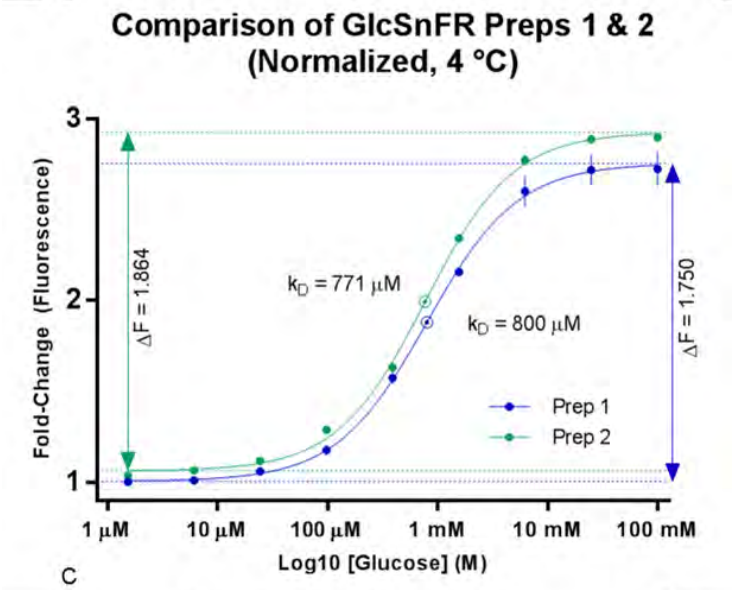
B
Comparison of GlcSnFR Preps 1 & 2
(Normalized, 4 °C)
Fold-Change (Fluorescence)
3
2
1
ΔF = 1.864
kD = 771 μM
kD = 800 μM
ΔF = 1.750
Prep 1
Prep 2
1 μM
10 μM
100 μM
1 mM
10 mM
100 mM
Log10 [Glucose] (M)

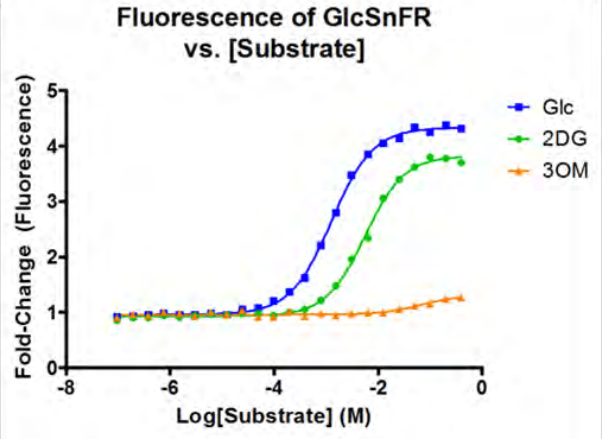
C
Fluorescence of GlcSnFR
vs. [Substrate]
Fold-Change (Fluorescence)
5
4
3
2
1
0
-8
-6
-4
-2
0
Log[Substrate] (M)
Glc
2DG
3OM

Figure 2.2 Equilibrium glucose binding and response by GlcSnFR. A: Excitation scan of GlcSnFR in fluorimeter with glucose titration. Abscissa: excitation wavelength (nm); Ordinate: Voltage of photomultiplier tube (% maximum) after monochromator filtering at 510 nm (3 nm slit width). His-purified GlcSnFR protein was scanned with a range of excitation wavelengths to determine which is optimal for fluorescent output. Scanning was conducted in incremental glucose concentrations to demonstrate probe sensitivity, Local maxima detected at 488 and 492 nm. **B:** Equilibrium binding kinetics and response in two different GlcSnFR preps. Abscissa: Glucose concentration (log_{10}[M]); Ordinate: Ratio of fluorescence at given concentration to that at 0 glucose (fold change). Purified preparations of GlcSnFR probe were incubated in geometric dilutions (1/4) of glucose from 100 mM to ~1 μM at 4 °C for 30 minutes and then analyzed by plate reader for emission at 510 nm following excitation at 488 nm. Results were normalized to 0 glucose reading and fit with a four-parameter sigmoidal curve. Best fit parameters estimate k_Ds of 800 and 771 μM with maximum ratios of output to background of 2.75 and 2.86-fold (blue and cyan data sets, respectively). **C:** GlcSnFR equilibrium binding to glucose and the glucose homologues 2-deoxyglucose (2DG) and 3-O-methylglucose (3MG). Abscissa: Substrate concentration (log_{10}[M]); Ordinate: Ratio of fluorescence at given concentration to that at 0 substrate (fold change). This experiment was conducted as in **B**, but at 20 °C and with (1/2) dilutions of each of the three substrates. Best fit parameters estimate the k_D for glucose binding to increase to 1.3 mM and the maximum signal ratio to increase to 3.3-fold over background. The k_D and maximum output for 2DG were measured to be 5.6 mM and 3.82-fold, respectively. GlcSnFR binding of 3MG was too weak to accurately measure either parameter.

Sensitivity of GlcSnFR to pH, calcium ion, and crowding

Because of its potential use in a variety of biological settings, we evaluated changes to GlcSnFR's glucose response profile to two common environmental variables, pH and free calcium ion. Kaline buffer was titrated to pH values above and below the normal physiological range in the presence and absence of 1 mM calcium ion. Due to limiting protein quantities, we could not titrate the calcium concentration and instead decided to begin testing with a high concentration to evaluate whether the probe was sensitive to the cation in calcium-dependent output would lead to more precise testing of the phenomenon.

The variable pH buffers (no calcium) were used to create a series of glucose titrations into which we added purified GlcSnFR protein. Samples were allowed to equilibrate at ice temperature for ten minutes before measuring fluorescence in a plate reader. The results demonstrated a clear sensitivity of the probe to pH values with acidity and alkalinity having negative and positive effects, respectively, on the sensor's fluorescent efficiency (Figure 2.3A). From the first experiment (panel A), it is clear without any help from data modeling that the magnitude of maximal fluorescent increase is directly proportional to the pH value. Unfortunately, these data were not of high enough quality to allow meaningful comparisons between the observed k_Ds under these conditions. When this experiment was repeated with the addition of calcium to half of the experimental conditions, we observe the same trend regarding the effect of pH on fluorescent capacity, but are also able to get a clearer picture of the affinity constants (Figure 2.3B). The k_Ds reported by the nonlinear regression for calcium-free samples indicate a slight apparent increase in affinity in acidic buffer compared to the more alkaline conditions. This is not seen in calcium-containing samples, however, with the k_D showing less deviation with pH (Table 2.1). The most significant result from both experiments is the large shift in fluorescent output as a result of pH changes within one log scale of the physiological norm.

We considered the possibility that expression of GlcSnFR in a cellular context, in which it is in a much higher concentration of local proteins and structures, might also result in altered expression patterns. We concentrated the purified sensor to 2x and 4x concentrations using centrifugal protein concentrators. These samples were individually titrated against a glucose and fluorescence measured in a plate reader. There was no significant difference between the three conditions (data not shown).

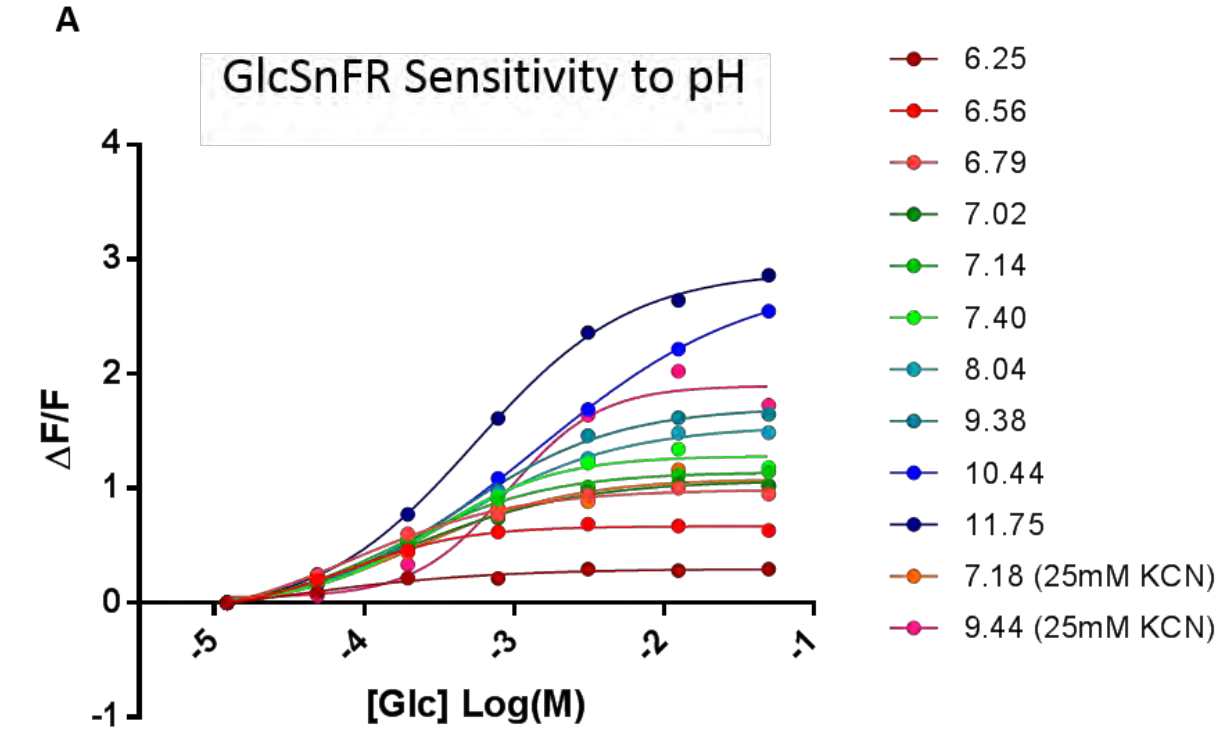
A
GlcSnFR Sensitivity to pH
ΔF/F
[Glc] Log(M)
6.25
6.56
6.79
7.02
7.14
7.40
8.04
9.38
10.44
11.75
7.18 (25mM KCN)
9.44 (25mM KCN)

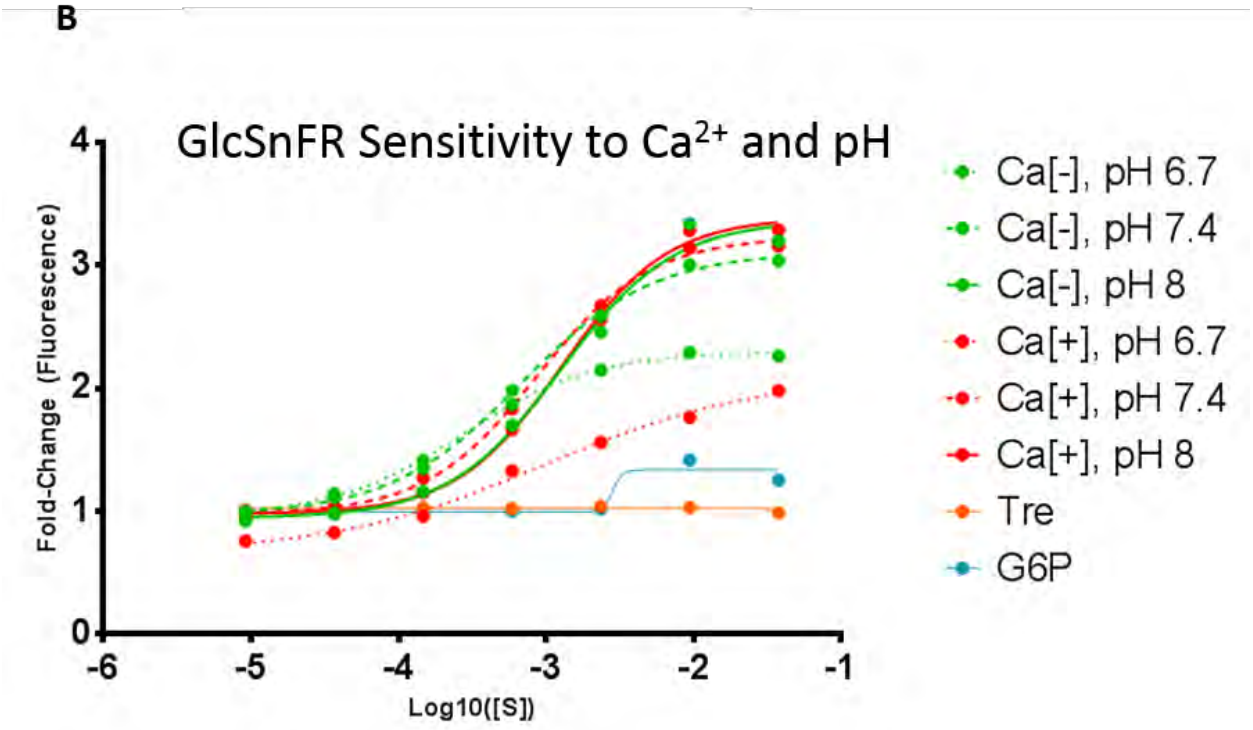
B
GlcSnFR Sensitivity to Ca2+ and pH
Fold-Change (Fluorescence)
Log10([S])
Ca[-], pH 6.7
Ca[-], pH 7.4
Ca[-], pH 8
Ca[+], pH 6.7
Ca[+], pH 7.4
Ca[+], pH 8
Tre
G6P

Figure 2.3 Sensitivity of GlcSnFR to pH and Ca2+ ion. **A:** Equilibrium fluorescence of GlcSnFR with titrated glucose and pH. Abscissa: Concentration of glucose ($\log_{10}$[M]); Ordinate: Fractional increase of response at given concentration versus 0 glucose ($\Delta F/F$). GlcSnFR demonstrates two clear trends with the pH of its solvent: maximum fluorescence increase goes down with acidity and up with alkalinity (relative to pH 7.4), and affinity (k_D^{-1}) goes up with acidity and down with alkalinity (relative to pH 7.4). **B:** GlcSnFR calcium sensitivity. Abscissa: Concentration of glucose ($\log_{10}$[M]); Ordinate: Fold increase of response at given concentration versus 0 glucose. The sensitivity of the GlcSnFR fluorescent response to glucose binding to Ca^{2+} ion was measured in acidic (pH 6.7, dotted lines), normal (pH 7.4, dashed lines), and alkaline (pH 8.0, solid lines) kaline buffers at 4 °C. Normal and alkaline solutions showed little effect from Ca^{2+}, but acidic buffers indicated a marked increase in sensitivity to pH when calcium is present.

Glucose homologue affinity mutants

Our previous results demonstrated that 3MG is a poor substrate for GlcSnFR. However, the potential utility of being able to use 3MG in experiments in which the sensor will be in a cellular context inspired us to attempt the creation of GlcSnFR affinity mutants. With the availability of a crystal structure for the glucose binding protein (GBP) used in the construction of the GlcSnFR probe, we attempted mutant design from a rational design standpoint.

The GBP structure we analyzed contained a glucose molecule in the substrate binding pocket. We used built-in PyMOL functions to evaluate potential contacts between the glucose and nearby GBP residues (Figure 2.4A). We hypothesized that the methyl group on carbon 3 in 3MG (C3 hydroxyl on glucose is highlighted with red in figure 2.4A) could be sterically incompatible with tryptophan 9. We created three GlcSnFR mutants at that point, W9A, W9N, and W9Q. These were expressed and purified as described above. Glucose titration in the fluorescent plate reader assay revealed that all three mutants demonstrated significantly worse affinities and fluorescent shifts with all three substrates (data not shown).

In the wildtype GBP, residue 66 is a histidine, but was changed to alanine during the engineering of GlcSnFR. This was done to reduce the hexose affinity of the GBP subunit and bring the k_D closer to the physiological range of glucose in humans. We considered that our first set of GlcSnFR mutations, compounded with the pre-existing H66A, was too disruptive to the binding pocket of the GBP subunit. We proceeded by reverting the mutation at residue 66, creating GlcSnFR variants A66H, A66H:W9A, A66H:W9N, and A66H:W9Q. Following expression and purification, we analyzed their hexose affinities by plate reader assay. We found that A66H:W9A was not sensitive to any of the three substrates (data not shown), but the remaining three each had an altered affinity profile compared to the 'wildtype' GlcSnFR (Figure 2.4B). We were able to generate mutants capable of binding 3MG with affinities across four orders of magnitude, but none which did so with a greater affinity than that of glucose. A summary

of the affinity properties observed in these mutants and the original GlcSnFR construct are shown in figure 2.4.

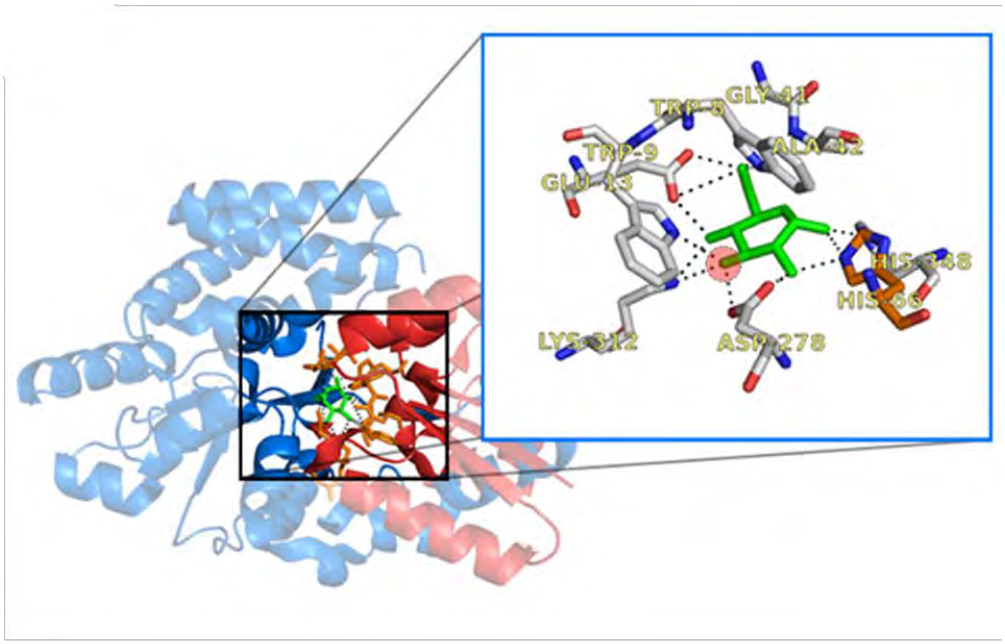
TRP-8
GLY-41
TRP-9
ALA-42
GLU-43
HIS-148
HIS-66
LYS-212
ASP-278

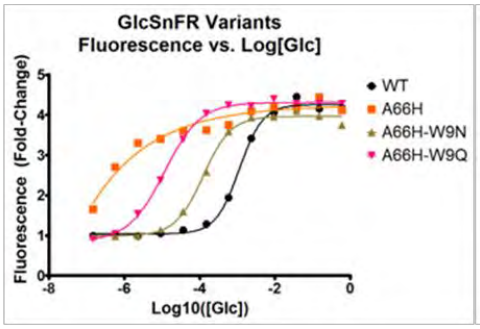
GlcSnFR Variants
Fluorescence vs. Log[Glc]
Fluorescence (Fold-Change)
Log10([Glc])
WT
A66H
A66H-W9N
A66H-W9Q

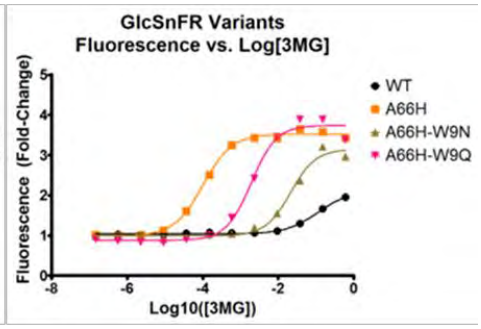
GlcSnFR Variants
Fluorescence vs. Log[3MG]
Fluorescence (Fold-Change)
Log10([3MG])
WT
A66H
A66H-W9N
A66H-W9Q

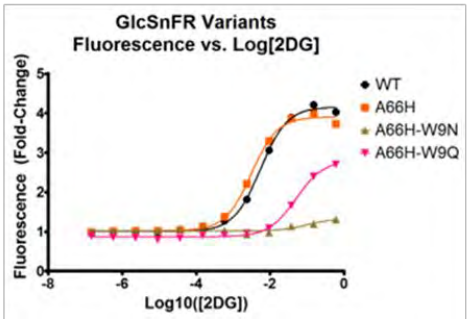
GlcSnFR Variants
Fluorescence vs. Log[2DG]
Fluorescence (Fold-Change)
Log10([2DG])
WT
A66H
A66H-W9N
A66H-W9Q

Figure 2.4 Rational design of GlcSnFR affinity mutants. We endeavored to create GlcSnFR affinity mutants which were capable of 3MG binding with higher affinity than glucose. **A:** Crystal structure of GBP with bound glucose (PDB: 2B3B) with detail of glucose:GBP interactions. The location of the methyl group in 3MG is highlighted in red. We used the interactions shown in this crystal structure to inform our selection of residues to mutate and the choice of substituted residue. **B:** Equilibrium binding data from mutants A66H, A66H|W9N, and A66H|W9Q. Abscissa: Substrate concentration (log_{10}[M]); Ordinate: Ratio of fluorescence at given concentration to that at 0 substrate (fold change). The data were fit to a four-parameter sigmoidal using nonlinear regression in GraphPad Prism. The kDs and maximum fold increases for: [WT] Glucose – 1.13 mM and 3.22, 2DG – 5.45 mM and 3.16, 3MG – 113 mM and 1.08; [A66H] Glucose – Affinity too high for either measure, 2DG – 3.09 mM and 2.88, 3MG – 102 μM and 2.53; [A66H|W9N] Glucose – 123 μM and 2.98, 2DG – 103.5 mM and 0.317, 3MG – 21.1 mM and 2.16; [A66H|W9Q] Glucose – 11.5 μM and 3.46, 2DG – 50.5 mM and 1.94, 3MG – 1.9 mM and 2.86.

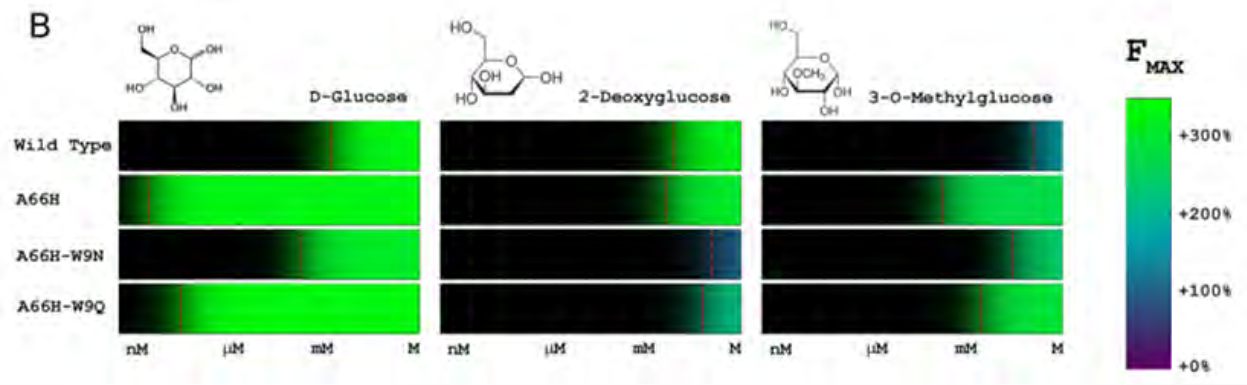

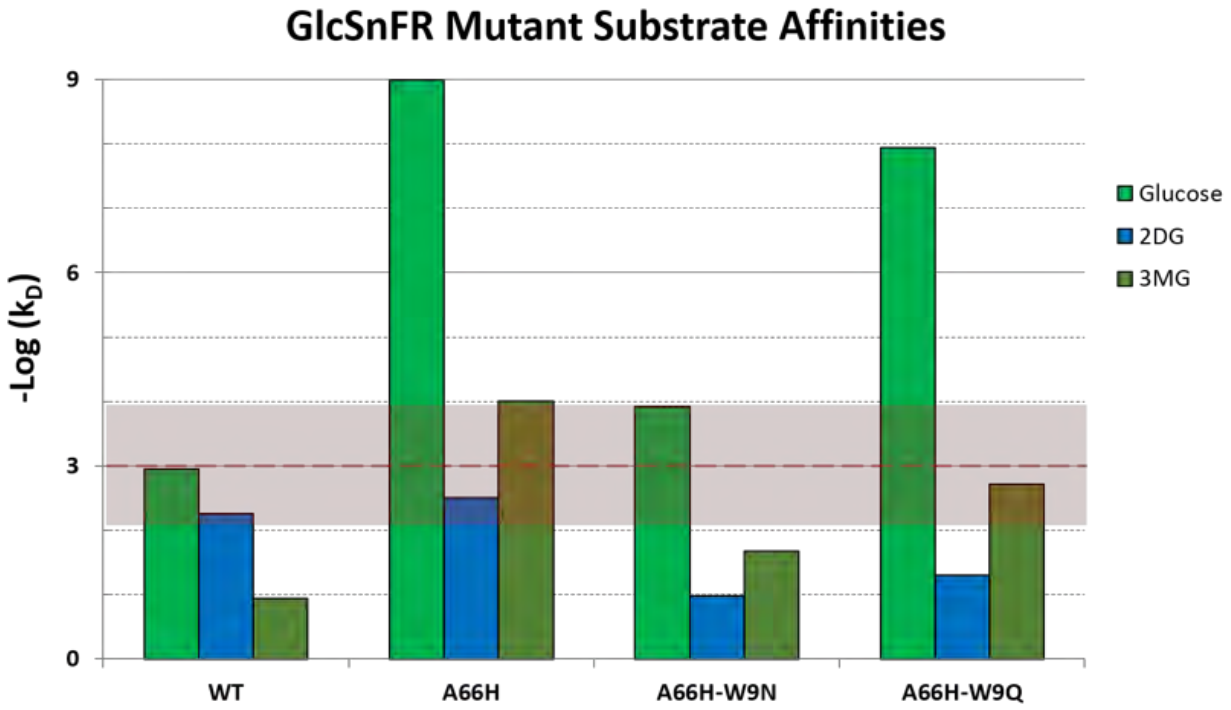

Figure 2.5 Characterization of GlcSnFR affinity mutants. Two visualizations of the data from Figure 2.4. **A:** Colorimetric representations of equilibrium binding data. Scale on right indicates color representation of fold increase. **B:** Bar chart summarizing binding k_Ds. Note the log scale on the ordinate. The red band represents the approximate normal physiological range for glucose concentrations (0.1 – 10 mM).

Measuring the GlcSnFR k_{on} and k_{off} rate constants

In previous sections, we observed that equilibrium binding of GlcSnFR with glucose produces changes in fluorescence with linear response in the area of physiological glucose concentrations. However, using the GlcSnFR probe, or any of its derivative versions, to measure dynamic [glucose] in the

context of a living cell will depend on the individual rate constants for binding and dissociation. These values were measured by using a stopped-flow system to observe time courses of GlcSnFR fluorescence shifts resulting from glucose binding. Purified GlcSnFR protein was mixed with varied concentrations of glucose to generate a series of response curves which were used to perform global fit analysis. This was repeated with multiple batches of purified protein and three separate regression models were applied. When using single phase exponentials to fit the individual data traces (Figure 2.6A), linear regression of k_{app} estimated a k_{on} of 349 $M^{-1}s^{-1}$, a k_{off} of 0.299 s^{-1}, and a k_D of 859 μM. There was no precedent against which to compare the first two parameters, but the k_D was in agreement with that measured by equilibrium at 4 °C while these experiments were conducted at 20 °C. Converting the time axis to log(time) revealed a hysteresis in the sub-second domain. Fitting the data with a two-phase exponential fit the data very well (Figure 2.6B), but the parameters calculated from the linear regression of k_{app} were not easily interpreted in the context of equilibrium data. We then hypothesized that the early behavior of the fluorescent record could be the result of mixing in the tubing prior to the sample cell. We tested this by convolving the positive domains of exponential and gaussian curves. This was accomplished using Mathematica and simplification resulted in equation 2.5. Fitting this while holding all parameters positive resulted in a good fit to the data and parameters that were in good agreement with expectation as well as previous results (Figure 2.6C).

Conclusions

The GlcSnFR probe demonstrates fluorescence with emission proportional to local glucose concentrations. By equilibrium kinetics, the kD of its binding to glucose is around 1.5 mM at 20 °C and 800 μM at 4 °C. We measured the kon and koff rate constants and analyzed the results in three different ways. While each of the three models generated very good fits to the data, it is our conclusion that the single exponential and convolution fits are most accurate. The two-exponential model generated rate constants for the rapid phase that are far out of the expected range and we have not

generated any reliable interpretations of their significance. However, the slow phase constants are near those seen in the other fits and generate a k_D that is in fair agreement with equilibrium data. The convolution by mixing model predicts very reasonable constants, though the k_D that results is about twice that measured at equilibrium. In turn, the single exponential fit is about half what is expected at room temperature. Ultimately, the disparity between the measurements is not very large and in practice we will use the mean values for calculations that require numeric inputs for those parameters.

We created several affinity mutants in an attempt to create a 3-O-methylglucose sensor and were successful to a point. Each version we generated with 3MG sensitivity demonstrated significantly higher affinity for glucose. As such, each mutant would be inadequate for use within the context of a living cell where glucose is abundant and very difficult, if not impossible, to control. For the remainder of this work, we will proceed only with the original version of the GlcSnFR sensor.

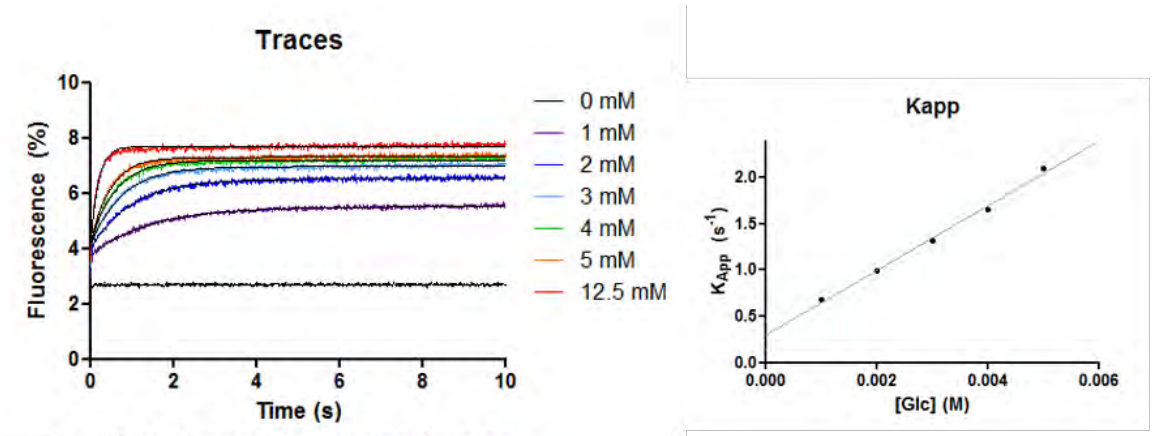
Traces
Fluorescence (%)
Time (s)
0 mM
1 mM
2 mM
3 mM
4 mM
5 mM
12.5 mM
Kapp
K_{App} (s^{-1})
[Glc] (M)

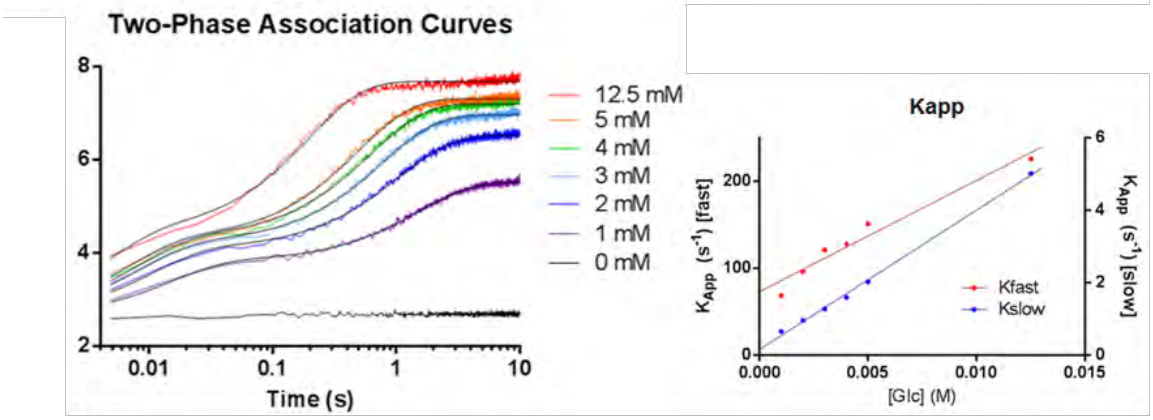
Two-Phase Association Curves
Time (s)
12.5 mM
5 mM
4 mM
3 mM
2 mM
1 mM
0 mM
Kapp
K_{App} (s^{-1}) [fast]
K_{App} (s^{-1}) [slow]
Kfast
Kslow
[Glc] (M)

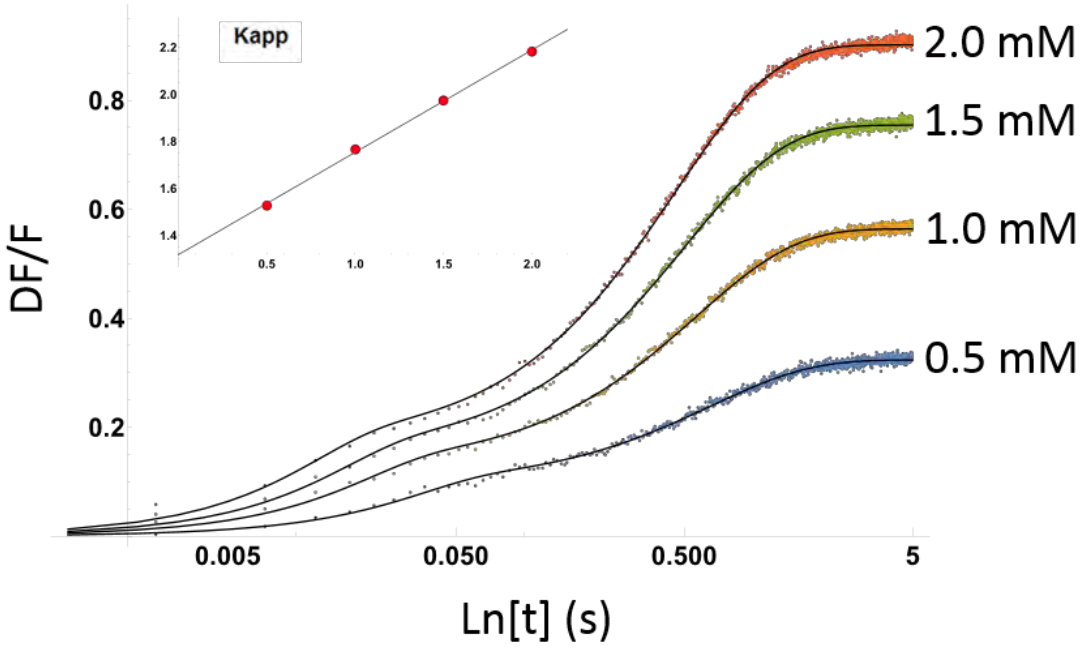
Kapp
2.0 mM
1.5 mM
1.0 mM
0.5 mM
DF/F
Ln[t] (s)

Figure 2.6 Measuring the on-and-off rates of GlcSnFR. The forward and reverse binding constants were calculated by various data models. In all cases we assumed pseudo-first order kinetics of binding. Varied glucose concentrations were rapidly mixed with purified GlcSnFR protein and time courses of fluorescence observed. **A:** Single exponential fit. [Time Courses] Abscissa: time (s), Ordinate: signal (% max voltage); [Kapp vs. Glucose concentration] Abscissa: Glucose concentration (M), Ordinate: k_{app} (s^{-1}). These fits did not force the curve to begin at the origin. The estimated k_Ds (K_{app}) were plotted against glucose concentration and fit with linear regression. Slope (k_{on}): 348.9 ± 14.77 ($M^{-1}s^{-1}$), Y-Intercept (k_{off}): 0.2999 ± 0.04898 (s^{-1}), X-Intercept ($-k_D$): -860 μM. **B:** Two exponential fit. [Time Courses] Abscissa: time (s), Ordinate: signal (% max voltage); [Kapp vs. Glucose concentration] Abscissa: Glucose concentration (M), Left Ordinate: $k_{app, fast}$ (s^{-1}), Right Ordinate: $k_{app, slow}$ (s^{-1}). In this model the curves were forced to start at the origin. The estimated K_{app}s were plotted versus concentration and fit with linear regression. [Fast Component] Slope (k_{on}): 12788 ± 1388 ($M^{-1}s^{-1}$), Y-Intercept (k_{off}): 73.26 ± 8.236 (s^{-1}), X-Intercept ($-k_D$): -5.7 mM [Slow Component] Slope (k_{on}): 384.6 ± 9.353 ($M^{-1}s^{-1}$), Y-Intercept (k_{off}): 0.1617 ± 0.05550 (s^{-1}), X-Intercept ($-k_D$): -2.6 mM **C:** Convolved single exponential and positive normal fit. [Time Courses] Abscissa: $\log_{10}$[time (s)], Ordinate: signal (% max voltage); [k_{app} vs. Glucose concentration] Abscissa: Glucose concentration (mM), Ordinate: k_{app} (s^{-1}). We assumed an impulse response due to mixing time caused data convolution. Assuming the impulse function to be the positive domain of a gaussian with mean 0, we fit these data to the convolution of the impulse function and a single exponential. The k_{app} from this fit was plotted versus glucose concentration and fit by linear regression. Slope (k_{on}): 435 ($M^{-1}s^{-1}$), Y-Intercept (k_{off}): 1.32 (s^{-1}), X-Intercept ($-k_D$): -3.03 mM

Chapter 3

ASSESSING MODEL SYSTEMS FOR KINETIC ANALYSIS

Abstract

The investigation of glucose flux across the plasma membrane requires an experimental regime which provides the capacity to disambiguate transport from other processes that alter glucose concentration. We tested the use of the fluorescent probe GlcSnFR in several model systems to evaluate which would provide suitable environments for its use as a reagent to study glucose transporter kinetics. We sought to establish experimental systems that could provide the following: i) concurrent control over the presence of GlcSnFR and application of stimulus, ii) unambiguous discrimination of signal response to changes in glucose versus environmental parameters with at least partial separation of glucose modulating fluxes (i.e., transport versus metabolism), and iii) provide the opportunity to answer current questions in the field of GLUT1 kinetics. We evaluated three different scales of system throughout this process. We expressed combinations of GlcSnFR, channelrhodopsin, and rCaMP using the promoter-specific UAS and QUAS genetic methods in brain tissues of *D. melanogaster* including neurons, glia, astrocytic glia, antellal lobe neurons and sub glomeruli. We created enriched and/or clonal cell populations expressing cytosolic and membrane-bound GlcSnFR variants derived from three different immortalized cell lines: HEK293, CHO-K1, and C8-D1A. Finally, we adapted a protocol for the use of resealed human erythrocyte ghosts to create membrane-sequestered volumes with GLUT1-specific permeability to glucose and minimal existence of competing glucose-interactive entities. Our investigation led us to conclude that erythrocyte ghosts satisfied the three conditions above and the other systems either presented properties incompatible with our line of investigation (cultured cell lines) or whose results would be too difficult to assess (*D. melanogaster*) prior to establishing the technique in a simpler experimental regime. We reliably demonstrate that resealed ghosts containing

purified GlcSnFR maintain an intact solvent/cytosol barrier and exchange glucose with their solvent in a carrier-specific manner.

Introduction

Cultured cells provide a powerful as well as convenient environment in which to observe basic biological activities. The use of immortalized cell lines allows the genetic manipulation of their behavior and contents, a technique used widely in the scientific community and extensively in this laboratory, contributing greatly to our study of many kinetic phenomena that would have not been otherwise possible. Our collaborators at Janelia provided two forms of the GlcSnFR probe, a cytosolic version which was the subject of the analysis above, and a membrane-bound version, herein referred to as GlcSnFR.C and GlcSnFR.M, respectively. The membrane-bound GlcSnFR was constructed using the pDisplay vector from Invitrogen which adds an IgKappa signaling peptide and the transmembrane domain of the platelet-derived growth factor receptor (PDGFR) gene at the N- and C-termini, respectively. The IgKappa peptide directs the fusion protein to the export pathway and the PDGFR transmembrane domain anchors it in the membrane with all portions N-terminal of this domain exposed on the extracellular face of the cell. As just mentioned above, this lab has generated many cell lines expressing high levels of several of the GLUT family members as well as mutants and chimerae which demonstrate a variety of interesting variant functionalities. We aspired to use these sensors as a means of first recapitulating such results and then extending them with the increased temporal resolution and continuity of sample they provide. Our first goal was to transfect the sensors into a few basic cell lines and establish stable, highly expressing transgenic lines. We decided to evaluate this strategy first using CHO-K1 (Chinese hamster ovary), HEK-293 (human embryonic kidney), and C8-D1A (mouse astrocyte). Here we describe this effort, the basic observations it provided about controlling cytosolic glucose concentrations, and the technical limitations which must be overcome to achieve accurate measurements of transporter activity.

Concurrently, we explored the possibility of using the glucose sensors to answer questions related more to qualitative trends in a physiological arena as opposed to those mentioned above which relate more to the precise quantification of characteristics specific to the transporter alone. A currently unresolved topic involves the metabolic production and utilization of lactate and glucose in the central nervous system (CNS) and how it changes during periods of neuronal activity. The interactions between neurons and astrocytes have been studied in great detail in recent years and found to be increasingly important for the development and maintenance of neural circuitry. Once thought of as structural cells that provided metabolic support to neurons, it is now clear that they are far more important. Astrocytes have been implicated in developmental roles (Müller and Best 1989), synapse formation (Pfrieger and Barres 1997; Ullian et al. 2001; Christopherson et al. 2005), response to injury and axonal degradation (reviewed in Eroglu and Barres 2010), and synaptic plasticity (Perea and Araque 2007; D'Ascenzo et al. 2007), though their modulation of synaptic activity is most relevant to the work proposed here. Many studies have demonstrated that astrocytes are associated with synapses, but the extent to which this occurs varies spatially and temporally. Ventura and Harris (1999) estimated that 57% of synapses in rat hippocampus were adjacent to astrocytic processes and Spacek (1985) showed the majority (74%) of Purkinje cells were covered by glia while this was the case for only 29% of pyramidal neurons. Additionally, these associations have been shown to be dynamic, changing over time (Nishida and Okabe 2007; Haber et al. 2006). This union of cells has been dubbed the "tripartite synapse" (Araque et al. 1999) and great effort has been made to decipher its activities.

Astrocytes play many potential roles at synaptic junctions, many of which are only partially understood. It is generally accepted that astrocytes are involved in clearing excess extracellular potassium released by firing neurons, though the molecular mechanism by which this occurs is not known (reviewed in Walz 2000). This issue may be aided through the analysis of recently generated transcriptome data from astrocytes, neurons, and oligodendrocytes (Lovatt et al. 2007; Cahoy et al.

2008). Neuronal activity also triggers astrocytic release of chemical transmitters such as D-serine, ATP, and glutamate. The effects these have on neuron activity are only partially characterized, but it has been proposed that astrocytic modulation helps neural network organization (reviewed in Fellin 2009). Astrocytes are also purported to play a major role in neuronal metabolism following activation, though the nature of this role is not agreed upon. Pellerin and Magistretti, having observed the stimulation of astrocytic glycolysis and an increase in interstitial lactate concentration following the onset of neuronal activity, proposed the ANLS hypothesis (Pellerin and Megistretti 1994). Briefly, this proposes that pyruvate is converted to lactate in astrocytes and shuttled to neurons where it is converted back to pyruvate for oxidative phosphorylation. This hypothesis is not universally accepted, with evidence published claiming the opposite and the proposal of the NALS (Simpson et al. 2007). Other work claims a more complex metabolic interaction involving astrocyte and neuron redox coupling (Cerdán et al. 2006). Despite a large body of work on this subject, resolving these hypotheses into a single model has proven difficult.

Investigating this topic in the human brain through direct methods is quite difficult. Form and function are jointly at the core of CNS physiology and studying behavior of the tissues anywhere but in their natural environment introduces fundamental differences that cannot be overlooked. For this reason, studies taking place in the context of a living human are limited to indirect measurements which are unable to provide the accuracy and precision needed to answer the questions described above. Here we describe a strategy for investigating the use of GlcSnFR to study the role of glucose and lactate in the neurons and astrocytes of *D. melanogaster*.

Drosophila olfaction is well-characterized on a physiological and molecular level. Small hairs called sensilla on the antenna and maxillary palps house olfactory sensory neurons (OSNs) that are tuned to respond to specific odorants (de Bruyne M 1999). This tuning is achieved via a family of membrane-bound odorant receptors (ORs) with one odor-specific receptor gene expressed per OSN.

These neurons project into the antennal lobe (Laissue et al. 1999) where they target specific glomeruli based on their tuning (Vosshall et al. 2000; Couto et al. 2005). Such specificity makes it possible to express engineered genes in a small subset of neurons with predictable geometries of dendritic processes. Further, characterization of astrocyte-like glia in Drosophila was achieved with confocal microscopy of the antennal lobe (Doherty et al. 2009), so the presence of astrocytes in this region is expected. The ORNs synapse with projection neurons (PNs) that relay signals to higher processing sensors. The GH146 gene is expressed in 90 of the 200 PNs from the antennal lobe which have representation within 34 of the 43 antennal lobe glomeruli (Laissue et al. 1999). Using this information, functional imaging of ORNs and their PNs has been done previously. Wang et al. (2003) were able to record neuronal activity following stimulation of the antenna with specific odors using the fluorescent calcium sensor G-CaMP (Nakai et al. 2001) and two-photon microscopy, though this was done following dissection of the brain from the fly. This was later achieved using live flies (Jayaraman and Laurent 2007).

Specific expression of the GlcSnFR sensors was achieved using the UAS/GAL4 system (Brand and Perrimon 1993). Neural expression will be confined to specific glomeruli of the antennal lobe using OR promoters (reviewed in Ronderos and Smith 2009) while pan-astrocytic expression will be driven by the *alarm* promoter (Doherty *et al*. 2009). We describe the construction of this system and its study below.

Materials and Methods

Materials

Human whole blood (#100-17) was purchased from Biological Specialty Corporation. Any other chemicals not mentioned above were purchased from Sigma Chemicals.

Solutions

Kaline buffer contains 150 mM KCl, 5 mM HEPES, 0.5 mM EDTA, and the pH is adjusted to 7.4 at experimental temperature. Erythrocyte lysis buffer contains 10 mM Tris·HCl, 4 mM EDTA, and the pH is adjusted to 7.4 at 4 °C.

Cell culture

HEK-293 (ATCC CRL-1573) and C8-D1A (ATCC CRL-2541) cells were cultured in DMEM (Gibco) with 1% Pen/Step (Gibco) and 10% FBS (Gibco). CHO-K1 (ATCC CRL-61) cells were cultured in HAM-F12 (Gibco) media with the same additives as above. Cells were passaged by incubating with 0.25% Trypsin-EDTA solution at 37 °C for 2 minutes, detaching with warm culture media, centrifugation at 800 rpm in a tabletop centrifuge for 3 minutes, aspirating media, resuspending cells in growth media and splitting at 1:10 by area into new plates.

Cell Transfection and Generation of Stable Lines

For evaluation of mammalian cell expression, GlcSnFR-pcDNA3.1 (cytosolic expression) and GlcSnFR-pDisplay (extracellular expression) were transfected into HEK293, CHO-K1, and C8-D1A cells using Lipofectamine reagent (Life Technologies) according to the product insert. Cells were passaged once and then placed into selection media (growth + 50 μg/mL Geneticin (Invitrogen)). Media was changed to remove dead cells and monitored until cell death stopped. They were then transferred to new plates while maintaining selective pressure. This was repeated until cells stabilized at which point stocks were frozen back.

Preparation of fluorescent RBC ghosts

Ghosts were prepared by mixing 1 volume of blood with 3 volumes ice-cold kaline followed by centrifugation in a 4 °C centrifuge at 5,000 x *g* for 4 minutes. The supernatant was aspirated and this process was repeated 2-3 times. Next, pelleted cells were resuspended into 20-40 volumes of RBC lysis buffer and incubated on ice for 10 minutes. It was imperative that all subsequent steps be conducted as close to ice temperature as possible and that buffers and tubes remained chilled throughout. Lysed cells

were centrifuged for 10 minutes in a 4 °C centrifuge at 14,000 x *g* in 50 mL conical tubes or 21,000 x *g* in larger containers. Supernatants were aspirated carefully, as initial pellets are wispy and loose. Cells were washed in RBC lysis buffer and centrifuged as above, repeating until supernatant was clear. For every 2 mL of ghosts to be resealed, a mixture of 1 mL concentrated GlcSnFR in kaline buffer and 1 mL kaline with 16 mM AMP or ATP in 20 mM $MgCl_2$ (adjust pH to 7.4 after addition of adenosine reagent) was prepared. We mixed 2 mL packed lysed RBCs with 1 mL sensor and 1 mL adenosine $MgCl_2$ for a final solution of lysed cells in 4 mM adenosine and 5 mM $MgCl_2$. These cells were incubated on ice for 10 minutes then transfer to a 37 °C water bath for 1 hour. After incubation, cells were centrifuged at 10,000 x *g* for 5 minutes and resuspended in 10 volumes room temperature kaline buffer. This was repeated 2 times and then pellets allowed to equilibrate to experimental temperature before proceeding to assay. Temperature of the samples was maintained as carefully as possible throught use in each assay as fluorescent output is a function of temperature.

Preparation of RBC Ghost Standard Curve

Resealed ghosts were prepared as above, resuspended in one volume of room temperature kaline buffer (50% hematocrit), and equilibrated to room temperature. Fluorimetry was conducted by excitation with 488 nm light and detection of emission of 510 nm light perpendicular to the excitation source. Samples were prepared by adding 50 μL (V_{RBC}) of resealed ghosts to 1.5 mL (V_i) of kaline buffer in a quartz cuvette constantly mixed with a small magnetic stirrer. This mixture was used to read initial fluorescence (F_i) prior to addition of glucose media. While reading, 750 μL (V_G) of new media with G_i mM glucose was added to the cuvette. Uptake was monitored until equilibrium fluorescence (F_{eq}) was reached. The baseline fluorescence (F_0) following addition of glucose, but prior to any transport, was calculated as a dilution of F_i:

$$F_0 = \frac{V_i}{V_i + V_{RBC} + V_G} F_i$$

Similarly, we calculate the final concentration of glucose in the cuvette :

$$G_x = \frac{V_G}{V_i + V_{RBC} + V_G} G_i$$

Knowing F_0 allows calculation of ΔF_{eq} from F_{eq} :

$$\Delta F_{eq} = \frac{F_{eq} - F_0}{F_0}$$

Plotting ΔF_{eq} versus G_x gives a standard curve fit with the following equation:

$$\Delta F_{eq} = \Delta F_{max} \frac{G_x}{G_x + k_D} = \boldsymbol{f}(\boldsymbol{G_x})$$

where ΔF_{max} is the percent increase in fluorescence at sensor saturation and k_D is the dissociation constant of the sensor and glucose, assuming a simple E + S ↔ ES system.

Results and Discussion

Expression of GlcSnFR in cultured cell systems

Stable cell lines expressing the cytosolic and membrane-tethered varieties of the GlcSnFR probe were generated using standard transfection and culture techniques. Following transfection, stable lines were generated and maintained under selective pressure with geneticin. After the stable lines were established, they were sorted by FACS into bulk, high-expressing populations. Cells were gated by forward and side scatter, then sorted based on their intensity in the green channel. The top 2% of the cells in the fluorescence histogram were gated for sorting. After these lines were established, clonal lines were generated to maintain more consistent output in fluorescent assays. This was also done by single cell sorting FACS. We generated low, medium, and high expressing lines as we did not know what anomalous physiological phenotypes might result from pushing sensor expression too far. Example images from both constructs in all three lines can be seen in Figure 3.1. Cells transfected with GlcSnFR.C expressed the protein throughout their cytosol and maintained healthy morphologies, though CHO-K1

cells show exclusion of the protein from multiple internal compartments and appear to have accumulation of the sensor in what we presume is the endoplasmic reticulum (ER). Conversely, all three cell types demonstrate marked difficulty when expressing GlcSnFR.M. Internal aggregation of sensor, presumably within the ER and Golgi networks, is observed in all cells expressing the protein. Additionally, normal morphologies are absent and cells appear stressed.

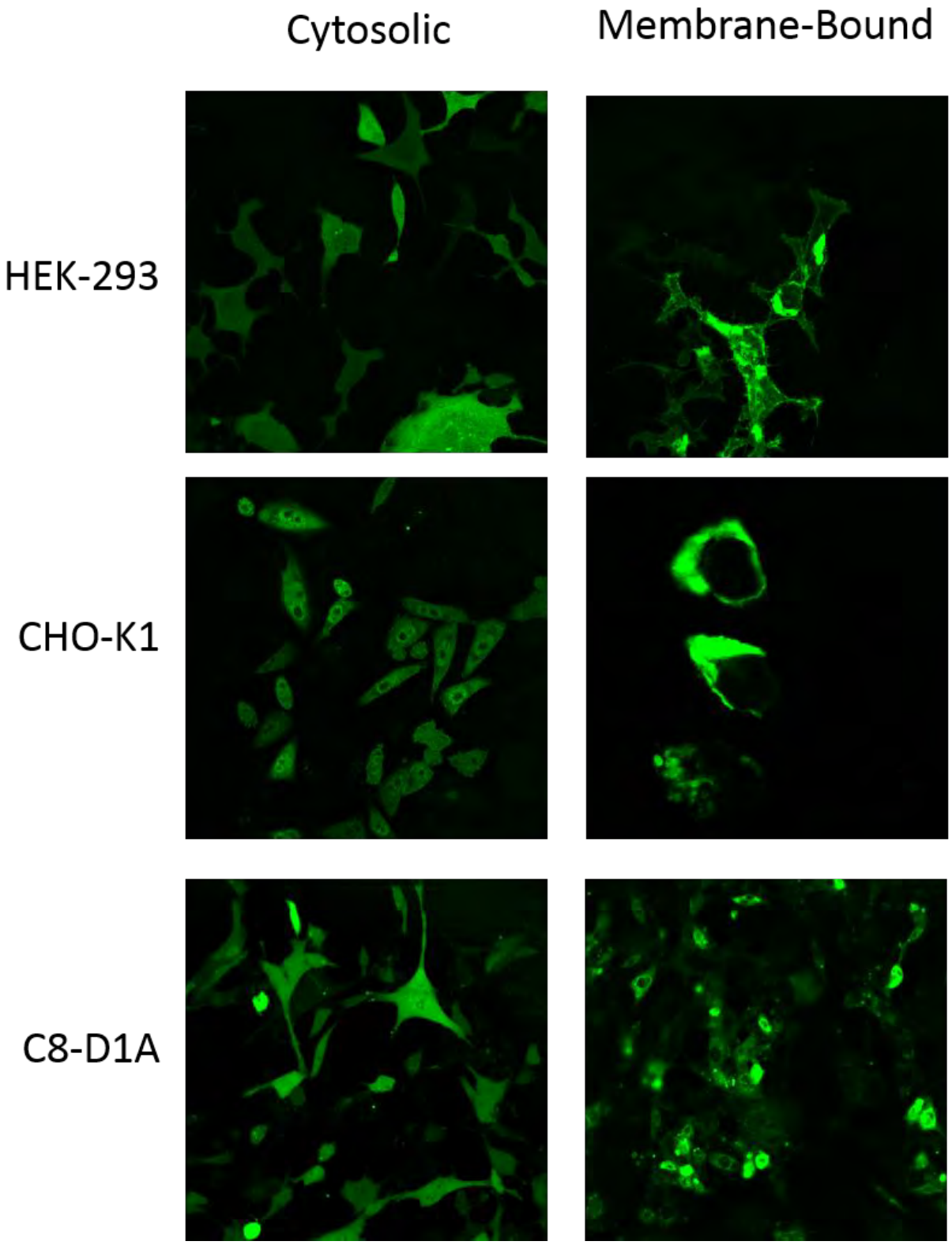
Cytosolic
Membrane-Bound
HEK-293
CHO-K1
C8-D1A

Figure 3.1 Expression of GlcSnFR.C and GlcSnFR.M cultured cell lines. Stable transfections of the cytosolic and extracellular sensor were established in cultured mammalian cells. Following plasmid transfection, selective pressure was maintained on cells transfected with expression cassettes containing the neomycin resistance gene using geneticin (G418). After recovery, cells were bulk sorted by fluorescence-activated cell sorting (FACS) into top 2% pools. Examples of each cell line containing both versions of GlcSnFR are seen in this figure.

Responses to glucose challenge in cultured cells

We assessed the GlcSnFR cell lines for fluorescent sensitivity to changes in glucose concentration using plate reader assays to assess equilibrium responses and fluorescent and confocal microscopy techniques to observe time courses of response. Stable cells were cultured in clear-bottom 96 well plates and exposed to titrations of glucose solution. Following incubation for 60 minutes in the incubator, plates were read, and fluorescence response recorded. This assay was used to inform our selection of high, medium, and low expressing clones. Colonies which began to grow in the sorted plate could be evaluated after their first passage into new wells. This helped us prevent carrying forward a large number of clones which would ultimately be discarded. Once the clone was established, we could challenge it with titrations of glucose to better classify its expression levels (Figure 3.2A). In all three cell types expressing GlcSnFR.C we observe our [qualitatively] expected results. Cells demonstrate fluorescent output in proportion to the concentration of glucose exposure, though signal still doesn't appear saturating at what would be considered overwhelming glucose concentrations (up to ~400 mM; Example of these data in Figure 3.2B). This is surprising as we expected that even in extremely metabolically active cells we could surpass their capacity to outpace cytosolic equilibration. Further, this effect is not seen when cells are treated with 2DG or 3MG, indicating that the signal is glucose-specific and not simply related to other possible physical effects caused by such high concentrations of extracellular solute. This is further confirmed by the effects of coincidental exposure of cells to high glucose and cytochalasin B (CCB), a potent inhibitor of GLUT1 function. We attempted to force more rapid solute:cytosol equilibration using the membrane permeabilizing α-toxin protein from *Staphylococcus aureus*. This toxin has been shown to insert into plasma membranes and create pores around 2-3 nm in diameter, providing membrane permeability preferentially to small molecules and ions. We expected that application of the toxin to cells in the plate assay would result in a rapid gain of

fluorescence as glucose equilibrated without the need for carrier-mediated transport. Instead, we saw an inhibition of signal gain (Figure 3.2C).

A

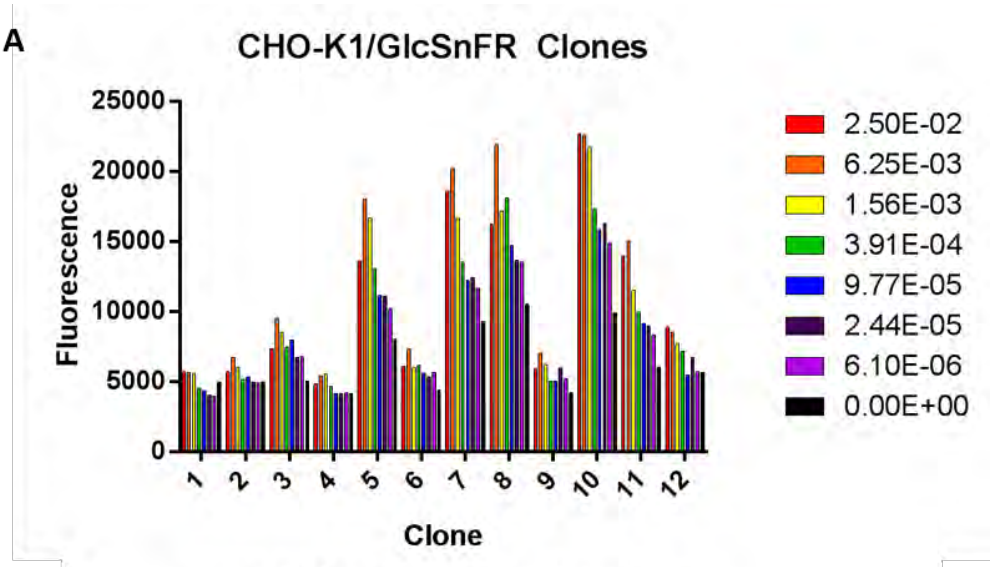
CHO-K1/GlcSnFR Clones
Fluorescence
25000
20000
15000
10000
5000
0
1 2 3 4 5 6 7 8 9 10 11 12
Clone
2.50E-02
6.25E-03
1.56E-03
3.91E-04
9.77E-05
2.44E-05
6.10E-06
0.00E+00

B

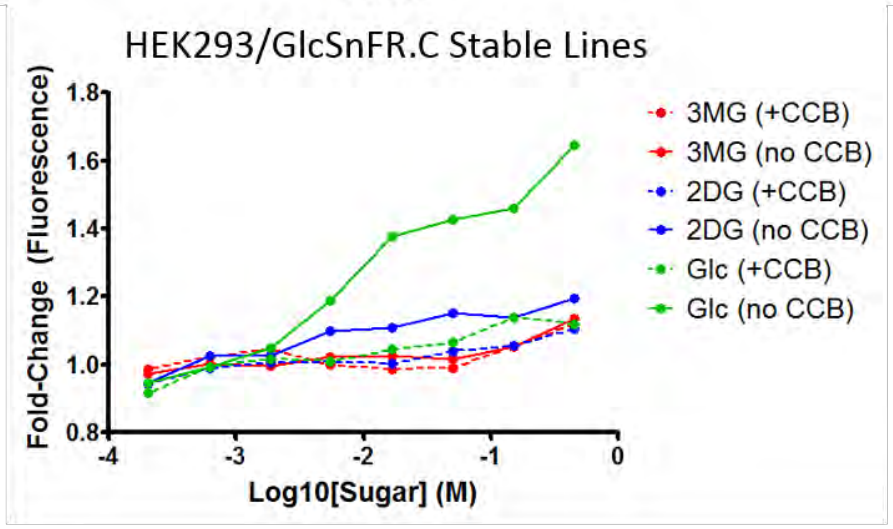
HEK293/GlcSnFR.C Stable Lines
Fold-Change (Fluorescence)
1.8
1.6
1.4
1.2
1.0
0.8
-4
-3
-2
-1
0
Log10[Sugar] (M)
3MG (+CCB)
3MG (no CCB)
2DG (+CCB)
2DG (no CCB)
Glc (+CCB)
Glc (no CCB)

C

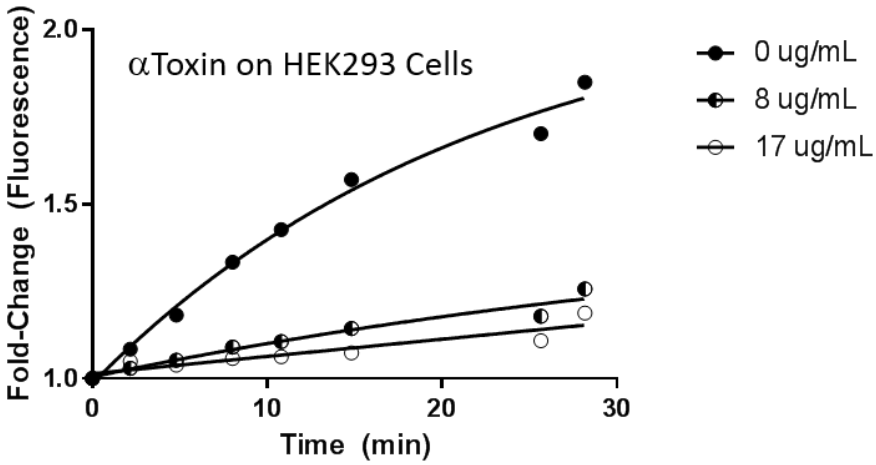
αToxin on HEK293 Cells
Fold-Change (Fluorescence)
2.0
1.5
1.0
0
10
20
30
Time (min)
0 ug/mL
8 ug/mL
17 ug/mL

Figure 3.2 Cultured cell response to glucose and pharmacological toxins. **A:** Single-sorted CHO-K1 cells were established as clonal cell lines. Abscissa: clone number and glucose concentration (mM); Ordinate: Fluorescence (A.U.). Single cells were selected by FACS and sorted into 96 well plate according to low, medium, and high fluorescence. Plates were monitored over the subsequent weeks for surviving clones. Four of each class were selected for expansion. We grew each in wells of clear-bottom 96wp and treated with glucose titrations in kaline buffer. Following incubation at 37 °C for 30 minutes we read the samples on a plate reader. **B:** Bulk-sorted (top 2%) HEK-293 cells expressing GlcSnFR.C were cultured in clear-bottom 96wp. Abscissa: concentration of substrate (M); Ordinate: Increase in fluorescence compared to 0 sugar (fold change). We treated these with titrations of 3MG, 2DG, and glucose +/- CCB. Following incubation at 37 °C for 30 minutes, we read the cells on a plate reader. Regarding sugar specificity of the probe, results are qualitatively similar to the equilibrium binding done with purified protein. We also see that the addition of CCB inhibits cellular import of glucose. **C:** As in **B**, HEK-293 bulk-sorted populations were plated into 96 well plate. These cells were treated with 10 mM glucose and varied concentrations of α-toxin (0, 8, or 17 μg/mL), a cell permeating protein. Abscissa: concentration of substrate (M); Ordinate: Increase in fluorescence compared to 0 sugar (fold change). The plate was incubated at room temperature for the indicated times prior to each reading. We observed a marked decrease in fluorescence in treated wells compared to untreated.

We used confocal microscopy to visualize the effects of dynamic extracellular sugar concentrations on cells expressing GlcSnFR proteins. We first note that cells transfected with the GlcSnFR.M version of the probe continued to demonstrate poor capacity for surface presentation and, though very bright, showed little to no response to glucose manipulation in their media. This was the case for all assays attempted and we therefore decided to forego any more experiments using the GlcSnFR.M variant. However, those cells expressing the GlcSnFR.C variant (as noted above), were responsive to changes in glucose concentrations in both plate reader and microscope assays, if not in a way that can be fully rationalized. Continuous observation of cells by confocal microscopy verified the trend observed previously in the plate reader. Increasing concentrations of glucose in the media above cells in the field of view resulted in unsaturated signal up to a glucose concentration of 100 mM. An example series of images from some of these cells is seen in figure 3.3A-D. A bolus of high concentration glucose solution was added to the existing media every minute for ten minutes. Even at the highest concentration the sensor output gain seemed to be in the linear range of response.

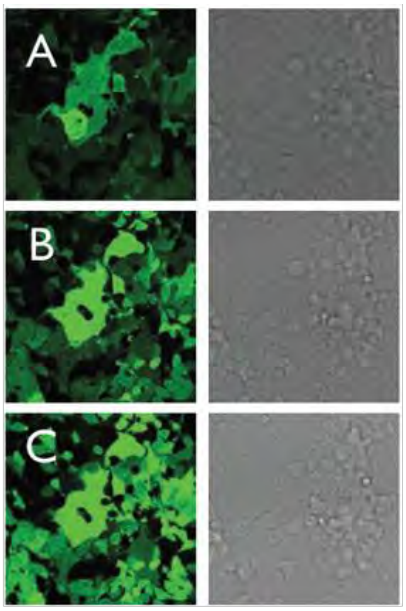
A
B
C

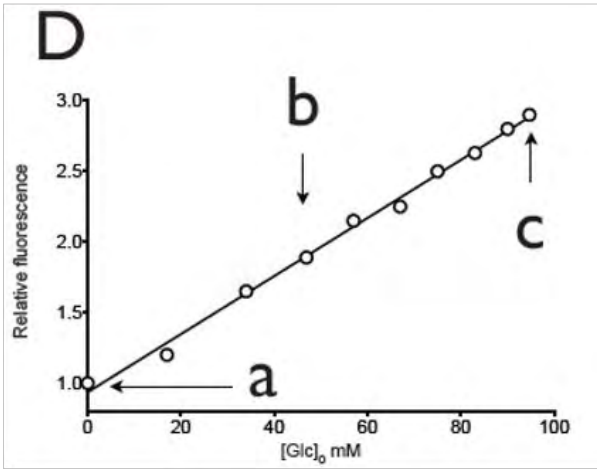
D
b
c
a
Relative fluorescence
3.0
2.5
2.0
1.5
1.0
0
20
40
60
80
100
[Glc]o mM

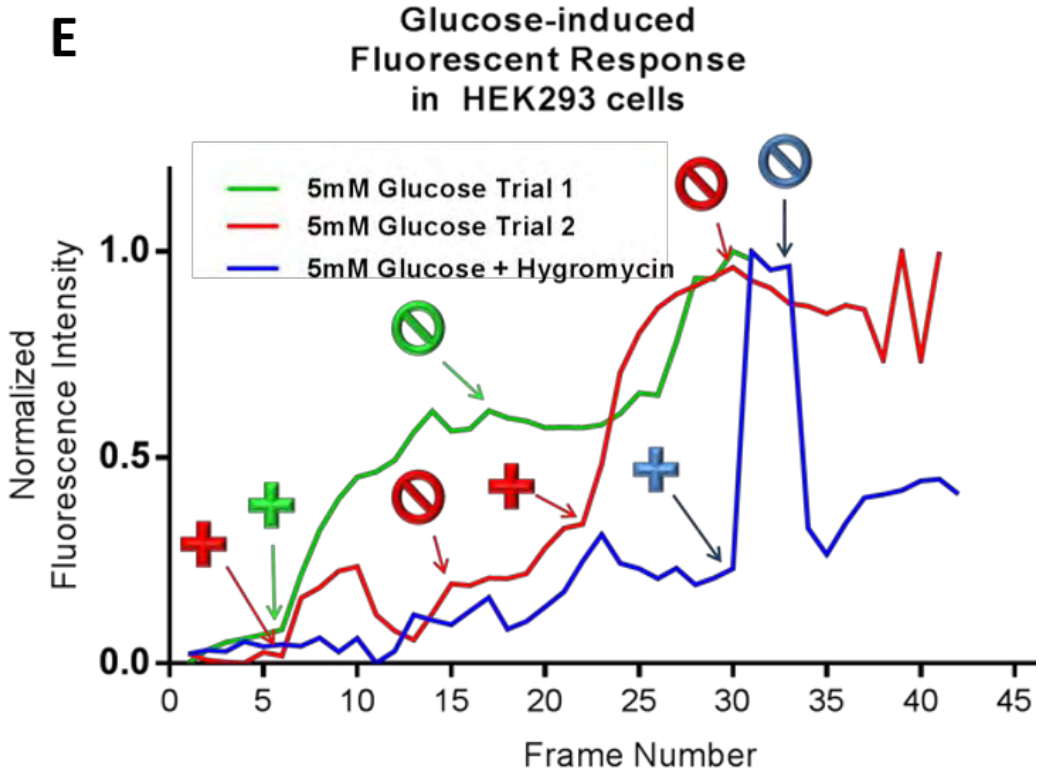
E
Glucose-induced
Fluorescent Response
in HEK293 cells
5mM Glucose Trial 1
5mM Glucose Trial 2
5mM Glucose + Hygromycin
Normalized
Fluorescence Intensity
1.0
0.5
0.0
0
5
10
15
20
25
30
35
40
45
Frame Number

Figure 3.3 Cultured cell response to glucose is unpredictable. **A-C:** We cultured HEK-293 cells in Mattek dished with glass coverslip bottoms. Cells were observed by confocal microscopy during the addition of boluses of high concentration glucose buffer. **D:** Total field integration of signal. Abscissa: External glucose conventration (mM); Ordinate: Fluorescent increase over 0 mM glucose (fold change). We measured the total fluorescent signal from the field of view 10 minutes after the addition of each glucose bolus and normalized to the original fluorescence. The inset letters indicate the view of cells at each of the marked data points. **E:** Signal evolution from newly translated GlcSnFR. HEK-293 bulk sorted cells were plated and grown on 35 mM round coverslips. At 80% confluence, they were glucose starved overnight with or without the translation inhibitor hygromycin. Under perfusion, we added and removed 5 mM glucose in PBS, exchanging with 0 mM buffer (PBS). We observed that in untreated cells, the addition of glucose caused an increase in signal. However, its removal did not cause the expected decrease. In translation-inhibited cells, however, we saw a similar increase in signal upon glucose addition, but also saw the signal decrease following removal.

Standard fluorescent microscopy was used to visualize the effects of increasing and decreasing glucose concentrations. Cells were cultured on microscope coverslips and carefully placed, inverted, on a glass slide with two strips of vacuum grease which allowed the passage of liquid across one side of the slip to the other. This provided the means to exchange the solvent surrounding the cells adhering to the coverslip using a pipette and a vacuum and gave us more experimental control in regards to the solvent glucose concentration. Stably transfected HEK-293 cells were plated 48 hours prior to experiment and glucose starved for 16 hours overnight prior to their use. The addition of a physiological glucose concentration (5 mM) resulted in the expected increase in cellular fluorescence. However, replacing the solvent with zero-glucose buffer only served to slow the rate of fluorescence increase and then was followed by an unexpected rapid increase in the absence of any glucose (Figure 3.3E, green trace). However, when cells were treated with the translation inhibitor hygromycin for one hour prior to imaging followed by a buffer exchange into zero glucose medium, we see the expected fluorescent responses to high and low glucose buffers (Figure 3.3E, blue trace). This indicates that the unexpected increases in fluorescence in the absence of glucose observed in untreated cells arises from increased production of GlcSnFR protein with the post-starvation availability of glucose. Glucose taken up during the initial dosage of high-glucose medium was entered into the metabolic pathway and subsequent anabolic pathways.

Development of *D. melanogaster* strains expressing GlcSnFR: We generated the following plan to examine glucose utilization in neurons and astrocytes of the *D.* melanogaster antennal lobe. Tissue specific gene expression can be accomplished using the UAS/GAL4 and QUAS/QS binary expression systems. We sought to use this to drive expression of GlcSnFR in all glomeruli of the antennal lobe by crossing UAS.GlcSnFR with OR83b.GAL4. Channelrhodopsin, a light-gated sodium channel, would be expressed in one glomerulus of the antennal lobe using a direct fusion of the gene and either Or24a, Or42b, or Or82a. Finally, expression of the red calcium sensor RCaMP would be driven by the other

binary system in the same glomerulus using the appropriate QUAS/QS pair. With this system in place, we would use confocal microscopy to observe changes in apparent glucose levels in sub regions of the antennal lobe while manipulating its behavior. Photo-activation of channelrhodopsin would allow us to train action potentials in only one glomerulus while observing how the green fluorescent signal changed in it and nearby glomeruli. The RCaMP co-expression in the activatable glomerulus would provide feedback of neuronal activity. We took the following steps to achieve this result. The GlcSnFR.C open reading frame was cloned into pUAST and pQUAST vectors. These constructs were then sent to BestGene for injection into embryos. We received back 10 and 11 G_2 transformants for the pUAST/GlcSnFR and pQUAST/GlcSnFR vectors, respectively. We isolated mutants with insertions on chromosomes 2 and 3 for each vector and balanced them over CyO and TM3,Sb. UAS.GlcSnFR/TM3,Sb flies were crossed repeatedly with Or83b.GAL4 flies until we isolated a crossed-over fly with both cassettes on chromosome 2. As proof of concept for functional expression of GlcSnFR in the fly, we crossed UAS.GlcSnFR flies with a *repo*.GAL4 strain to achieve pan-neuronal expression. The successful cross clearly demonstrated the expression of GlcSnFR in the central nervous system of both larvae and adults (Figure 3.4A). We dissected *repo*.GAL4/UAS.GlcSnFR first instar larvae and observed whether the expressed sensor could respond the glucose in that context. While imaging, 10 mM glucose was applied to the dissecting dish in which the larva was held. We imaged continuously for 23 minutes before applying a large dose of CCB (1 μM) to the dissecting buffer. Very quickly we observed a decline in the fluorescent output of the cells (Figure 3.4B). These two simple observations demonstrated to us that GlcSnFR provides glucose-related signal and that we could use it to evaluate, at least qualitatively, the effects of specific physiological activities. However, given the unexpected difficulties observing the effects of sugar modulation in cultured cells, we decided to delay further development of this project until we had definitive evidence we could use GlcSnFR effectively.

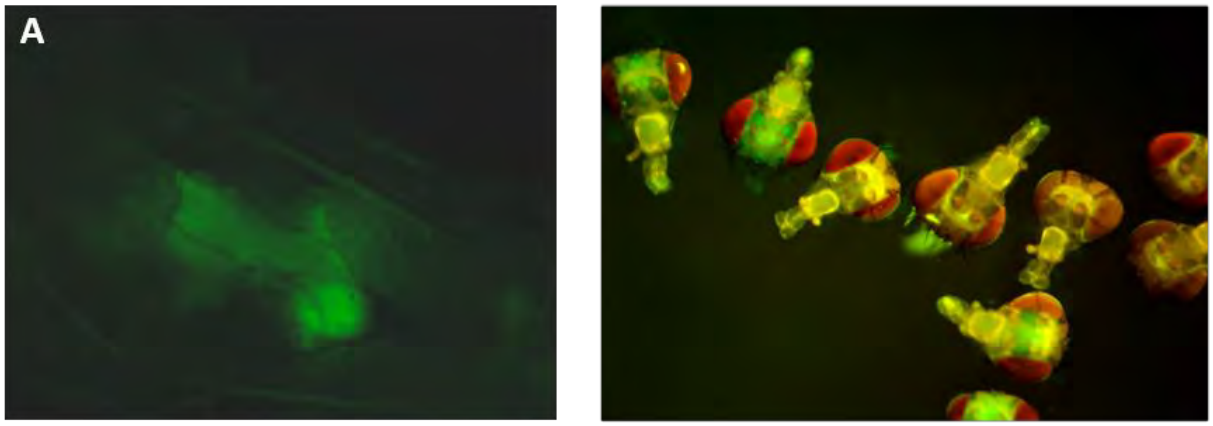
A

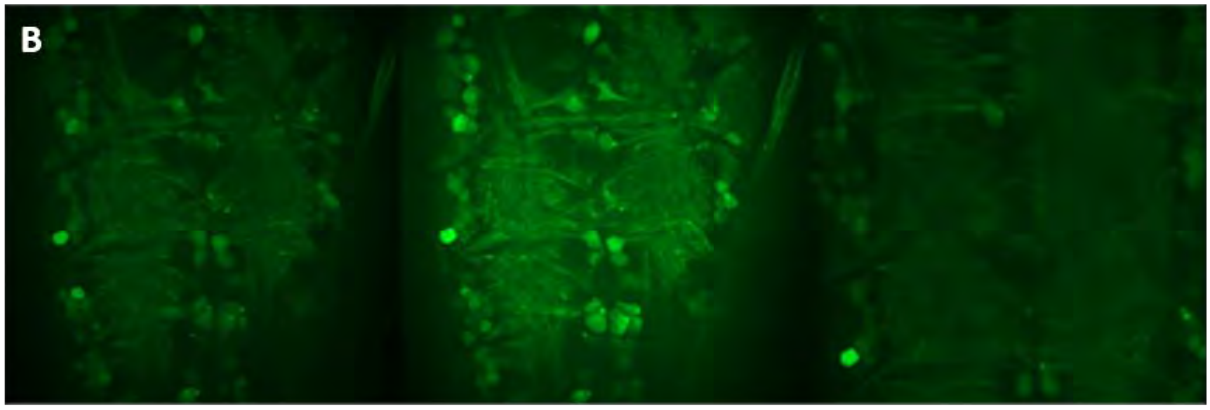
B

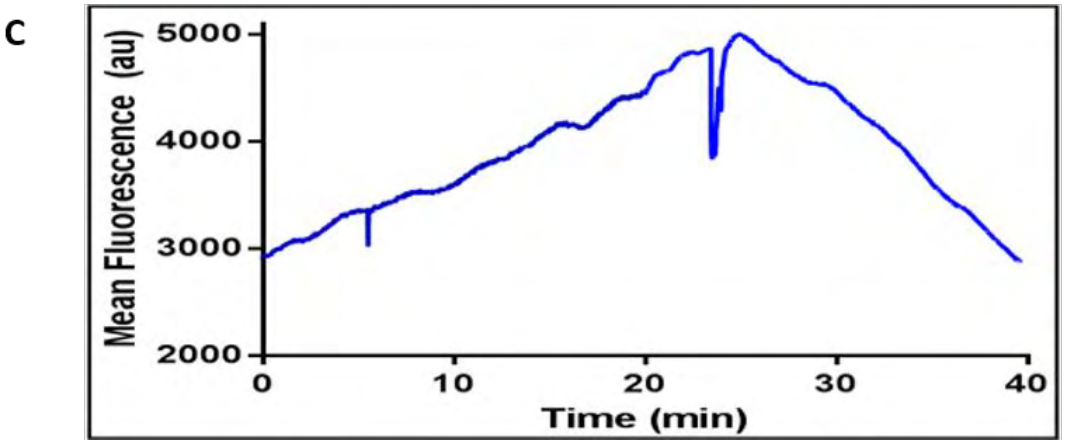
C
Mean Fluorescence (au)
5000
4000
3000
2000
0
10
20
30
40
Time (min)

Figure 3.4 Expression of GlcSnFR in D. Melanogaster. The expression of GlcSnFR in the *Drosophila* central nervous system is driven by the pan-neuronal promoter *elav*. This is accomplished using the UAS-GAL4 binary expression system. The neuronal *elav* promoter drives tissue-specific expression of the yeast GAL4 gene, a powerful transcription factor that activates the UAS promoter. The GlcSnFR open reading frame (ORF) is downstream of the UAS promoter, and thus is expressed in a tissue-specific manner in all neurons. Other pairings of the UAS/GlcSnFR fly line with a different GAL4 line would result in expression in the tissue-specific manner specified by that GAL4 line. **A:** Expression of GlcSnFR in the developing CNS of a first instar larva. Visibility is diminished by the larval cuticle. **B:** Expression of GlcSnFR in the brain of adult *Drosophila*. Successful crosses were examined by fluorescence-enabled microscopy with a dissecting scope. Samples were illuminated with blue light and filtered through yellow plastic. Brains were later dissected and analyzed in different glucose buffers. **C:** A third instar larva dissected by the "glove" method. Nicks are placed in the cuticle and then, with forceps, pulled back and inside out, leaving the exposed tissue with greater visibility for microscopy.

Monitoring glucose flux in erythrocyte ghosts: Fluorescent red blood cell (RBC) ghosts were hypotonically lysed and then resealed in the presence of purified GlcSnFR protein and 0 or 4 mM ATP or AMP. We assessed the successful encapsulation of fluorescent probe and ATP/AMP using a fluorescent microscope. To ensure our protocol was not disrupting normal RBC physiology, we looked for hallmarks of ATP vs. AMP resealed ghosts. Ghosts containing ATP create the familiar bi-concave diskoid while those without ATP or with AMP will show a rounded, spiculated morphology. We confirmed the presence of GlcSnFR, its encapsulation in the ghost interior, and the morphology of the ghosts using lipophilic dyes to stain the plasma membrane red. We confirmed GFP presence in the green channel. We also confirmed morphology remained intact by SEM. The panels in Figure 3.5 show that each of the considerations above is addressed and resealing GlcSnFR in ghosts preserves the cell as well as the protein.

The fluorescent response of GlcSnFR in the context of the ghost was evaluated first by equilibrium kinetics. Resealed fluorescent ghosts were added to a 96 well plate and mixed with glucose titrations at ice temperature. We also tested free solution GlcSnFR to observe any differences in behavior between the two conditions (Figure 3.6A-B). The equilibrated fluorescence curve indicated a kD of 1.17 mM for the free sensor and 2.4 mM for the RBC-encapsulated sensor with maximum fluorescent ratios of 3.22 and 2.05-fold, respectively. We hypothesize that the decreased apparent affinity and output of the ghost-enclosed sensor is a result of greater temperature sensitivity in a more crowded environment, but we will perform more evaluations of the sensor to ensure we can interpret results from future experiments.

Time courses of uptake were recorded in a 96wp at 20 °C in ghosts treated with varied concentrations of CCB (0-100 μM). Rates of equilibration with 10 mM glucose were slowed proportional to concentration of drug in the CCB-treated wells (Figure 3.6C). However, the ghosts were almost completely equilibrated during the time taken moving the plate from the benchtop to next to the plate reader into the device. This might indicate a failure for the ghosts to reseal, especially in the context of our previous results, except the temperature is significantly higher and the CCB-specific inhibition in the other wells speaks to an intact membrane.

There is a long history of studying GLUT1 kinetics using RBC ghosts, so we wanted to compare ghosts prepared with and without sensor using a standard technique as final confirmation of this system as capable of generating reliable transport records. We compared uptake of radiolabeled 3MG between ghosts +/- GlcSnFR using 0-5 mM 3MG and observed KM values of 0.45 and 1.04 mM with and without sensor, respectively (Figure 3.6D). Variability in sample composition prevented normalization of the two data sets, so we do not have a definitive measure of the Vmax. However, we were sufficiently satisfied that the ghost resealed with sensor does not demonstrate marked differences in behavior compared to one resealed without and thus makes for a suitable environment for studying glucose transport kinetics.

In order to conclusively demonstrate that glucose equilibration in the fluorescent ghosts was a product of GLUT1-facilitated diffusion rather than incomplete recovery of membrane integrity, we conducted counterflow experiments using a fluorimeter. Conventionally, this experiment involves initial conditions in which “hot”, radiolabeled substrate is on the exterior

of the cells and “cold”, unlabeled substrate is inside. This is accomplished by equilibrating cells with a large concentration of cold substrate in a small volume and then beginning the experiment by diluting them in a large volume of buffer with a comparatively low concentration of hot substrate. Initially, net sugar flux is from in to out, but the radiolabel allows tracking of the relatively small flux from out to in. In the early stages of equilibration, the hot substrate which is transported inside can be transported back out, but does so very slowly owing to enormous competition from the highly concentrated cold substrate. This results in a transient accumulation of labeled sugar above its equilibrium concentration which persists until the cold sugar concentration decreases sufficiently to relieve the inhibition of its exit (Figure 3.7A). Differential labeling of two subpopulations of glucose is not possible in a fluorometric assay, but we have developed an analogous system using glucose and 3MG. As described in the previous chapter, the affinity of GlcSnFR for 3MG is extremely low compared to glucose ($k_{D,3MG}$ > 100 mM, $k_{D,Glc}$ ≈ 2.5 mM, Figures 2.4 & 2.5), and as such changes in signal can be almost completely attributed to changes in glucose concentrations. Here, we use 3MG as the “cold” substrate and glucose as the “hot” to achieve the counterflow transient in our fluorometric assay. Fluorescent RBC ghosts were prepared with 4 mM ATP or AMP and incubated for 1 hour at room temperature in kaline at a final concentration of 80 mM 3MG. While already recording in the fluorimeter, ghosts (50 μL) were added to the cuvette containing a large volume (3.0 mL) of kaline with varied glucose concentrations (0.0, 0.5, 1.0, or 4.0 mM) and the subsequent time course of fluorescence observed. The counterflow overshoot was observed in all samples in which ghosts were injected into glucose-containing buffer (Figure 3.7B). This confirmed with certainty the restored integrity of the erythrocyte membrane and continued function of the

GLUT1 carrier. Additionally, we were able to recapitulate previous results obtained using radiolabeled substrate in which the effects of intracellular ATP are exhibited through a counterflow transient which begins later, reaches a smaller magnitude, and takes longer to return to the equilibration concentration (REF).

Conclusions

Our evaluations of different experimental systems for studying GLUT1 kinetics have ultimately resulted in the determination that the resealed erythrocyte ghost offers the best environment for unambiguous measurement of transporter kinetics. A brief evaluation of each system:

- Cultured cells – Cultured cell lines provide great benefits in the area of protein production due to this process being done automatically following transfection. Additionally, they offer a full cellular context which approximates physiological conditions. Unfortunately, controlling the metabolic profile of the cells proved highly variable if not impossible. Additionally, cytosolic conditions, protein content, and metabolic rates all follow patterns related to cell cycle, passage number, and incubator conditions. While it is possible to control for each of these factors, it is extremely difficult to relate the state of the sensor to each individually, not even considering glucose concentrations. With the additional goal of examining changes in fluorescence which are exclusively from glucose, we decided that the uncertainty was too high.
- *D. melanogaster* – The fly model is a more difficult system to establish than the cultured cells, but offers a far more relevant physiological setting. So, despite sharing the same (if not more numerous) concerns related to ambiguity in the source of signal changes, the qualitative changes that can be observed have a more direct significance to normal tissue function. The systemic behavior of cells in a living organism can help resolve questions about how it functions on a large scale (organ/tissue/body) while qualitative phenomena observed in a cultured cell system only serve to inform how a malfunctioning cell functions. However, because we had yet

to demonstrate a proof-of-concept methodology that allowed the use of GlcSnFR to recapitulate observations from previous studies, we concluded that such a series of experiments was needed before we could reliably interpret data from a complex system that was still under construction.

- Erythrocyte ghosts – The union and intersection of the sets of strengths and weaknesses of the erythrocyte as an environment for this study are almost the same. We are able to avoid sometimes unpredictable or unmeasured changes in metabolism, surface expression, and cell cycle because these things are either absent from the red blood cell already, or completely gone upon generation of resealed ghosts. This makes signal interpretation almost unambiguous (but not completely, see chapter 4) and greatly facilitates the quantitative measurement of glucose concentration from fluorescence data. However, the lack of the cellular programs which make other cells too complex also render the erythrocyte unable to provide any of the powerful biochemical tools that can be harnessed in said other cells. For example, erythrocytes are enucleated and thus cannot be genetically modified to create sensor on its own. Instead, it must be introduced through somewhat laborious methods each time an experiment is conducted (ghosts must be prepared fresh or results are too variable). This same deficiency prevents the use of engineered or disease-state GLUT1 transporter. It is serendipitous that human red blood cell membranes are dense with GLUT1 protein. Altogether, the benefits far outweigh the shortcomings and we concluded that the ability to measure glucose transport in the absence of interference from competing pathways was critical to establishing experimental techniques using the GlcSnFR probe.

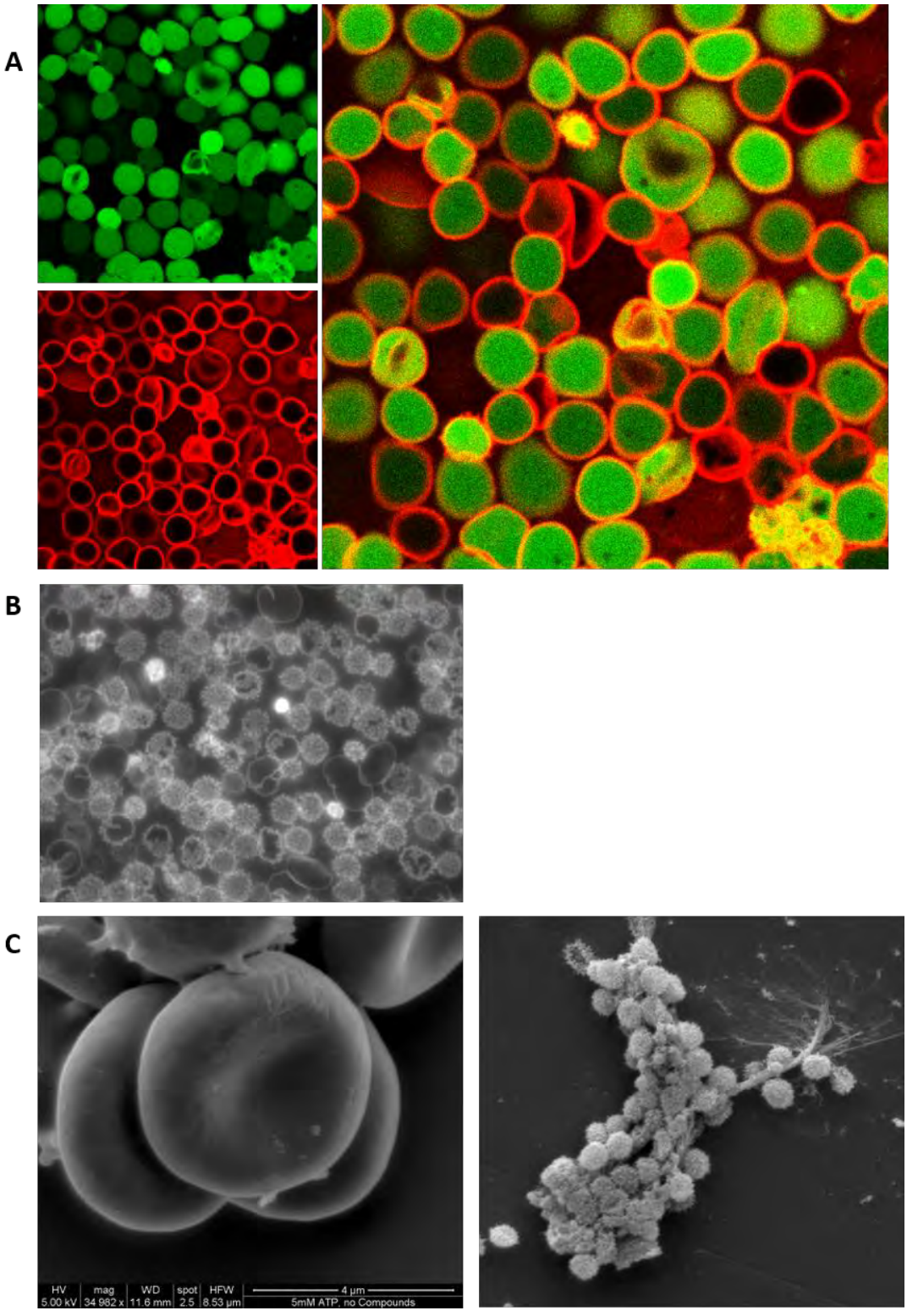
A
B
C
HV
5.00 kV
mag
34.982 x
WD
11.6 mm
spot
2.5
HFW
8.53 µm
4 µm
5mM ATP, no Compounds

Figure 3.5 Erythrocyte ghost morphology is not compromised by the enclosure of GlcSnFR.

Fluorescent, confocal, and scanning electron microscopy images of erythrocyte ghosts resealed +/- GlcSnFR with 5 mM AMP or ATP. **A:** Human red blood cells were biotinylated with NHS-ester-linked biotin prior to hypotonic lysis, resealing in isotonic buffer containing purified GlcSnFR protein and 5 mM ATP, and then attached to coverslips with adsorbed biotinylated BSA and streptavidin. Cells were counterstained with a lipophilic red dye to visualize their membranes. Images acquired using confocal microscope. Upper panel: green channel showing homogenous dispersion of GlcSnFR in cytosol of ghosts; Lower panel: red channel showing cell membranes (and the lack of interior membranes); Right panel: merged channels. **B:** Fluorescent scope imaging of ghosts prepared as in **A,** but resealed with 5 mM AMP and GlcSnFR. Note the echinocyte morphology characteristic of ATP-free ghosts. Cell membranes were visualized with fluorescent red streptavidin. **C:** Scanning electron microscope (SEM) images of ghosts resealed with GlcSnFR and 5 mM of either ATP (left panel) or AMP (right panel). Both images show the expected morphology for cells with the respective nucleotide.

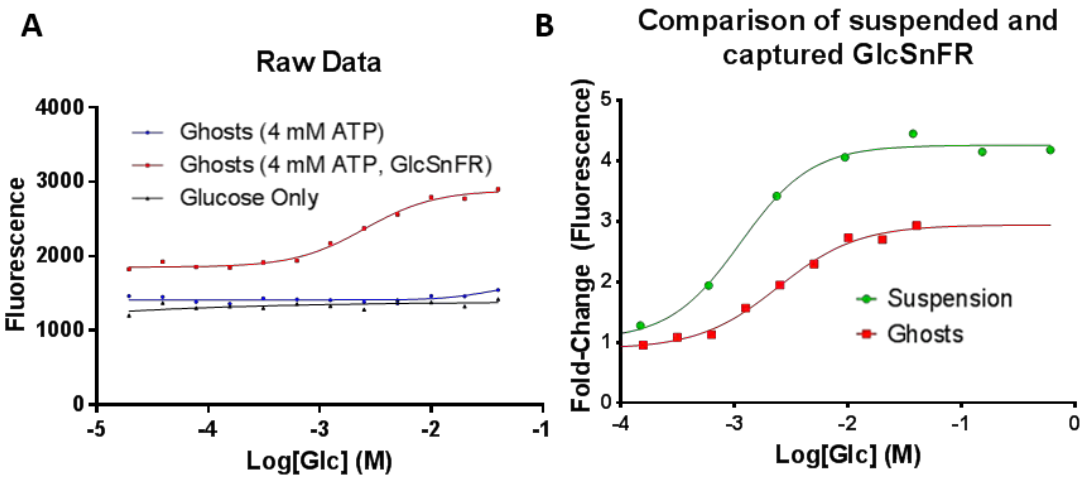
A
Raw Data
Ghosts (4 mM ATP)
Ghosts (4 mM ATP, GlcSnFR)
Glucose Only
Fluorescence
Log[Glc] (M)
B
Comparison of suspended and captured GlcSnFR
Fold-Change (Fluorescence)
Suspension
Ghosts
Log[Glc] (M)

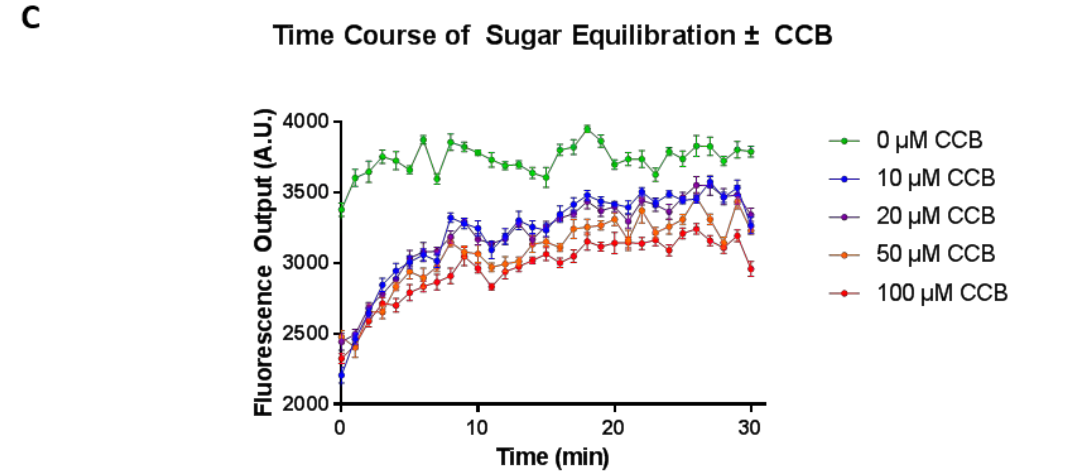
C
Time Course of Sugar Equilibration ± CCB
Fluorescence Output (A.U.)
0 µM CCB
10 µM CCB
20 µM CCB
50 µM CCB
100 µM CCB
Time (min)

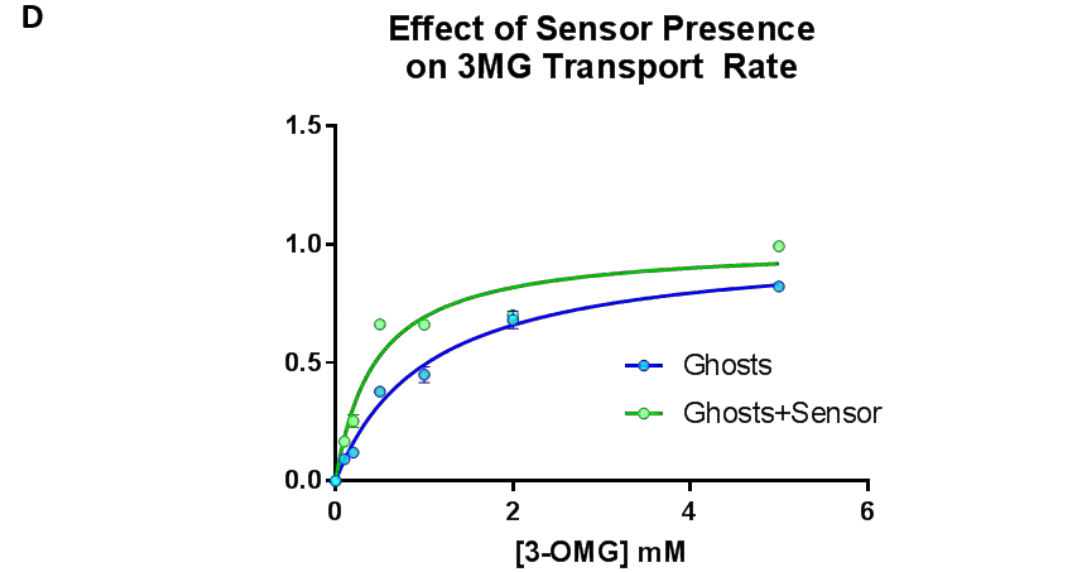
D
Effect of Sensor Presence on 3MG Transport Rate
Ghosts
Ghosts+Sensor
[3-OMG] mM

Figure 3.6 **Effects of sealing GlcSnFR within erythrocyte ghosts.** We explored the possibility that the presence of GlcSnFR within erythrocyte ghosts effects the kinetics of glucose transport or sensor fluorescence. **A:** Equilibrium kinetics of fluorescent ghosts. Abscissa: Concentration of glucose (log_{10}[M]); Ordinate: Fluorescence output (arbitrary units). Fluorescence of erythrocyte ghosts is dependent on inclusion of GlcSnFR and dynamic with glucose concentration. **B:** Comparison of GlcSnFR glucose response in ghosts and free in solution. Abscissa: Concentration of glucose (log_{10}[M]); Ordinate: Fluorescence output (fold change over zero glucose control). GlcSnFR's kD for glucose is elevated in ghosts, measuring at 2.5 mM at room temperature instead of 1.4 mM. Further, the maximum ratio of fluorescence is approximately 3:1, down from 4:1. **C:** Cytochalasin B attenuates rate of fluorescence response to glucose added to cell exterior. Abscissa: Time (minutes); Ordinate: Fluorescence (arbitrary units). Time courses of glucose uptake were measured as a function of fluorescence increase. Cells were pre-treated with CCB (0 – 100 μM) to inhibit glucose transport. **D:** Radiolabeled 3MG uptake. Abscissa: Concentration of 3MG (mM); Ordinate: Normalized transport rate.

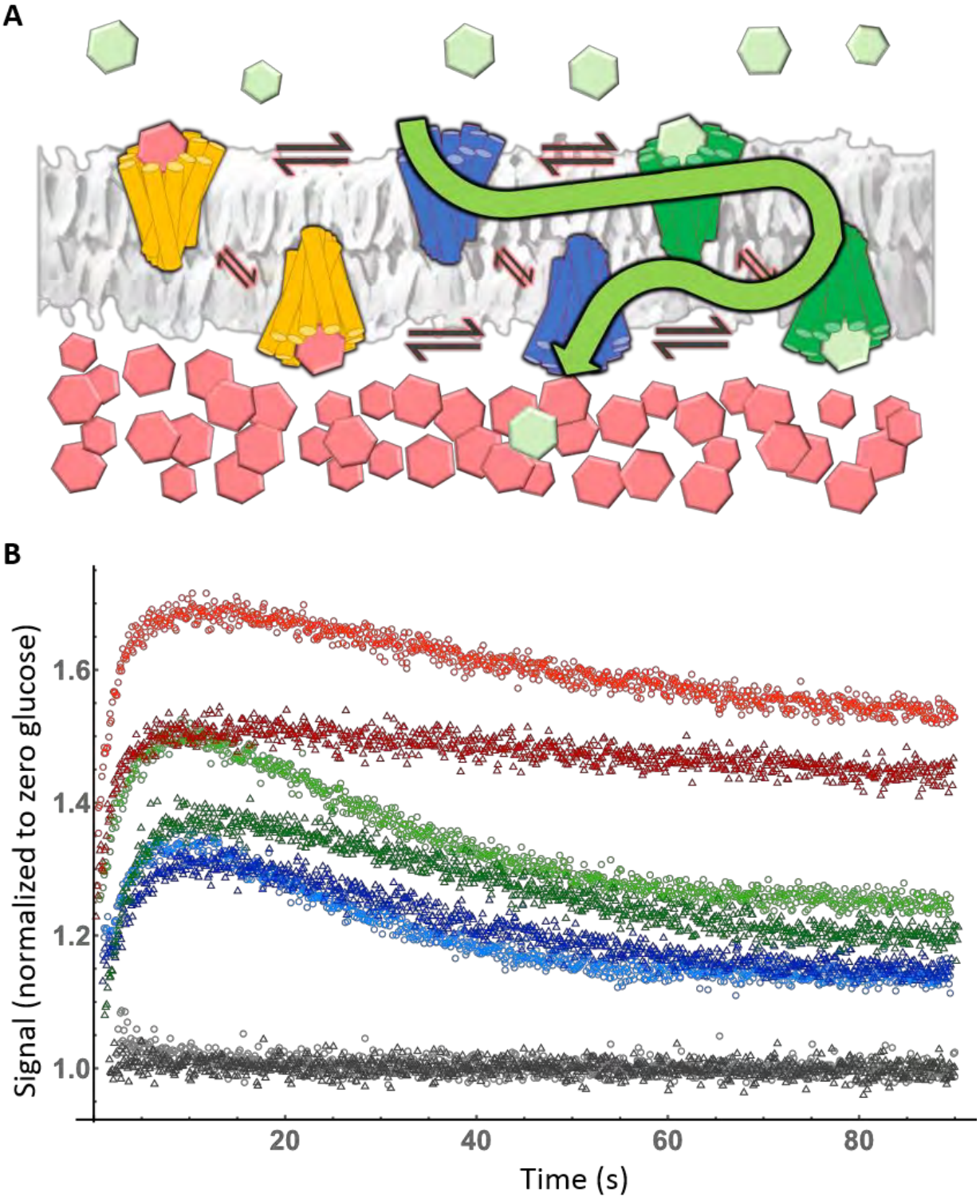
A
B
Signal (normalized to zero glucose)
1.6
1.4
1.2
1.0
20
40
60
80
Time (s)

Figure 3.7 Recapitulation of counterflow transient confirms equilibration is GLUT1-mediated.

A: This cartoon schematic shows the early stage of a counterflow experiment. Green hexagons: detectable sugar; Red hexagons: undetected sugar; Yellow cylinders: GLUT1 bound to undetected sugar; Green cylinders: GLUT1 bound to tracked sugar; Blue cylinders: Unbound GLUT1; Green arrow: path of translocating tracer sugar from out to in. We see from the diagram that in early stages of equilibration, exterior tracer sugar is transported in while cytosolic concentrations of undetected sugar are many times higher than the tracked sugar. Upon release into the cytosol, the tracer sugar is outcompeted for binding to the cytosolic face of the transporter. During this period, concentration of tracer sugar increases past the equilibrium value. As the untracked sugar concentration decreases, the tracer sugar occupies a more proportional fraction of carrier and returns to the equilibrium concentration. **B:** Demonstration of counterflow transients in AMP- and ATP-containing fluorescent ghosts. Abscissa: Time (seconds); Ordinate: Signal (normalized to initial value); Triangles: 4 mM ATP, Circles: 4 mM AMP; Gray traces: 0 mM glucose, blue traces: 0.5 mM glucose, green traces: 1.0 mM glucose, red traces: 4.0 mM glucose. Counterflow was observed in cells preincubated in 80 mM 3MG for one hour. Uptake was done in ATP- and AMP-containing ghosts injected into a cuvette containing varied glucose concentrations.

Chapter 4

SINGLE CELL ANALYSIS OF ERYTHROCYTE GHOSTS

Abstract

We applied confocal microscopy to resealed erythrocyte ghosts containing the fluorescent glucose sensor GlcSnFR to continuously monitor glucose transport with high temporal density and single cell resolution. We developed an assay to immobilize ghosts on glass coverslips which allowed the use of a perfusion-based oscillating stimulus transport assay (OSTA) to evaluate uninterrupted, alternating uptake and efflux of sugar in the observed cells. This experimental framework was first used to investigate standing question regarding GLUT1 phenomena observed in resealed ghosts: are the measured kinetic complexities of transport fundamentally derived from the nature of the transporter, or from a heterogeneous population of cells, each with variable transport capacity, generated by an inconsistent nature inherent in the resealing process. We observed that in ghosts resealed with GlcSnFR and 5 mM of either ATP or AMP, there is a single class of cells observed with shared kinetic profiles. The same study provides direct and conclusive evidence of another GLUT1 behavior, the ATP-dependent asymmetry of GLUT1 uptake and efflux. Evaluation of the rates of fluorescence change in the two cell types clearly shows equal and opposite flux in the AMP-containing population, but approximately half the rate of efflux compared to influx in ATP-containing ghosts. To date, this technique has been used only to provide semi-quantitative data for the direction and relative magnitude of glucose fluxes between cells under varied conditions due to operational constraints related to sensor photomodification that prohibit direct quantification of glucose concentrations from fluorescence, but we conclude that refinement of the protocol could mitigate these difficulties and provide access to a great deal of information about GLUT1 kinetics.

Introduction

The conventional philosophy applied to systems of chemical or kinetic reactions assumes that any spacial or temporal phenomena which might manifest from the evolution and equilibration of diffusion-regulated intrasolvent concentration gradients occur on a timescale where events proceed significantly faster than those in the aforementioned reaction scheme. This allows the practical presumption of an instantaneous homogeneity of solute concentrations whose dynamics are then completely defined by the equations describing the relatively slower kinetic and chemical reactions. Indeed, the effects of rapid kinetic mechanisms such as diffusion are bundled into the rate constants used in the rate equations of the slower reaction schema. It is for this very reason that the numeric value of each rate constant is valid only within the experimental conditions in which it was measured. Changes in physical or chemical properties of the reaction medium will not prevent the application of the instantaneous solvent homogeneity assumption, but will alter the kinetics of the rapid processes and subsequently determine the specific nature of the reaction environment experienced by the slower chemical activities. This is manifest in the mathematical relationships between reaction rate constants and systemic variables such as temperature.

As with most assumptions, the justification of their application to enable the simplification and reduction of the processes of a reaction system and its mathematical framework must be considered each time such a system is defined. In this case, instantaneous solvent homogeneity becomes less reasonable either as the solvent volume increases or the solvent composition becomes inherently heterogeneous. It is the latter consideration that has been hypothesized as a constituent factor in certain kinetic phenomena observed during various investigations into cellular glucose homeostasis. The time courses of sugar equilibration measured by a variety of experiments show multiphasic kinetic profiles. Further, this is usually only apparent on a logarithmic time scale, suggesting that distinct processes may be individually responsible for the equilibration seen during each phase. Naftalin, Smith,

and Roselaar put forward a hypothesis that the apparent kinetic partitioning of sugar equilibration is due to lowered rates of sugar diffusion in the cytosol versus the exterior solvent as well as sequestration of cytosolic glucose through associations with other intracellular molecules and/or structures (Naftalin et al., 1985). These ideas were later supported by the observations that equilibration of 3MG across the membranes of human RBCs and resealed ghosts is slowed proportionally to solvent viscosity while the poorly (and thus slowly) transported substrate 6-NBD glucosamine is not. Together, the observations that changing the diffusive properties of the solvent is rate-limiting for the rapidly transported substrate 3MG, but not rate-limiting for the slowly transported substrate, 6-NBD glucosamine, suggest that diffusion kinetics are taking place on a time scale closer to that of the heterogeneous reaction scheme than previously considered and that diffusion-mediated sugar exchange between adjacent solvent volumes within the erythrocyte cytosol should be considered a measurable dynamic process (Cloherty et al., 1995). Further study of the very early (~5 ms intervals) and late (8 hours) periods of equilibration revealed that there may be as many as three individual phases which were hypothesized to result from the binding of substrate to the transport proteins (GLUT1), binding of translocated substrate to intracellular structures, and diffusion between cytosolic solvent partitions (Blodgett and Carruthers, 2005). The idea that early phases of equilibration rates are derived from a rapid equilibrium of substrate:protein binding states was later contradicted by observation of multiphasic time courses of ^{3}H-3MG equilibrium when it was added as a minute tracer to the exterior of cells already at equilibrium with the solvent which contained a concentration of cold 3MG which was effectively unchanged by the addition of tracer solute molecules. This showed that the multiphasic time courses could not be attributed to a period of sugar:protein equilibration, as this has already occurred prior to the addition of labeled substrate (Leitch and Carruthers, 2007). The same study showed that the multiphasic equilibration is an ATP-dependent phenomenon, occurring in RBC ghosts only when they are resealed in the presence of ATP. It was also demonstrated that the human equilibrative nucleoside transporter-1

(ENT1) effects monophasic uridine transport in an ATP-independent manner. This led to an additional hypothesis that the diffusion rate dependence of sugar equilibration may also depend upon the distribution of GLUT1 within the cell membrane.

It became clear that the geometric homogenization of the theoretical framework for glucose equilibration kinetics was no longer an easily justifiable simplification. However, before we can draw any definitive conclusions about the contributions of translational kinetics to these observations, there remains an additional general hypothesis which can account for the existence of the multiple equilibration phases. Each of the studies mentioned above collected data by measuring populations of cells, not individuals. As such, there is no definitive proof that these populations are not composed of heterogeneous cell types as pertaining to the protein contents of their membranes, completeness of lysis, or the cytosolic contents introduced during the resealing process (ATP). The conclusions that can be claimed about GLUT1 kinetics and their role in the observed characteristics of glucose equilibration are vastly different depending on which class of hypothesis, the geometries of individual cells versus the stratification of the cell population, is shown to be correct. The first informs of a persistent behavior arising from the function of GLUT1 and the structure of the erythrocyte while the second provides the almost tautological conclusion that measuring the properties of a mixed cell population *en masse* will result in the observation of mixed behaviors.

We sought to address the ambiguity between these two hypotheses by observing populations of ATP- and AMP-containing resealed erythrocyte ghosts by fluorescent microscopy. In doing so, we will have access to single cell data as well as the entire population of cells in the microscope's field of view. This should allow a clear affirmation or rejection of the hypothesis that erythrocyte ghost populations are multimodal in their kinetic behavior. This will be especially important for the ATP-containing population as they have the greater potential for heterogeneous composition arising from non-uniform enclosure of ATP. This is true in the case of the AMP-containing ghosts as well, but there is no known

effect of AMP on the function of GLUT1 or the structure of the erythrocyte when compared to creating ghosts with no nucleotide at all.

Materials and Methods

Materials

Whole blood (#100-17) was purchased from Biological Specialty Corporation. 35 mm poly-D-lysine coated glass-bottom (#1.5) culture dishes were purchased from Mattek (#P35GC-0-14-C). Biotinylation reagent: EZ-Link Sulfo-NHS-LC-Biotin (Life Technologies # 21335). Streptavidin, tetravalent (Thermo Fisher Scientific #PI21125). Biotinylated BSA (Thermo Fisher Scientific #PI29130). Gravity-fed perfusion system was purchased from Automate Scientific. Any other chemicals not mentioned above were purchased from Sigma Chemicals. Fluorescence-enabled compound light microscopy was conducted using a Zeiss Axioscope with green and red filters, 100x 1.5 NA oil-immersion objective. Confocal images were acquired using a Leica TCS with 488 nm laser and 63x oil immersion objective.

Solutions

Kaline buffer contains 150 mM KCl, 5 mM HEPES, 0.5 mM EDTA, and the pH is adjusted to 7.4 at experimental temperature. Erythrocyte lysis buffer contains 10 mM Tris·HCl, 4 mM EDTA, and the pH is adjusted to 7.4 at 4 °C.

Biotinylation of human red blood cells.

Whole human blood was suspended in 4 volumes of room temperature PBS and then centrifuged at 6000xg for 5 minutes. The supernatant was removed and the pellet washed by resuspension in 5 volumes of PBS. This was repeated three more times (4x total dilutions). The pelleted blood cells were resuspended in PBS at 279 μL cell pellet per 1 mL of the final volume of biotinylation buffer/blood solution. Biotinylation reagent was dissolved in water (it will not dissolve directly into PBS) at a concentration of 50 mg/mL and then subsequently diluted to 5 mg/mL with PBS. This buffer was

used to resuspend the cell pellet in the ratio stated above. The reaction proceeded at room temperature for 30 minutes and then the reaction was quenched with 5 volumes of 100 mM glycine.

Adhesion of RBC ghosts to cover glass.

Cover glass was treated by incubating with a covering volume of 5 mg/mL biotinylated BSA solution (in water) for 5 minutes. The glass was rinsed 3x with diH_2O and then treated with 0.1 mg/mL streptavidin solution (water). This was incubated at room temperature for 5 minutes and then rinsed with water 3x. Prepared biotinylated fluorescent RBC ghosts were resuspended at various concentrations in 2-3 mL of kaline per dish and then centrifuged at 100-300xg for 3 minutes (they will not settle onto glass in fewer than 8 hours, data not shown) to attach them to the immobilized streptavidin on the glass. The buffer was exchanged for fresh, RBC-free kaline and they were kept in the appropriate experimental temperature and condition until imaging began.

Results and Discussion

Development of confocal microscope assay: We developed a method for immobilization of fluorescent ghosts on glass coverslips for use in perfused microscope assays. Prior to lysis, whole blood was washed and then biotinylated using NHS ester linkage. This was undertaken prior to creating ghosts to minimize access of the reagent to the cell interior and the GlcSnFR probe. Following biotinylation, ghosts were made as usual. Concurrently, biotinylated bovine serum albumin (BSA) was adsorbed onto clean coverslips, washed, and treated with streptavidin solution. Prepared ghosts were centrifuged gently (100xg) onto the treated cover glass. Because streptavidin is tetravalent with two axially aligned, outward facing dimers, one face can interact with the adsorbed, biotinylated BSA and the other will remain available for binding. When the ghosts are applied to the slip, they are bound by the immobilized streptavidin and the cover glass. We tested the proof of concept of this assay using whole RBCs without sensor and found that we were able to achieve cell immobilization without seeming to cause them harm (Figure 4.1A). To evaluate the degree of coverage of our biotinylation, we applied

fluorescent streptavidin to glass-bound RBCs. We found our biotinylation protocol provides diffuse, but complete coverage of the membrane (Figure 4.1B). Extension of the protocol to include post-biotinylation lysis and resealing with GlcSnFR demonstrated no apparent adverse effects with regard to the baseline fluorescence of GlcSnFR, nor did it show any difficulty in achieving membrane closure. This is evidenced by the lack of signal loss to protein diffusion out of the cell. This protocol was successful for both AMP- (Figure 4.1C) and ATP-containing ghosts (not shown). Because the biotinylation is non-specific and can result in linkage to effectively any surface protein, we confirmed that there were no resulting adverse effects on GLUT1 kinetics. This was accomplished using the canonical radiolabeled sugar transport assay. Zero-*trans* uptake into +/- biotinylated red blood cells was measured using 5 mM ^{3}H-3MG. We found that time courses comparing biotinylated and unbiotinylated RBCs demonstrated no significant differences in their kinetics (Figure 4.1D).

Having confirmed the preservation of both membrane and GLUT1 functionality post-immobilization, we evaluated sample integrity following a series of buffer perfusions. Additionally, continuous perfusion can result in cell detachment. Not only does this eventually result in the complete loss of the cell, but release is often preceded by gradual deformation and a shift in signal that results from the change in geometry, not sugar concentration. We performed imaging while perfusing using the OSTA method (Keller and Looger, 2016). Briefly, this assay is not fundamentally different from a standard continuous microscope assay with perfusion except for the pattern of buffer delivery which alternates between two solutions, typically one with substrate and the other without. With an optogenic sensor for said substrate present, the periodic oscillations can provide a great deal of information about the transport process responsible for translocation of the substrate. We conducted this assay using two sources of kaline buffer with 0 or 25 mM glucose. The zero glucose buffer contained the red dye rhodamine to provide verification of buffer exchange in the field of view and to indicate the time taken for complete exchange between the buffers (Figure 4.2A). Here we see a

complete exchange time of approximately 3 seconds (Figure 4.2B). We also report that over a time course of ten minutes of constant perfusion at a rate of 4.0 mL/min (66.1 uL/s), there were no detached or partially detached cells and morphology was consistent from start to finish (not shown). Additionally, we are able to reduce the buffer exchange time to approximately 1 second by increasing the flow rate from 4.0 mL/min to 12.0 mL/min without any negative effects on ghost adhesion or morphology (not shown).

We did observe a characteristic of the sensor that warrants further attention. The green channel recording from Figure 4.2A shows a gradual increase in the local minima and maxima following each buffer exchange. We originally hypothesized that this was because the net change in cytosolic glucose was only partially equilibrating following each cycle and that the signal would plateau as it approached this point. However, during more extended imaging, we observed an eventual reversal of this trend and the signal began to decline. This was not surprising, however, as fluorescent molecules are known to photobleach as imaging continues. What was surprising was that when, during the increasing baseline phase, we stopped imaging, removed glucose completely, and retained zero sugar conditions for 10 minutes then resumed imaging, we saw that the imaged cells were still bright compared to their unimaged neighbors (Figure 4.2C, inset). When we resumed imaging of the previously exposed field, the signal did begin to decline, and we verified as above that the decrease was due to photobleaching (not shown). This led us to conclude that there are two possible photomodifications of GlcSnFR and that they can be applied sequentially: photoactivation, or “kindling”, and photobleaching. These phenomena were not observed in our fluorimetry experiments because of the high turnover rate of which cells are in the light path due to the stirring in the cuvette. In the confocal microscopy assays, however, there is no turnover of exposed sensor molecules and those which are modified accumulate and reveal these events. As such, until rigorous testing of the kinetics of these modifications can allow disambiguation of changes in signal from sensor modification rather than

glucose binding, we will refrain from attempting direct analysis of glucose concentrations and only discuss qualitative and semi-quantitative measurements from the microscopy assay.

Single cell transport measurement: Using the confocal assay described above, we evaluated transport in individual ghosts within the field of view. Samples were prepared with 5 mM of either AMP or ATP. Buffers were alternated between 0 and 10 mM glucose in kaline for 20 seconds each (40 second total period). Individual cells were selected using a sequence of built-in functions in Mathematica and signal data was parsed based on image masks created for each cell (Figure 4.3A).

Total pixel intensity was calculated for each region of interest (ROI) and normalized to its value at t_0. We also applied a lowpass filter with cutoff 0.1 to remove high-frequency noise from the data traces. AMP- and ATP-containing cells were plotted on two graphs with each trace from the same group overlaid (Figure 4.3B). Comparing the two cell conditions does not reveal any clear differences between them. The AMP-containing ghosts appear to increase in signal faster, but only slightly. In both sets of traces, we see the effects of photoactivation and bleaching accumulating at different times in different cells. This is expected if we consider each ROI as a relatively small set of stochastic processes (pixels). Indeed, in the final period of each set we can see individual cells which are still increasing in fluorescence while others have already peaked and begun to dim.

We next sought to evaluate the rates of fluorescent signal movement in each condition. The derivative of each trace was approximated using first differences of the smoothed, normalized signal values (forward-facing) and dividing by the time step. These values are plotted in Figure 4.3C. Unlike the raw fluorescence values, the rate data show a clear difference between the AMP- and ATP-containing ghosts. In ghosts resealed with AMP, the magnitudes of the rates of fluorescent increases that accompany the uptake periods are approximately equal and opposite the subsequent negative efflux peaks. This symmetry is in line with observations made using radiolabeled substrate and matches

the simple presumptions (but not requirements) of a passive carrier. Looking at the ATP-ghost graph it is clear that the efflux period is only about half the magnitude of the preceding influx, a marked difference in behavior compared to the AMP-containing cells. Further, this validates previous observations that intracellular ATP slows GLUT1-mediated sugar efflux and that it does so asymmetrically, resulting in GLUT1 kinetics which demonstrate a higher capacity for influx rates compared to efflux. Even without the current existence of an experimental and computational framework to convert microscopy-derived fluorescence into glucose concentrations, the qualitative trends are distinct between the two groups, recapitulated on a single cell scale, and observed repeatedly during each period of buffer oscillation. These observations mark the most direct evidence of ATP-induced GLUT1 asymmetry in human erythrocytes.

While it appears to us from the collected data that the trend is shared among each cell in the AMP- and ATP-containing populations, we wanted to examine the distributions of the populations as a whole as well as during each cycle of the buffer exchange. Within each period of the OSTA data traces we calculated the ratio of the greatest observed positive and negative magnitudes of rate of change in fluorescence for each individual cell. For each cycle and condition, we created a histogram of influx:efflux ratios. We expected that if the behavior is shared among the cells of each population, these histograms should resemble normal probability distributions. Histograms of ratios were constructed by binning with 0.05 intervals and normalizing the area to unity. We then used nonlinear regression to fit a normal curve to each binned data set and saw good agreement between them (Figure 4.4, insets). Combining the individual histograms and fits results in the composites shown in Figure 4.4. At this point it is clear that while the unpartitioned histograms demonstrate a kurtosis not seen in a normal distribution, this is the result of a shift in population behavior over the course of the experiment as evidenced by the good agreement between individual cycle histograms and a normal fit. We are now confident in our assessment that each sample, ghosts with AMP or ATP, are of unimodal composition.

Further, we conclude that the addition of ATP to the cytosol of erythrocytes is sufficient to induce a change in GLUT1 kinetics from symmetric to asymmetric flux capacities.

Conclusions

In order to answer questions regarding the potential heterogeneity of populations of erythrocyte ghosts used to analyze kinetic data, we developed a confocal microscopy assay to monitor individual cells during periods of transport activity. We achieved this by biotinylating of RBC surface proteins and anchoring them to cover glass containing adsorbed biotinylated BSA and streptavidin. This allowed for constant perfusion of the cells with alternating buffers which alternated the direction of the glucose concentration gradient repeatedly during time courses of imaging, providing visualization of transport activity during influx and efflux. As such, our efforts to use the GlcSnFR probe to examine GLUT1-mediated transport in single cells was successful, but not without its limitations.

During these experiments we became aware of specific photomodifications which can be made to GlcSnFR as a result of exposure to excitation wavelengths of light. It demonstrates the potential to bleach, losing its fluorescent capacity, but this is a hallmark of all fluorescent molecules. What we did not expect was its potential for photoactivation, an event which increases its fluorescent output by way of covalent modification, permanently (on the scale of fluorescence life time) shifting its behavior toward being brighter. These two modifications can be sequentially applied, but the necessity of that is uncertain. That is, activated sensor molecules can still undergo the bleaching photomodification(s), but we assume bleaching may occur whether or not it is preceded by activation. In either case, the ability to quantitate glucose concentrations from changes in signal is diminished by this ambiguity.

We were able to answer definitively, however, the question regarding population heterogeneity. Our experiments revealed that while there is variability in the populations of fluorescent ghosts, it conforms to the statistics of a normal distribution, the expected type of irregularity for a

population sampling. The presence of subpopulations within each class of cells would be likely to manifest statistically as a smearing of a gaussian distribution or some variety of multimodal sum of distributions. One could argue this is seen in the total histogram of cells, but we demonstrate that this heterogeneity is manifest in the different laser exposure times of the cells following each cycle of activity. When grouped by cycle, this broad heterogeneity disappears. We are confident in our assessment that fluorescent erythrocyte ghosts, and RBC ghosts populations in general, demonstrate kinetic phenomena derived from the general nature of GLUT1 rather than the composition of the sample populations used to measure them.

We also demonstrated with these experiments that cytosolic ATP in erythrocyte ghosts induces the oft observed asymmetry in GLUT1 transport capacities into and out of the cell. We used 5 mM ATP or AMP and observed that the former treatment resulted in influx rates around 1.7 times those of efflux while the latter demonstrated close to a 1:1 ratio of the two rates.

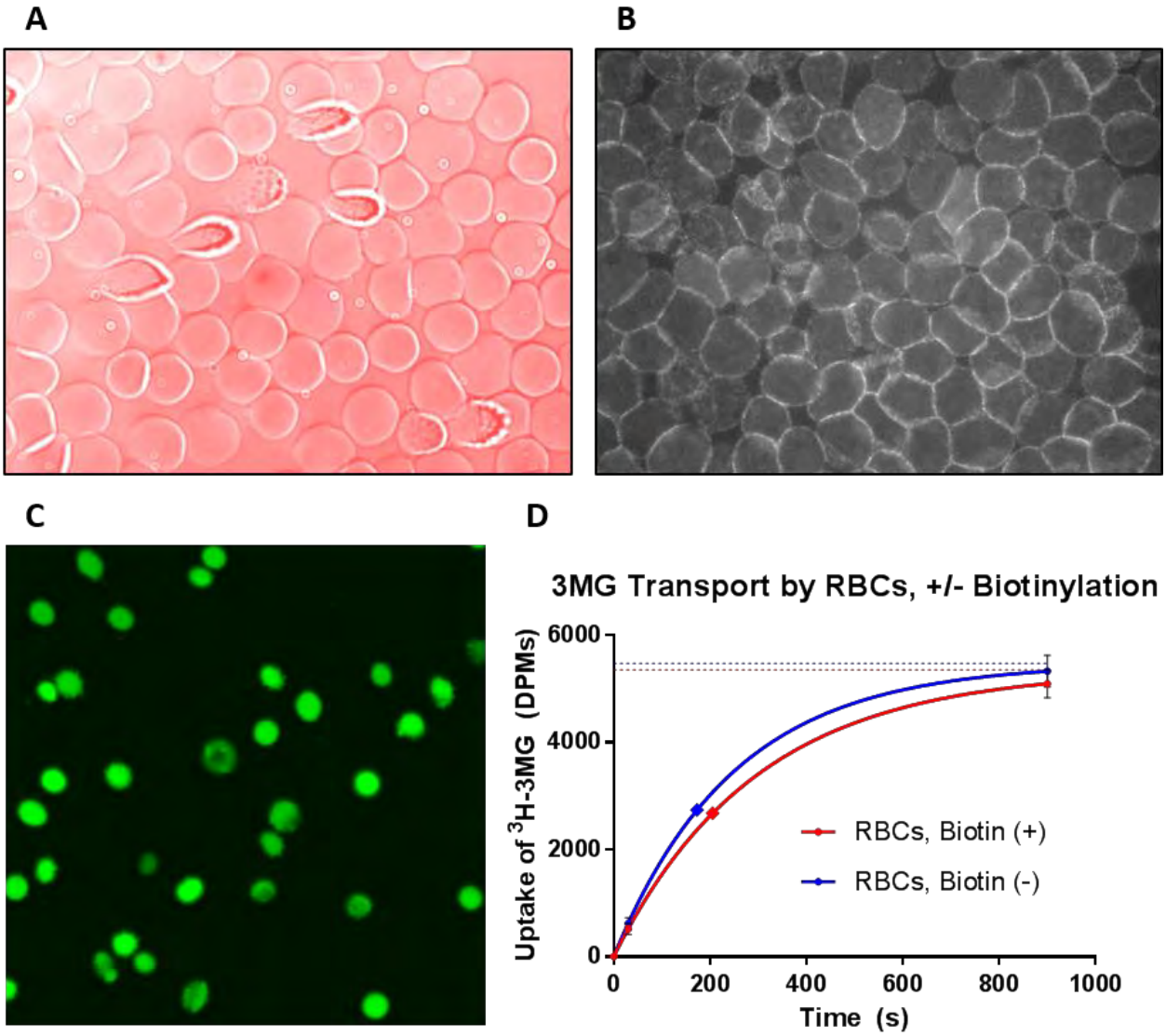

Figure 4.1 Biotinylation and slide adhesion of RBC ghosts.

A: Surface proteins of human red blood cells were biotinylated non-specifically and then bound to a biotinylated BSA :: streptavidin complex adsorbed to microscope cover glass. Cells were imaged at 1000x magnification on a fluorescence-enabled compound microscope. **B:** RBCs were prepared as in panel **A** and then treated with alexafluor-488-labeled streptavidin to visualize free biotin remaining on the RBC membranes. **C:** Human RBCs were biotinylated prior to hypotonic lysis and resealing with purified GlcSnFR protein to make fluorescent ghosts. These cells were then centrifuged onto glass-bottom dishes treated with the same complex described in **A** and **B**. Imaging by confocal microscopy demonstrates successful membrane closure and adhesion to glass. **D:** To test the effects of surface biotinylation on GLUT1 function in RBCs, the biotinylation protocol was repeated as described above and resulting cells were used in a radiolabeled 3MG uptake assay. Ordinate: Time (seconds); Abscissa: Total 3MG uptake (DPMs). We see no significant difference between uptake in biotinylated and untreated RBCs.

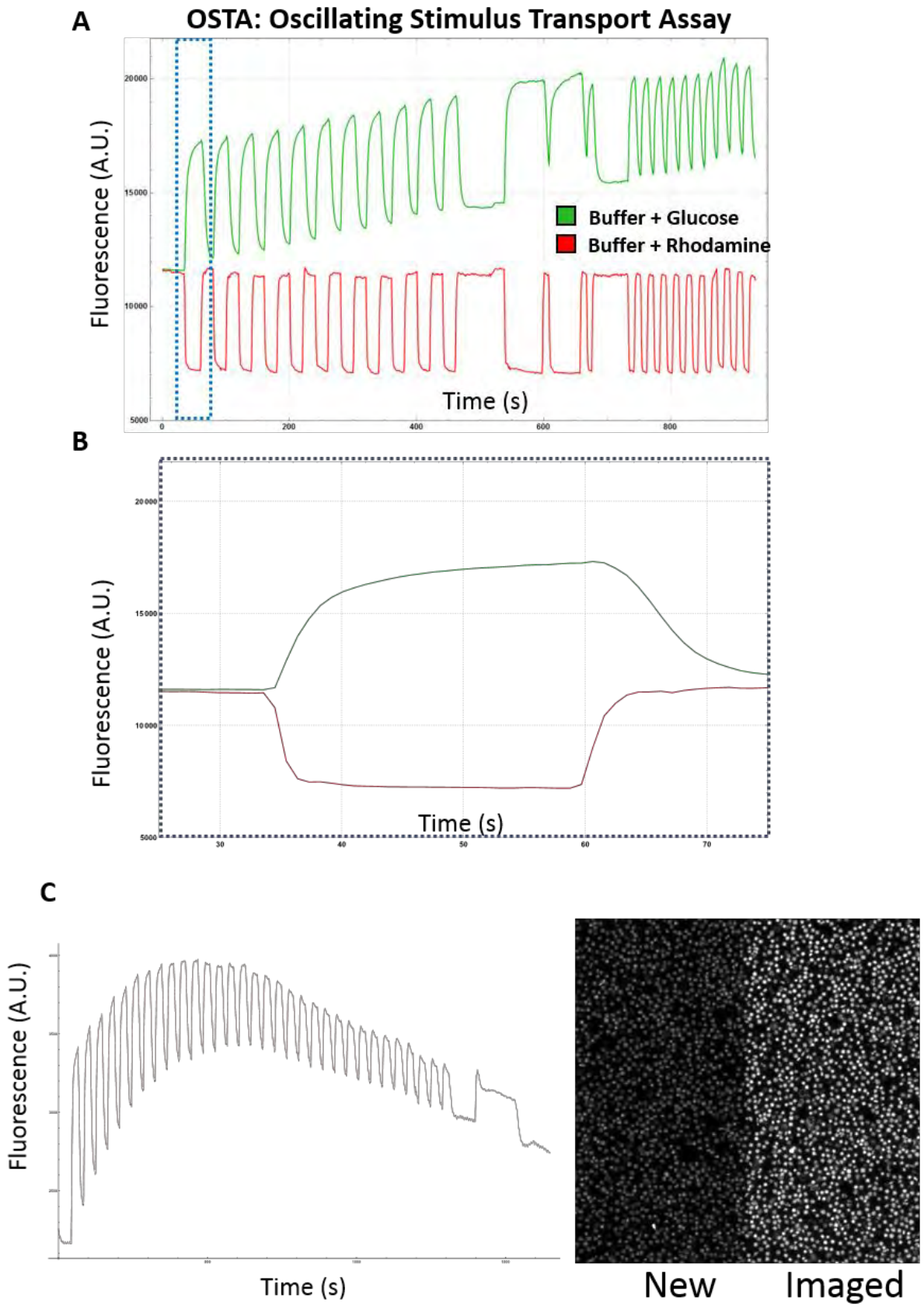
A
OSTA: Oscillating Stimulus Transport Assay
Fluorescence (A.U.)
Time (s)
Buffer + Glucose
Buffer + Rhodamine
B
Fluorescence (A.U.)
Time (s)
C
Fluorescence (A.U.)
Time (s)
New
Imaged

Figure 4.2 Development of OSTA-enhanced fluorescent ghost microscopy assay.

Confocal imaging of erythrocyte ghosts was used to monitor glucose flux during alternating periods of influx and efflux. **A:** Glucose uptake and exit transport experiments were combined by alternating perfusing buffers of high and low glucose concentrations. This graph shows whole field integration of fluorescence from a static field of view during exchange of kaline buffers containing 25 mM glucose or 0 mM glucose and rhodamine dye. Ordinate: Time (seconds); Abscissa: Fluorescence (arbitrary units). Green traces are from the green channel and red traces from the red channel. The green trace is shifted up to allow easier visualization of both data sets. **B:** Traces from a single period of buffer oscillation. The region in this panel is taken from the dotted region in **A**. Ordinate: Time (seconds); Abscissa: Fluorescence (arbitrary units). The rhodamine dye in the zero glucose buffer allows for estimation of buffer exchange rates. Here we see complete exchange takes place in approximately 3 seconds with a flow rate of 4.0 mL/min. Increasing the flow rate to 12.0 mL/min results in a decreased exchange time of approximately 1 second. Colors are as indicated in panel **A**. Green traces translated vertically for visual clarity. **C:** Photomodifications of GlcSnFR include photoactivation and bleaching. Ordinate: Time (seconds); Abscissa: Fluorescence (arbitrary units). Fluorescent ghosts were imaged by confocal microscopy during OSTA buffer exchange perfusion of 10 mM and 0 mM glucose for 30 minutes. The graph shows glucose transport transients as well as a steady increase in baseline fluorescence until about 8 minutes into imaging whereupon the trend reverses and the baseline begins to decline. A repeat of this experiment was conducted, but stopped at 8 minutes at which point imaging was stopped and the sample was flushed with 0 mM glucose for 10 minutes. The field of view was shifted to the right by half of the horizontal dimension to concurrently view previously imaged and unimaged ghosts (inset). The previously imaged ghosts show a significantly higher background fluorescence compared to unimaged ghosts. The ten minute perfusion with zero glucose buffer should have removed any residual glucose. Any remaining cytosolic concentration would be present in imaged and unimaged cells. This indicates that the increase in fluorescence is the result of photomodification. Resuming imaging in the original field of view eventually results in total loss of fluorescence from the cells and is confirmed by juxtaposition with unimaged cells (not shown). This suggests that both photoactivation and bleaching can occur sequentially, though it is unclear how often bleaching occurs first.

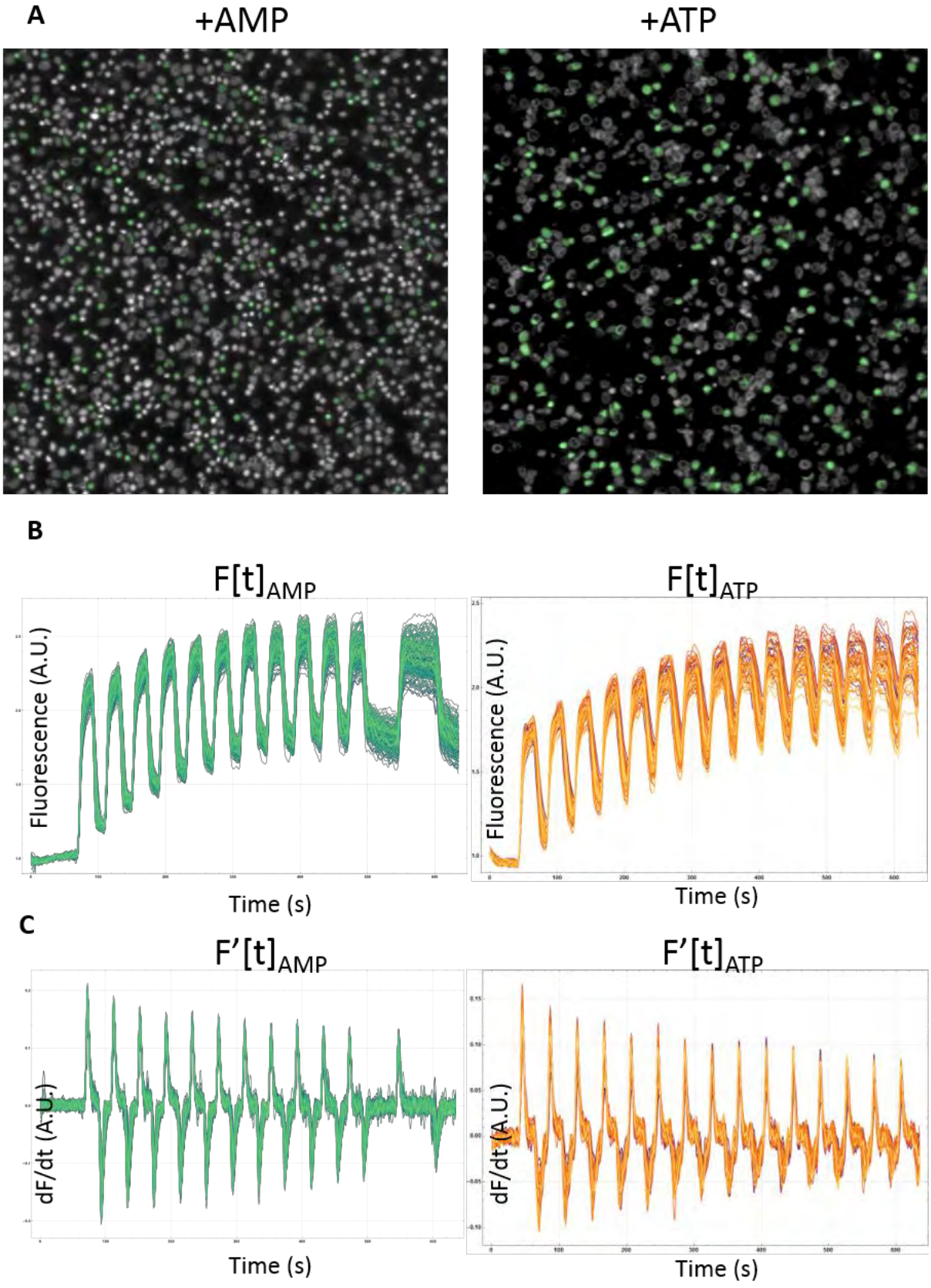
A
+AMP
+ATP
B
F[t]AMP
F[t]ATP
Fluorescence (A.U.)
Time (s)
C
F'[t]AMP
F'[t]ATP
dF/dt (A.U.)
Time (s)

Figure 4.3 Single cell analysis of glucose transport by GLUT1.

Adherent fluorescent erythrocyte ghosts were prepared with 5 mM AMP or ATP and attached to glass-bottom culture dishes. Cells were observed by confocal microscopy during OSTA buffer exchange. Individual regions of interest (ROIs) were selected using an algorithm constructed in Mathematica software. All cells were selected with identical criteria. A set of 180 individual cell ROIs were selected from each condition. **A:** Confocal field of view and individual regions of interest for AMP- and ATP-containing ghosts. Each ROI is indicated with green pseudo coloring. We also note that cells exhibited morphologies consistent with expectations for each nucleotide. **B:** Signal was collected from each ROI, processed, and plotted here. Ordinate: Time (seconds); Abscissa: Fluorescence (fold change). Signal data were processed for each ROI by normalizing average pixel intensities at each time point to initial intensity and then applying a lowpass filter (0.5 cutoff). It is clear that the optical properties of each ROI mature heterogeneously during the course of imaging, with a greater disparity between ROIs appearing in the ATP-containing cells. **C:** The signal traces from **B** were used to calculate rates of change of fluorescence. Ordinate: Time (seconds); Abscissa: Discrete rate of change of fluorescence (Fold change per second).

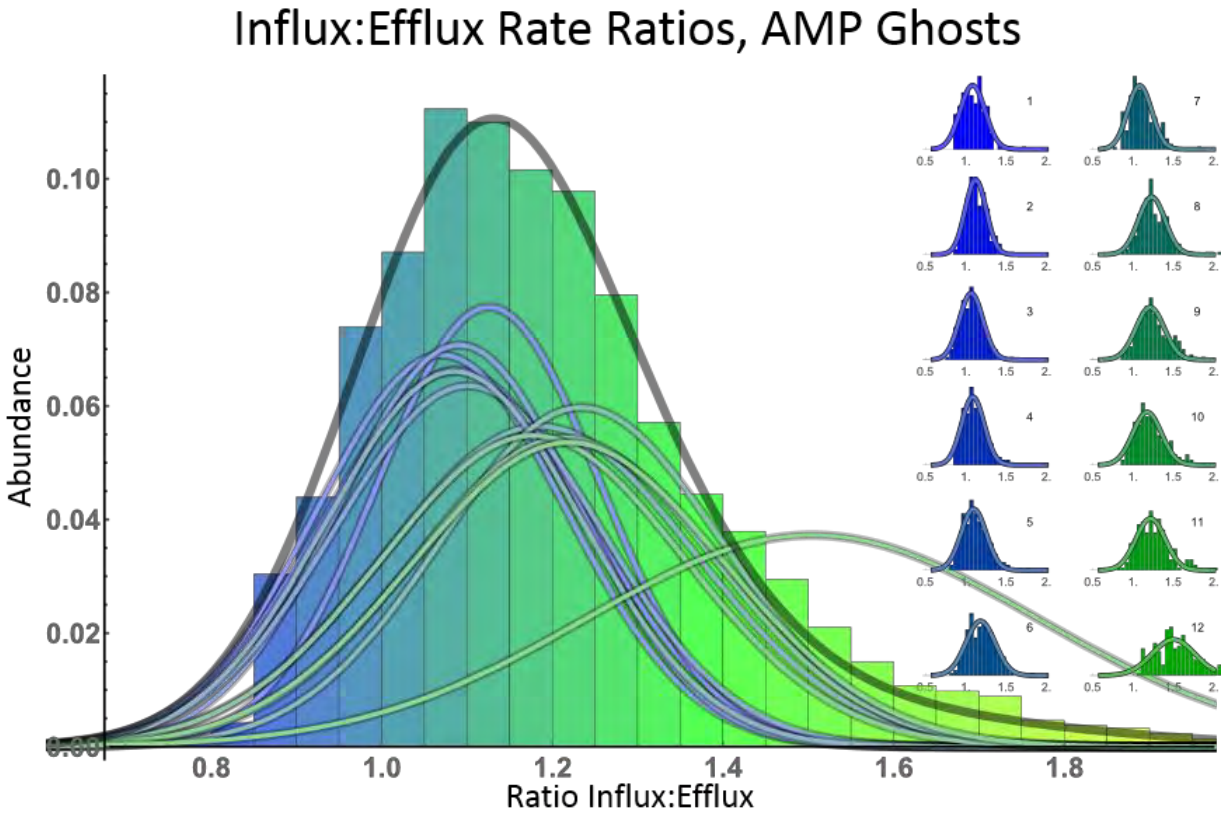
Influx:Efflux Rate Ratios, AMP Ghosts
Abundance
0.10
0.08
0.06
0.04
0.02
0.8
1.0
1.2
1.4
1.6
1.8
Ratio Influx:Efflux

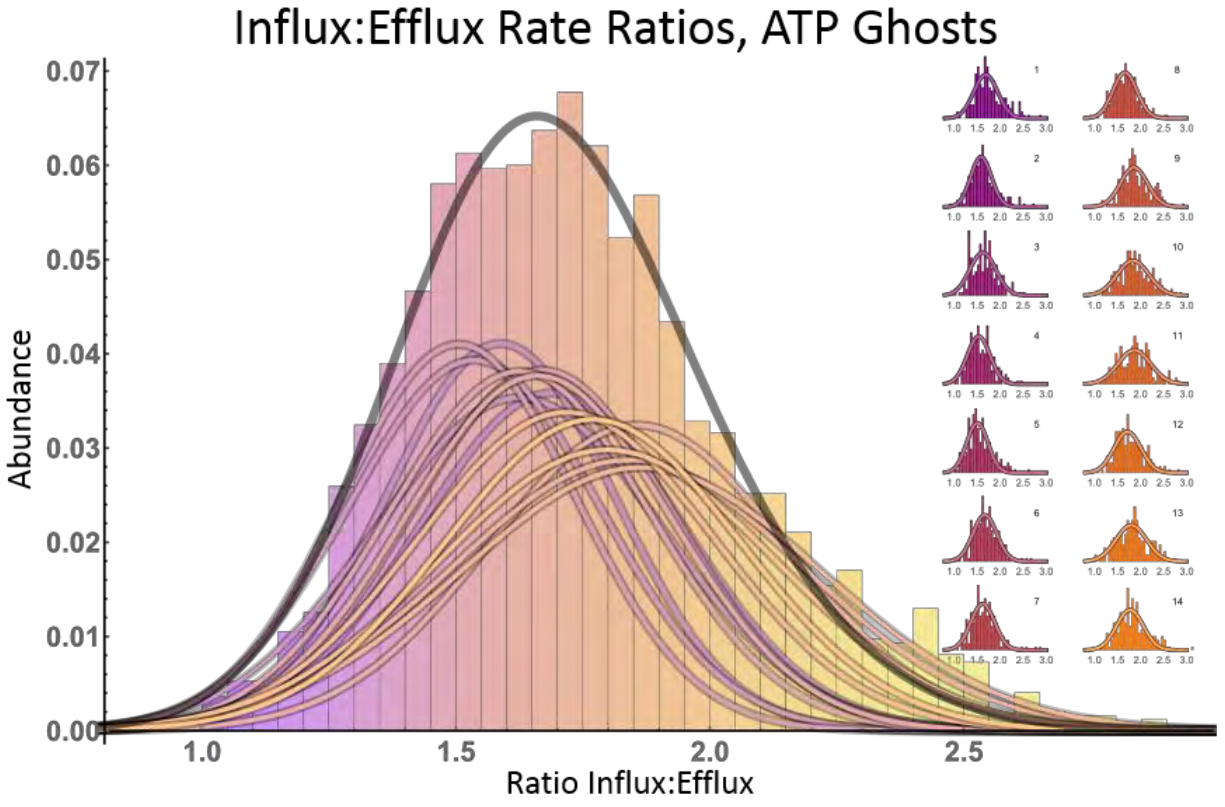
Influx:Efflux Rate Ratios, ATP Ghosts
Abundance
0.07
0.06
0.05
0.04
0.03
0.02
0.01
0.00
1.0
1.5
2.0
2.5
Ratio Influx:Efflux

Figure 4.4 Populations of AMP and ATP fluorescent ghost are unimodal by cycle.
Analysis of single cell microscopy recordings of glucose uptake and efflux in AMP- and ATP-containing cell populations. **A:** Erythrocyte ghosts prepared with GlcSnFR and 5 mM AMP were monitored during 12 cycles of OSTA buffer exchange, alternating between 0 and X mM glucose for 20 seconds each. Single cell traces were smoothed by lowpass filtering (0.1 cutoff) and derivatives estimated by taking forward-facing differences. Individual traces were partitioned by cycle and ratios of maximum influx and efflux rates were calculated. Single cycle histograms (insets) were normalized to unity and fit with a single gaussian distribution. The large histogram shows all ratios from all cycles and the sum (black) of each individual cycle's best fit gaussian (colored by inset). **B:** As with **A**, but for cells resealed with 5 mM ATP. Additionally, these cells experienced 14 cycles of OSTA with the same conditions as above.

Chapter 5

POPULATION KINETICS IN ERYTHROCYTE GHOSTS

Abstract

The utility of GlcSnFR in studying glucose transport kinetics relies upon the ability to convert fluorescence measurements into glucose measurements. Here we describe a systematic treatment of this problem in which we establish a rational framework for the calculations, determine the technical requirements to produce suitable data sets, and develop a fluorometric assay that supports the requirements of the theory. Following data collection and proper normalization, we use custom software to apply nonlinear curve fitting algorithms to systems of unsolved differential equations with a high degree of parameterization to find smooth curves through each data set. Rather than define the parameters of a model used to describe the data collected, this provides the means to generate smooth, differentiable curves that can be used in the calculations mentioned above. With these tools in place, we demonstrate that GLUT1-mediated kinetics of glucose transport as measured by the fluorescent sensor GlcSnFR recapitulate previous findings which demonstrate intracellular ATP (versus AMP) lowers the V_{max} for sugar entry, but increases the K_M. We are also able to show a previously unresolved linear dependence of internal K_M, when measured as the concentration of internal sugar needed to slow influx rates to half the original value, on subsaturating external glucose concentration.

Results and Discussion

Fluorimetry with red blood cell ghosts (equilibration curve standard): Ghosts were made from fresh whole blood and resealed with GlcSnFR protein in isotonic solution at 37 °C. We placed these in fixed volumes into a cuvette with zero glucose buffer and while monitoring the cuvette added glucose solution to it. The time course of sugar uptake was observed by measuring the change in fluorescent

signal in the cuvette (Figure 5.1A). Records of glucose entry were collected at varied starting extracellular sugar. Additionally, we allowed equal volumes of ghosts to equilibrate to various concentrations of sugar on the benchtop for an hour. These were then read in the cuvette at the same total volume of buffer, cells, and glucose concentration as the equilibration conditions. These were used to generate a standard curve of sensor:glucose binding (Figure 5.1B). The form of this curve is found by integrating the rate equation for the complex in a simple binding scheme and then taking the limit of t toward infinity. This reveals:

$$\frac{[Glc]\,F_{tot}}{[Glc]+K_D} \qquad \textbf{EQ 4.1}$$

where $[Glc]$ is the glucose concentration of the sample, F_{tot} is the total sensor concentration and K_D is the affinity of the substrate:sensor complex. We assume F_{tot} is a direct relation of signal converted to zero baseline and thus represents the maximum signal output in EQ3.1. Our first thought was to use this curve to back-calculate [Glc] from a time course of fluorescence data using the standard curve above, but that was flawed for two reasons: i) the standard curve form we used has already assumed steady state conditions, so would be inaccurate when used on dynamic fluorescent data, and ii) the asymptotic nature of the model results in wildly varying data as the input approaches saturation. This is clear in practice, as seen in Figure 5.1C. This presents a moderate problem as the solutions to the systems of differential equations behind most kinetic schema are unknown. As such, back-calculating [Glc] from fluorescence, F[t], does not have an explicit solution and equilibrium-based results are inadequate. These conclusions caused us to attempt to fit our data using numeric simulations of our reaction models. Using Berkeley Madonna simulation software, we set up an instance of the simple carrier model and performed parameter minimization on the error of our approximated fluorescence output function, resulting in the fit seen in Figure 5.1D. The fit is quite reasonable and has the added

benefit of concurrently simulating the time course of glucose concentration. We also realize here that our method of standardizing the fluorescence of each sample is insufficient for determining [Glc]. We developed a modified method for collecting and evaluating data with the fluorimeter and describe it here.

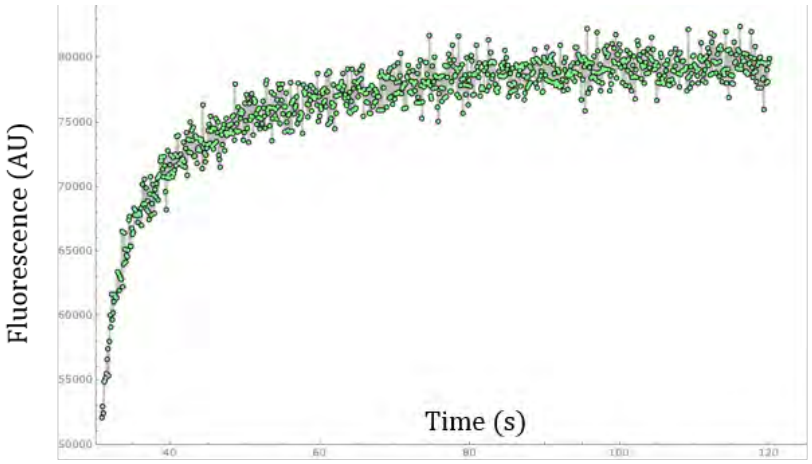

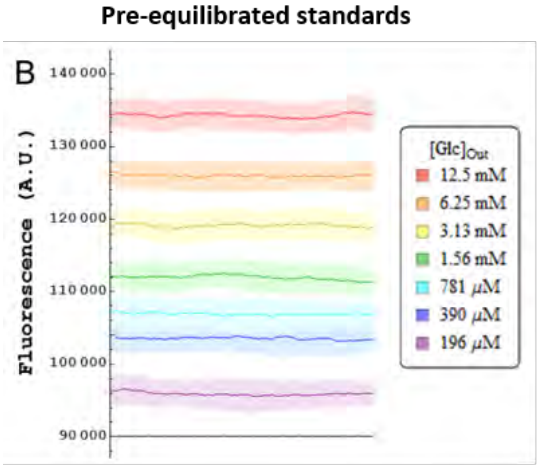

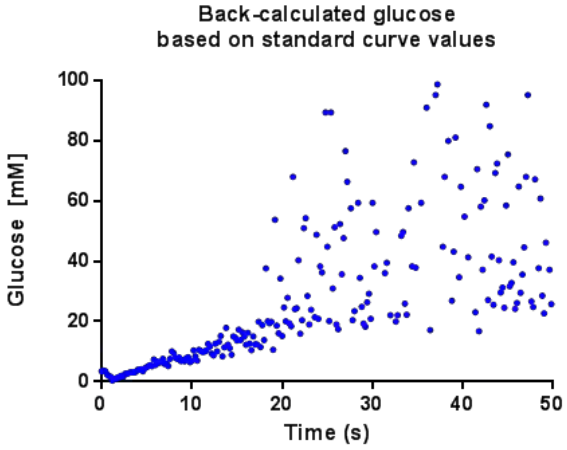

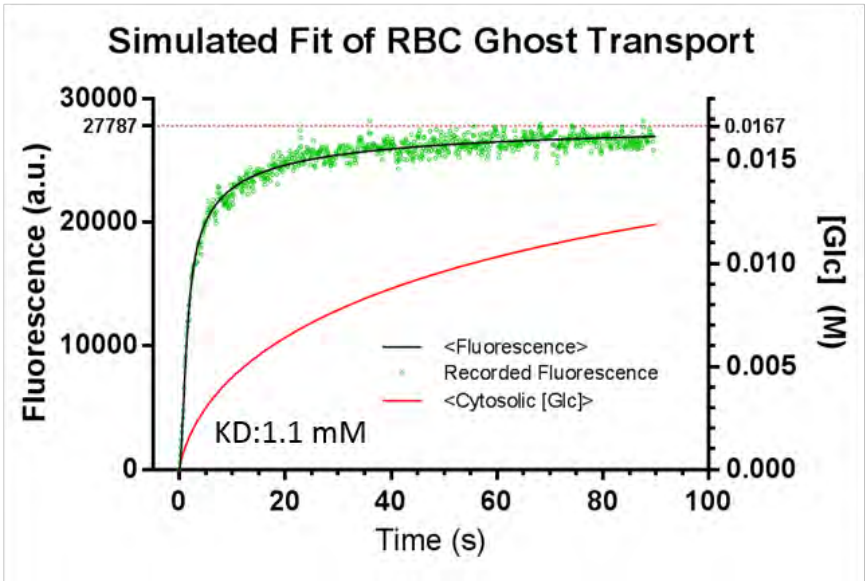

Figure 5.1 Creation of standard curve for the back-calculation of glucose concentration in fluorimeter

Fluorimetry with red blood cell ghosts (dilution curve standard)

Using fluorescence data as a precise quantitative measure requires being able to set the relative scale between individual measures. For the experiments described above, the addition of cells to the cuvette prior to the substrate provides a baseline reading of the sample which later serves as a normalizing value. However, we sought to design experiments which required the addition of cells to the cuvette at very small volumes. Signal begins to increase immediately due both to its baseline fluorescence mixing into the light path, but also because it begins interacting with the experiment. Without knowing its initial fluorescence, we can't normalize the signal and probably can't use the data. For this reason, we devised a method for establishing the full normalized range for a sample provided it is observed at some point in an equilibrium state.

A sequence of uptake experiments is conducted as above with varied glucose and the volume of diluting substrate is used to calculate for each sample what the baseline would be without any transport taking place. Each of these projected baselines is used to normalize the sample and the final equilibrium fluorescence value is matched to the concentration, generating the curve described above. Then, any sample with a time when the signal is at equilibrium and the glucose concentration is known can calculate its baseline with equation 4.2:

$$F_0 = \frac{F_{eq}}{m\left([Glc]_{EQ}\right) + 1} \qquad \textbf{EQ 5.2}$$

Where F0 is the unobserved baseline being calculated, m(x) is the best fit function for the standard curve, Feq is the fluorescence at equilibrium and [Glc]eq is the known equilibrium glucose concentration. This process is outlined in Figure 5.2.

Calculation of [Glc] from non-equilibrium F[t]

Here we describe our method for calculating the dynamic glucose concentration from a time course of fluorescence data. The chemical and rate equations for glucose:GlcSnFR binding is assumed to be as follows:

$$f + G \Leftrightarrow F$$

$$F'[t] = k_{on} f[t] g[t] - k_{off} F[t]$$

Solve for g[t]:

$$\boldsymbol{g[t]} = \frac{\boldsymbol{F'[t]} + k_{off} F[t]}{k_{on} f[t]}$$

With T = f[t] + F[t] being total probe concentration, replace f[t] with 1-F[t] and divide top and bottom by T and replace F[t]/T with P[T]:

$$\boldsymbol{g[t]} = \frac{\boldsymbol{P'[t]} + k_{off} P[t]}{k_{on}(1 - P[t])} \qquad \textbf{EQ 5.3}$$

Here, P[t] is the fraction of sensor bound and, since we have methods to normalize our data sets, we can scale from the domain [0,F_{max}] to [0,1] by dividing our data by F_{max} , which is also the maximum of our calibration curve. Thus, if we have our sensor's range and affinity constants, we can get glucose by measuring fluorescence and the derivative thereof. This presents one final issue before the analysis can be completed: noisy data produce very rough derivatives, so we must find a way to smooth our data sets before applying the above analysis.

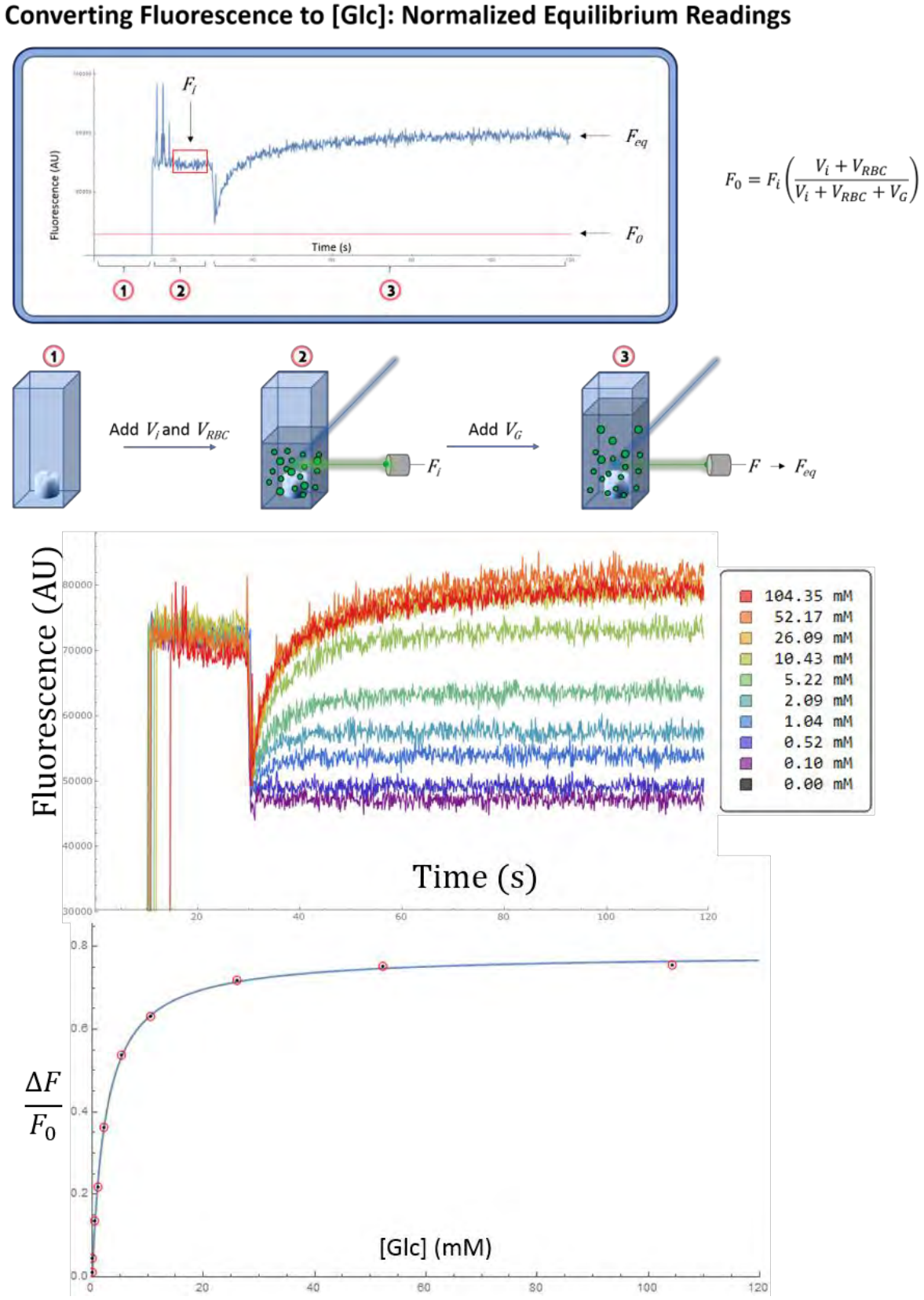

Figure 4.2 Conversion of fluorescence to glucose concentration

Data set smoothing by nonlinear regression of differential equations

We desired a regression method to that allowed for simultaneous fitting of multiple variables, parameters, and data sets. Further, it would be able to do this using differential equations in place of an explicit function. As this was highly valuable to our work, we have generated in-house software to accomplish this task. We will refer to it here as Deltaχ. In principle, the algorithm enacts regular Levenberg-Marquardt nonlinear regression, but with adaptations to include global fitting and non-explicit functions and parameters. We have also built in a smoothing routine which allows broadly applicable fits to data using over-parameterized systems. This is not useful for the direct analysis of the data, but approximates a curve through it. The fitted curve then provides a means of finding rates in data sets without the difficulty of other smoothing methods. Below we demonstrate the entire sequence of techniques described in the chapter to generate, smooth, and analyze data from fluorescent ghosts +/- ATP under zero-*trans* uptake conditions.

Counterflow is observed in ∞-*trans* entry experiments when saturating cold sugar on the cell interior is in extreme excess of external labeled sugar. When the labeled sugar enters the cell, it is unlikely to leave due to competition for exit sites with the more abundant cold sugar. Eventually both populations even out, but there is a transient state in which the labeled sugar surpassed its equilibrium concentration due to the aforementioned competition effect. The fluorescence assay using GlcSnFR has a functional equivalent in the form of 3MG. Because it is such a poor substrate for GlcSnFR, the 3MG acts as the cold sugar in counterflow when loaded at high initial concentrations in the cell. We loaded fluorescent ghosts with 80 mM 3MG and let them equilibrate at 20 °C for 1 hour. We then injected them in to a massively diluting volume of variable glucose concentration kaline in the cuvette. This was done with ATP and AMP-containing ghosts. The end of each run results in equilibrated cells with a known glucose concentration. These concentration values (Figure 4.3A) are used with the standard curve previously generated (Figure 4.3B) to find the expected fold-increase in fluorescence. This

provides the necessary information to normalize a set of curves relative to each other, not only themselves. This process prepares related data sets for global fits or smoothing using the Deltaχ software.

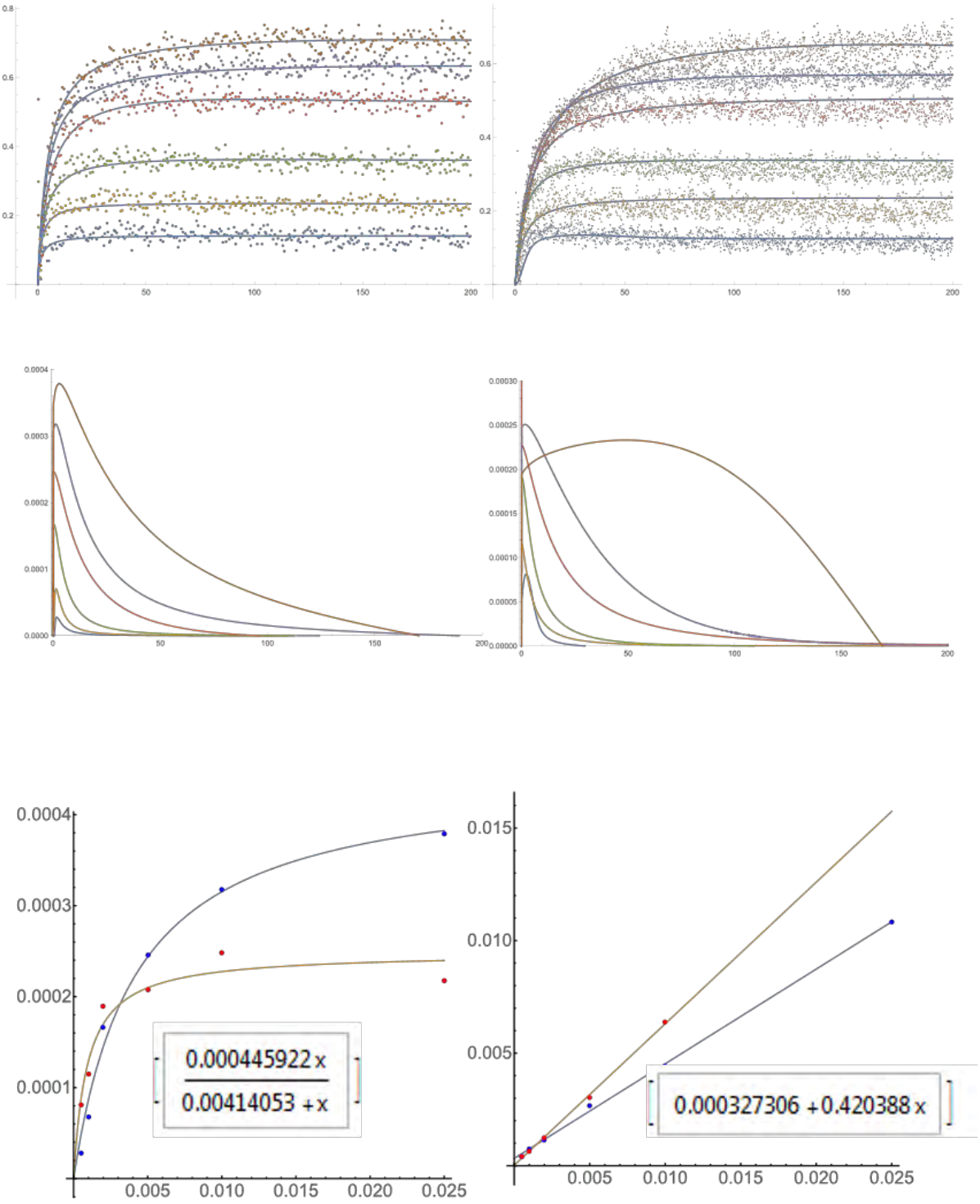

Figure 4.3 Initial velocity analysis using smoothing data fits, Km interior, and Vmax uptake

We proceeded with smoothing on two full data sets to analyze the early behaviors of their rates. These sets include zero-*trans* entry of glucose into ATP and AMP-containing ghosts. We

establish a system of differential equations akin to those used in the simple carrier model, but we did not hold any of the parameters between the data sets as shared or restricted to known values. The utility sought in this application of the program is to generate analytic curves whose shape will be used, not their parameters. We processed 6 data sets (0.5, 1.0, 2.0, 5.0, 10.0, and 25.0 mM Glc) for each condition and analyzed the resulting interpolating functions (Figure 4.3 A-B). We looked at properties of the simulated data sets which are analogous to V_{max} and K_m values. This was done by numerically differentiating the smoothing fits to the data sets and then finding the max value near t=0. We then used these to look at the concentration of intracellular sugar when the entry rate falls to half its original value, something analogous to an interior Km. Plotting each set vs. $[Glc]_{out}$ gives the graphs seen in 4.3E-F.

Chapter 6

DISCUSSION

GlcSnFR as tool to measure glucose transport and regulation

The engineering of a fluorescent glucose probe has provided access to a new experimental vista for the investigation of cellular glucose homeostasis. We found that the careful application of this technology allowed for glucose transport experiments which yielded unprecedented data density, resolution, and continuity. However, before we were able to execute these studies, it was also clear that the probe, GlcSnFR, is not a panacea for studying glucose regulation. Indeed, because of the continuous and ubiquitous presence of glucose and its dual role within the human physiology as a major source of chemical energy and biomass, local concentrations are maintained in relative equilibrium through the action of multiple biochemical programs. As such, the magnitude of a glucose flux effected by any one system can be significant while the overall change in concentration is near zero. This presents a significant barrier to an experimental strategy which cannot disambiguate individual glucose streams. As this is the case with GlcSnFR, extra care must be taken when designing experiments in order to preserve the specificity of the data gathered. However, the power of the ability to collect data continuously and immediately after the start of an experiment (in fact, during all phases of an experiment) should not be underestimated. Further, the sensor does demonstrate good substrate specificity and a high signal-to-noise ratio, making data sets obtained with good controls very rich sources of kinetic information. Indeed, a large amount of the effort exerted in the creation of this work was spent developing a reliable set of assays that could take into account the aforementioned risks while maximizing the rewards. We discuss here the basic information learned about the probe and its interactions with glucose and its experimental environment, the assays we developed along with the

difficulties and benefits inherent in each, and the future work which could be done to make it an even better tool.

The single greatest weakness of the GlcSnFR probe is the lack of certainty that can be assigned to the data it generates. In the case of a radiolabeled substrate, there can be little doubt of the source of the signal. Certainly, one might question whether all factors pertaining to its accumulation have been accounted for, but the decay of radioisotope is nearly as specific a signal as any used in an experimental setting. Additionally, a radiolabel can be applied to subpopulations of a chemical, allowing for certain delineation of the source and current location of said population. Both of these traits are absent when using GlcSnFR. The change in fluorescent signal can certainly be a result of shifting glucose concentrations, but can also be an indicator for changing pH, temperature, or photo-modification. In order to attribute the generated signal to flux in local glucose concentration, experimental design must take these confounding factors into account, even if they cannot be controlled completely. This places many restrictions on design that are not present in assays utilizing radiolabeled substrate. Additionally, the probe's inability to specifically track one subpopulation of substrate versus any others confounds data analysis in a different way. As mentioned above, there are several pathways in living cells with strong influence over the fate of an individual glucose molecule, and controlling these pathways is often difficult, if not impossible. Because the GlcSnFR probe can only detect net changes in total glucose, even more design considerations must be made to account for this. These reasons, individually and in composite, are what led us to ultimately choose erythrocyte ghosts as our environment for experimental analysis of GLUT1 kinetics. The pre-existence of a large membrane presence of carrier, homogeneous structure and geometry, lack of systemic complexity, and the evacuation of cytosolic contents, including the relatively small amount of metabolic activity to begin with, made the ghost an ideal choice for our studies.

While there are certainly limitations inherent in GlcSnFR's utility, it provides powerful benefits which still serve to make it a very attractive tool for kinetic analysis. First among these is the relatively non-disruptive nature of its reporting. In the canonical case of radiolabeled substrate experiments, the amount of translocated substrate can only be measured once per cell as the process of doing so requires the collection and destruction of said cell. This requires the use of many samples of the transport-effecting subject and introduces a discontinuity to the data which ultimately lowers accuracy and precision, especially at early time points where the assignment of an elapsed time to each sample carries the greatest degree of uncertainty. When using fluorescence as a signal, however, data can be collected without disruption of the integrity or location of the subject cell. This provides the capacity to follow the cell's complete transport history. The difference between the two techniques is analogous to the difference between a collection of biographies and a census. Importantly, the lack of disruption allows a previously unrealized resolution of early time points in the transport process. Because so many kinetic analyses use initial velocity as a central calculation, and because there is no guarantee that the initial rate of transport is maintained for a substantial length of time, this access to early data is of critical importance.

The successful completion of the affinity mutant work we began would help turn GlcSnFR into a more powerful tool for glucose transport kinetics. One of its shortcomings, as mentioned above, is the inability to differentiate between glucose fluxes inside the cell, namely those of transport and metabolism. A common technique adopted by radiolabeled substrate assays is the use of glucose homologues which interact with the cellular metabolism to different degrees. Among these alternate substrates is 3MG, a hexose which is transported by GLUT1 with similar kinetics as glucose, but has no level of interaction with hexokinase. As such, 3MG is a substrate for the transport process, but not metabolism. This provides a certainty that signal dynamics measured in experiments in which it is used are the result of carrier activity, uninfluenced by the metabolic state of the cell, at least with regard to

its direct consumption of glucose. While we were able to make a version of GlcSnFR with 3MG sensitivity in several ranges, none of these showed a preference for 3MG over glucose. Because glucose is at relatively high concentrations in most cultured cells and many primary cells, and can be generated through gluconeogenesis at unpredictable times and rates, this preference would be critical. However, if such a probe could be constructed, it would allow access to all sorts of cell types as environments for kinetic analysis. One of the greatest barriers to our studies in living cells was the inability to disambiguate the transport and metabolic glucose fluxes. A 3MG-specific sensor would be a great boon to the analysis of glucose transporter mechanisms.

GLUT1 Transport

Our use of GlcSnFR to study the nucleotide-modulated behavior of GLUT1 was able to confirm previous observations, establish answers to a few basic questions which had remained unanswered, and demonstrate some novel behavior.

When analyzing the transport of glucose through GLUT1, we expected to recapitulate a few basic observations which have been previously well-established regarding ATP-induced shifts in kinetic behavior. Namely, the presence of ATP, and not AMP, in the cytosol of erythrocyte ghosts has been shown to decrease the maximum rate of influx as well as decrease the K_M for import. Additionally, there should be a concurrent and more severe decrease in V_{max} for efflux, a hallmark of ATP-induced GLUT1 asymmetry. The apparent K_M for efflux is also predicted to decrease. Our studies in both single cells and cell populations confirmed these observations. In the single cell studies, we observed that efflux rates were significantly reduced compared to influx rates exclusively in ATP-containing cells. In our population studies, we observed the expected decrease in influx V_{max} and K_M. Additionally, we observed a trend for apparent K_M at the cell interior to increase with external glucose concentration. This observation was made in conditions of non-saturating external glucose, a condition previously

unexplored due to the difficulty in accurately measuring initial rates with the presumption of saturation. We see a linear increase in the half-max cytosolic glucose concentration which does not necessarily indicate a saturating trend as concentration goes up. However, such a saturation is presumed as there is conclusive evidence of a maximum velocity of entry. The passive nature of the GLUT1 transporter demands that the internal sugar concentration at which this is slowed to half demonstrate an asymptotic trend similar to that of the maximum velocity. This does highlight one stark fact, however. Many previous studies have found the half-max cytosolic glucose concentration (k_{50}) to be lower (around 4 mM) than predicted values (around 20 mM). Our study demonstrates that the linear dependence of the k_{50} has a predicted maximum value well above the 4 mM range. Indeed, this value of 4 mM is already determined to be lower than the unsaturated values we have calculated. In addition to these findings, we have also demonstrated conclusively that the kinetic phenomena observed in resealed erythrocyte ghosts are inherent characteristics of GLUT1 regulation, not artifacts of the experimental protocol. That is, a potential explanation for certain behaviors in GLUT1-mediated sugar equilibration, e.g. studies demonstrating multiphasic time courses, are not artificial results whose basis derives from the formation of a heterogeneous population of cells during the resealing process. Our confocal microscopy data confirms that both AMP- and ATP-containing ghosts demonstrate different transport parameters and that they do so as an entire population, not a collection of subpopulations.

We believe that these studies represent the beginning of what could be a very important kinetic data set. Many questions remain to be answered about the basics of GLUT1 function which can be studied in the erythrocyte. From the studies we have already conducted, several extending analyses present themselves. First among these is the continuation of the fluorimeter data set and the extension of the k_{50} trend. Because our experimental conditions did not extend beyond subsaturating conditions at the exterior of the cell, we do not yet have a clear indication of when the endofacial k_{50} will saturate. The working hypothesis of previous studies is that the limit of this value as the external glucose

concentration goes to infinity represents the affinity (K_M) of GLUT1 for glucose on its intracellular face. While the current study would not necessarily answer why much lower values were detected in previous assays, it would be able to determine the value of the endofacial catalytic affinity constant in a more definitive manner. That is, previous studies were designed such that their data would reveal the concentration of cytosolic sugar that would half the rate of sugar influx from an exterior solvent with completely saturating sugar concentration. This is simply the asymptotic value of the trend we observed with GlcSnFR. Our results already indicate that we have a reliable method for measuring this value for both saturating and non-saturating exterior glucose concentrations. This will allow the construction of the complete numeric relationship between exterior glucose and k_{50} which subsequently provides the asymptotic limit thereof. Additionally, it appears from the data already collected that the maximum k_{50} constants, or apparent K_Ms, for both AMP and ATP are more consistent with theoretical values than indicated by previously reported measurements. Similar studies should be conducted in the future using the reflected conditions: increasingly saturating initial cytosolic glucose exiting into very low external glucose. This experimental paradigm already highlights a variable yet unconsidered in these analyses which is the ratio of compartment volumes. In the uptake experiments, we can assume that the effective external volume is infinite compared to that of the cytosol. This allows our analysis to assume the concentration in the external buffer is invariant while that in the cytosol approaches equilibrium. As such, when measuring the k_{50} on the inside, we can estimate the internal glucose concentration while maintaining our assumption of a constant external concentration. However, in the case of sugar efflux, a nearly infinite volume of external buffer into which the sugar exits will force us to assign a value of nearly zero to the external sugar concentration. This means that every observation of half-maximum exit rate will be associated with a constant value. This suggests that the parameter being measured is not solely dependent on the static values of concentrations on the inside and outside, but a

function of the two and the volumes they occupy (and by extension the potential of the glucose gradient constructed by the experimental conditions).

Bibliography

Alberts B, Johnson A, and Lewis J (2002). Molecular Biology of the Cell. , Vol 4th edition, 4th edn (New York: Garland Science; 2002.).
Anderson, R.A., and Lovrien, R.E. (1981). Erythrocyte membrane sidedness in lectin control of the Ca2+–A23187-mediated diskocyte ⇄ echinocyte conversion. Nature *292*, 158.
Argüello, J.M., Patel, S.J., and Quintana, J. (2016). Bacterial Cu(+)-ATPases: models for molecular structure-function studies. Metallomics : integrated biometal science *8*, 906-914.
Augustin, R., and Mayoux, E. (2014). Mammalian Sugar Transporters. In Glucose Homeostasis, L. Szablewski, ed. (InTech).
Bachelard, H.S. (1972). Deoxyglucose and brain glycolysis. Biochem J *127*, 83P.
Bell, G.I., Murray, J.C., Nakamura, Y., Kayano, T., Eddy, R.L., Fan, Y.S., Byers, M.G., Shows, T.B.I., Yazaki, Y., and et, a.l. (1989). Polymorphic human insulin-responsive glucose-transporter gene on chromosome 17p13. Diabetes *38*, 1072-1075.
Blodgett, D., Graybill, C., and Carruthers, A. (2008). Analysis of glucose transporter topology and structural dynamics. J Biol Chem *283*, 36416-36424.
Blodgett, D.M., and Carruthers, A. (2005). Quench-Flow Analysis Reveals Multiple Phases of GluT1-Mediated Sugar Transport. Biochemistry *44*, 2650-2660.
Brook-Carter, P.T., Peral, B., Ward, C.J., Thompson, P., Hughes, J., Maheshwar, M.M., Nellist, M., Gamble, V., Harris, P.C., and Sampson, J.R. (1994). Deletion of the TSC2 and PKD1 genes associated with severe infantile polycystic kidney disease--a contiguous gene syndrome. Nat Genet *8*, 328-332.
Calonge, M.J., Gasparini, P., Chillaron, J., Chillon, M., Gallucci, M., Rousaud, F., Zelante, L., Testar, X., Dallapiccola, B., Di Silverio, F*., et al.* (1994). Cystinuria caused by mutations in rBAT, a gene involved in the transport of cystine. Nat Genet *6*, 420-425.
Carruthers, A., and Helgerson, A.L. (1989). The human erythrocyte sugar transporter is also a nucleotide binding protein. Biochemistry *28*, 8337-8346.
Cheng, S., Gregory, R., Marshall, J., Paul, S., Souza, D., White, G., O'Riordan, C., and Smith, A. (1990). Defective intracellular transport and processing of CFTR is the molecular basis of most cystic fibrosis. Cell *63*, 827-834.
Cloherty, E.K., Levine, K.B., Graybill, C., and Carruthers, A. (2002). Cooperative nucleotide binding to the human erythrocyte sugar transporter. Biochemistry *41*, 12639-12651.
Cloherty, E.K., Sultzman, L.A., Zottola, R.J., and Carruthers, A. (1995). Net sugar transport is a multistep process. Evidence for cytosolic sugar binding sites in erythrocytes. Biochemistry *34*, 15395-15406.
Court, S.J., Waclaw, B., and Allen, R.J. (2015). Lower glycolysis carries a higher flux than any biochemically possible alternative. Nat Commun *6*, 8427.
De Zutter, J., Levine, K., Deng, D., and Carruthers, A. (2013). Sequence determinants of GLUT1 oligomerization: analysis by homology-scanning mutagenesis. J Biol Chem *288*, 20734-20744.
Deng, D., Xu, C., Sun, P., Wu, J., Yan, C., Hu, M., and Yan, N. (2014a). Crystal structure of the human glucose transporter GLUT1. Nature *510*, 121-125.
Deng, D., Xu, C., Sun, P., Wu, J., Yan, C., Hu, M., and Yan, N. (2014b). Crystal structure of the human glucose transporter GLUT1. Nature.
Elbourne, L.D., Tetu, S.G., Hassan, K.A., and Paulsen, I.T. (2017). TransportDB 2.0: a database for exploring membrane transporters in sequenced genomes from all domains of life. Nucleic Acids Res *45*, D320-D324.
Friis, U.G., Praetorius, H.A., Knudsen, T., and Johansen, T. (1997). Role of the Na+/K+-ATPase in regulating the membrane potential in rat peritoneal mast cells. Br J Pharmacol *122*, 599-604.

Gorga, F., and Lienhard, G. (1981). Equilibria and kinetics of ligand binding to the human erythrocyte glucose transporter. Evidence for an alternating conformation model for transport. Biochemistry *20*, 5108-5113.
Graybill, C., van Hoek, A., Desai, D., Carruthers, A., and Carruthers, A. (2006). Ultrastructure of Human Erythrocyte GLUT1. Biochemistry *45*, 8096-8107.
Heard, K., Fidyk, N., and Carruthers, A. (2000). ATP-dependent substrate occlusion by the human erythrocyte sugar transporter. Biochemistry *39*, 3005-3014.
Hebert, D.N., and Carruthers, A. (1991). Cholate-solubilized erythrocyte glucose transporters exist as a mixture of homodimers and homotetramers. Biochemistry *30*, 4654-4658.
Hebert, D.N., and Carruthers, A. (1992). Glucose transporter oligomeric structure determines transporter function. Reversible redox-dependent interconversions of tetrameric and dimeric GLUT1. J Biol Chem *267*, 23829-23838.
Hermansen, L., Hultman, E., and Saltin, B., JJ (1967). Muscle glycogen during prolonged severe exercise. Acta Physiol Scand *71*, 129-139.
Hertz, L., Peng, L., and Dienel, G.A. (2007). Energy metabolism in astrocytes: high rate of oxidative metabolism and spatiotemporal dependence on glycolysis/glycogenolysis. J Cereb Blood Flow Metab *27*, 219-249.
Hille, B. (2001). Ionic Channels of Excitable Membranes (Sinauer).
Jacquez, J.A. (1984). Red blood cell as glucose carrier: significance for placental and cerebral glucose transfer. Am J Physiol *246*, R289-298.
Jay, T., Dienel, G., Cruz, N., Mori, K., Nelson, T., and Sokoloff, L. (1990). Metabolic stability of 3-O-methyl-D-glucose in brain and other tissues. J Neurochem *55*, 989-1000.
Jones, P.M., and George, A.M. (2004). The ABC transporter structure and mechanism: perspectives on recent research. Cell Mol Life Sci *61*, 682-699.
Jones, P.M., George, A.M.i., M., and Boutelle, M.G. (2000). Symmetry and structure in P-glycoprotein and ABC transporters. European Journal of Biochemistry *267*, 5298-5305.
Joost, H.G., Bell, G.I., Best, J.D., Birnbaum, M.J., Charron, M.J., Chen, Y.T., Doege, H., James, D.E., Lodish, H.F., Moley, K.H*., et al.* (2002). Nomenclature of the GLUT/SLC2A family of sugar/polyol transport facilitators. Am J Physiol Endocrinol Metab *282*, E974-976.
Jung, C.Y., Carlson, L.M., Whaley, D.A.M.N., and Haas, M.N. (1971). Glucose transport carrier activities in extensively washed human red cell ghosts. Biochim Biophys Acta *241*, 613–627.
Kapoor, K., Finer-Moore, J., Pedersen, B., Caboni, L., Waight, A., Hillig, R., Bringmann, P., Heisler, I., Müller, T., Siebeneicher, H*., et al.* (2016). Mechanism of inhibition of human glucose transporter GLUT1 is conserved between cytochalasin B and phenylalanine amides. Proc Natl Acad Sci U S A *113*, 4711-4716.
Keller, J.P., and Looger, L.L. (2016). The Oscillating Stimulus Transporter Assay, OSTA: Quantitative Functional Imaging of Transporter Protein Activity in Time and Frequency Domains. Mol Cell *64*, 199-212.
Leitch, J., and Carruthers, A. (2007). ATP-dependent sugar transport complexity in human erythrocytes. American journal of physiology Cell physiology *292*, C974-986.
Levine, K.B., Cloherty, E.K., Hamill, S., and Carruthers, A. (2002). Molecular determinants of sugar transport regulation by ATP. Biochemistry *41*, 12629-12638.
Lieb, W., and Stein, W. (1971). New theory for glucose transport across membranes. Nat New Biol *230*, 108-109.
Long, W., and Cheeseman, C. (2015). Structure of, and functional insight into the GLUT family of membrane transporters. Cell Health and Cytoskeleton *7*, 167—183.
Lowe, A.G., and Walmsley, A.R. (1986). The kinetics of glucose transport in human red blood cells. Biochim Biophys Acta *857*, 146-154.

Marger, M.D., Saier Jr, M.H., and Sobrevia, L. (1993). A major superfamily of transmembrane facilitators that catalyse uniport, symport and antiport. Trends Biochem Sci *18*, 13-20.
Mueckler, M., Caruso, C., Baldwin, S.A., Panico, M., Blench, I., Morris, H.R., Allard, W.J., Lienhard, G.E., and Lodish, H.F. (1985). Sequence and structure of a human glucose transporter. Science *229*, 941-945.
Mueckler, M., and Thorens, B. (2013). The SLC2 (GLUT) family of membrane transporters. Molecular aspects of medicine *34*, 121-138.
Naftalin, R.J., and Holman, G.D. (1977). Transport of sugars in human red cells. In Membrane transport in red cells, J.C. Ellory, and V.L. Lew, eds. (New York: Academic Press), pp. 257-300.
Naftalin, R.J., Smith, P.M., Roselaar, S.E.A., and Munday, K.A. (1985). Evidence for non–uniform distribution of D–glucose within human red cells during net exit and counterflow. Biochim Biophys Acta *820*, 235–249.
Pao, S.S., Paulsen, I.T., and Saier, M.H., Jr. (1998). Major facilitator superfamily. Microbiol Mol Biol Rev *62*, 1-34.
Perland, E., and Fredriksson, R. (2017). Classification Systems of Secondary Active Transporters. Trends in pharmacological sciences *38*, 305-315.
Richter, E.A. (2010). Glucose Utilization (John Wiley & Sons, Inc.).
Rigaud, J.L., and Levy, D. (2003). Reconstitution of membrane proteins into liposomes. Methods Enzymol. Methods Enzymol, 65-86.
Romano, A.H., and Conway, T. (1996). Evolution of carbohydrate metabolic pathways. Res Microbiol *147*, 448-455.
Schurmann, A., Doege, H., Ohnimus, H., Monser, V., Buchs, A., and Joost, H.G. (1997). Role of conserved arginine and glutamate residues on the cytosolic surface of glucose transporters for transporter function. Biochemistry *36*, 12897-12902.
Stein, W.D. (1986). Transport and diffusion across cell membranes (New York: Academic Press).
Taurino, F., and Gnoni, A. (2018). Systematic review of plasma-membrane ecto-ATP synthase: A new player in health and disease. Exp Mol Pathol *104*, 59-70.
Taylor, L., and Holman, G. (1981). Symmetrical kinetic parameters for 3-O-methyl-D-glucose transport in adipocytes in the presence and in the absence of insulin. Biochim Biophys Acta *642*, 325-335.
Travis, A., Tutuncu, L., Jorgez, C., Ord, T., Jones, B., Kopf, G., and Williams, C. (2004). Requirements for glucose beyond sperm capacitation during in vitro fertilization in the mouse. Biol Reprod *71*, 139-145.
Uldry, M., Ibberson, M., Horisberger, J., Chatton, J., Riederer, B., and Thorens, B. (2001). Identification of a mammalian H(+)-myo-inositol symporter expressed predominantly in the brain. EMBO J *20*, 4467-4477.
Wasserman, D.H. (2009). Four grams of glucose. Am J Physiol Endocrinol Metab *296*, E11-21.
Widdas, W.F. (1952). Inability of diffusion to account for placental glucose transfer in the sheep and consideration of the kinetics of a possible carrier transfer. J Physiol (London) *118*, 23–39.
Wood, R.E., Wirth, F.P., and Morgan, H.E. (1968). Glucose permeability of lipid bilayer membranes. Biochimica et Biophysica Acta (BBA) - Biomembranes *163*, 171-178.
Wright, E.M. (2009). Diseases of Renal Glucose Handling (Academic Pr).
Yan, N. (2013). Structural advances for the major facilitator superfamily (MFS) transporters. Trends in Biochemical Sciences *38*, 151-159.
Yu, S., and Ding, W.-G. (1998). The 45 kDa form of glucose transporter 1 (GLUT1) is localized in oligodendrocyte and astrocyte but not in microglia in the rat brain. Brain Research *797*, 65-72.